IMPACT OF AN ARTIFICIAL CIRCULATION DEVICE

ON THE

HEAT BUDGET OF AN ICE-COVERED MID-LATITUDE LAKE

by

Christopher Kavanagh Rogers

B. A. Sc. (hons.), University of Waterloo

A THESIS SUBMITTED IN PARTIAL FULFILLMENT OF

THE REQUIREMENTS FOR THE DEGREE OF

MASTER OF APPLIED SCIENCE

in

THE FACULTY OF GRADUATE STUDIES

Department of Civil Engineering

We accept this thesis as conforming

to the required standard

THE UNIVERSITY OF BRITISH COLUMBIA

December 1992

In presenting this thesis in partial fulfilment of the requirements for an advanced degree at the University of British Columbia, I agree that the Library shall make it freely available for reference and study. I further agree that permission for extensive copying of this thesis for scholarly purposes may be granted by the head of my department or by his or her representatives. It is understood that copying or publication of this thesis for financial gain shall not be allowed without my written permission.

(Signature)

Department of CIVIL ENGINEERING

The University of British Columbia
Vancouver, Canada

Date DEC. 17/92

DE-6 (2/88)

ABSTRACT

Two lakes located in the Southern Interior Plateau of British Columbia were selected for a field investigation in order to assess the impact of artificial circulation on the heat budget of a small mid-latitude ice-covered lake. The heat transfer algorithm developed by Patterson & Hamblin (1988) for high latitude lakes was extended to include the impacts of snowmelt due to rain, sediment heat transfer, snow-ice formation, and day to day variations in snow density, snow conductivity and albedo. Since the lakes considered are nearly isothermal in winter, the new model ignores the internal hydrodynamics of the problem. This model was tested on Harmon Lake, which was selected as a control for the study. The model was further modified to include the effects of artificial circulation at nearby Menzies Lake. These effects include polynya development, and a substantial reduction in average temperature. Heat losses due to free convective evaporation and direct snowfall on open water were added to the set of standard aerodynamic formulae used to determine the net meteorological heat flux across a water surface. Turbulent heat transfer from the circulated water to the ice cover was estimated based on an empirical surface velocity relationship derived from field measurements. The size of the polynya is estimated by means of a simple heat balance which also involves the surface velocity function.

The Harmon Lake predictions agree well with the field data. All discrepancies could be accounted for by parameter uncertainties and expected observation error. It was found that sediment heat transfer may be important in early winter in preventing a net loss of heat from the lake water. Significant heat gains in the latter part of winter, however, are attributed to the penetration of solar radiation. Once calibrated, the Menzies Lake predictions are also good. It was found that, over the period in which lake temperature dropped, the average heat loss due to turbulent heat transfer between water and ice was

three times that across the polynya surface. The former heat flux continued to increase as the lake warmed up again, while the latter fell, on average, over a short period until increased solar heating resulted in a reversal in the direction of heat transfer across the polynya. Discrepancies between early winter ice thickness predictions and observations, could not be accounted for. It is suspected, however, that these discrepancies are a result of the impact which the heat flux across the polynya may have on the heat flux through the ice and snow cover. In this thesis, it is assumed that these two fluxes are independent of one another.

TABLE OF CONTENTS

LIST OF FIGURES

LIST OF TABLES

LIST OF SYMBOLS

The following is a list of the most common symbols in this thesis.

A .....spectral fraction
.....area
C.....fraction of sky which is cloud-covered
C_{pi} .....heat capacity of ice
C_{pw}.....heat capacity of water
C_t.....turbulent heat transfer coefficient
d .....number of days since snowfall
H .....net meteorological flux
h.....thickness of medium
h_{en} .....latest snow-ice accumulation
h_{sm} .....maximum possible snow thickness
I_o .....non-reflected solar radiation at surface
I_w.....solar radiation reaching water
K .....conductivity
L.....latent heat of fusion
P .....rainfall
P_{atm} .....atmospheric pressure
q_f .....heat flux in ice at ice-water interface
q_o.....heat flux at the surface
q_{sed}.....sediment heat flux
q_t .....turbulent heat transfer from water to ice
q_w .....heat conduction from water to ice
Q .....volumetric flow rate
Q_c .....sensible heat flux
Q_e.....evaporative heat flux
Q_{fc}.....heat flux due to free convection
Q_o.....incoming solar radiation
Q_r .....heat due to rainfall
Q_{si}.....heat due to snow-ice formation

Q_{sp} ..... heat flux due to snowfall on water
$\bar{Q}_t$ ..... total turbulent heat transfer to ice
r_p ..... polynya radius
r_∞ ..... $r_p + \Delta r$
R_{li} ..... incoming long-wave radiation
R_{lo} ..... outgoing long-wave radiation
svp0 ..... saturated vapour pressure at surface temperature
svpd ..... vapour pressure of air
S ..... Stefan Number
SW ..... observed total daily short-wave radiation
S_w ..... wind sheltering coefficient
SWCS ..... total daily short-wave radiation on clear day
T ..... temperature
U ..... radial jet velocity
U_w ..... wind velocity
V ..... lake volume
z ..... vertical coordinate (depth)
z_{max} ..... maximum depth
$\bar{z}$ ..... mean depth

Subscripts

1 ..... visible spectrum of radiation
2 ..... infrared spectrum of radiation
e ..... snow-ice
f ..... freezing
i ..... ice
m ..... melting
o ..... surface
p ..... polynya
pe ..... polynya edge
s ..... snow
sed ..... sediment
w ..... water

Greek Symbols

α ..... albedo

β ..... solar angle at solar noon

Δr ..... radial distance over which $\bar{Q}_t$ is active

ε ..... emissivity

λ ..... solar attenuation coefficient

ρ ..... density

ρ_1 ..... snow density 24 hrs after snowfall

ρ_m ..... maximum snow density

ρ_n ..... density of new snow

σ ..... Stefan-Boltzmann Constant

ACKNOWLEDGMENT

A great deal a support was provided for this project in terms of financing, technical consultation and field assistance. Funding was provided by the Natural Sciences and Engineering Research Council (N.S.E.R.C), the Science Council of British Columbia, and the University of British Columbia. Equipment purchases and field expenses were paid for by N.S.E.R.C. and the B.C. Ministry of the Environment. The author would like to thank Dr. P.F. Hamblin for his patient explanations regarding the complexities of lake modeling, and Dr. G.A. Lawrence for lending a sympathetic ear in times of frustration. The suggestions and comments provided by these two individuals were crucial to the successful completion of this thesis. Dr. Craig Stevens and Dr. Noboru Yonomitsu are also recognized for their help in this regard.

The field study component of this project could not have been carried out without the guidance of Mr. K.I. Ashley who has been an excellent tutor in the area of field limnology. The students and staff of the U.B.C. Department of Civil Engineering (as well as many friends) who volunteered their time as field assistants are too numerous to list here, but their help has been greatly appreciated. In particular, the author wishes to thank Mr. B. Laval for the many long days he has dedicated to the acquisition of field data.

Chapter 1
INTRODUCTION

1.1 WINTERKILL

1.1.1 The Oxygen Depletion Problem

Many of the small kettle lakes of the B.C. Interior are naturally eutrophic, and therefore experience high oxygen depletion rates due to the decay of organic material. Over the winter season, replenishment of oxygen is prevented by ice and snow cover. The ice and snow constitute a physical barrier to the diffusion of oxygen into the water and can also inhibit photosynthetic production of oxygen due to light limitation. As a result, the dissolved oxygen content in these lakes may drop below levels which can support fish life. Deleterious effects on aquatic life may occur below about 1°C (pers. comm., Ashley, 1991). The B.C. Ministry of the Environment (Fisheries Branch) has addressed this problem, commonly termed winterkill, by implementing an extensive winter aeration programme throughout the Southern B.C. Interior.

1.1.2 The Artificial Circulation Solution

The aeration scheme simply involves artificially circulating the water in order to maintain a polynya (ice-free patch) over part or all of the winter season. This is often done using a commercial unit called the Air-o-lator®, which is shown in Figure 1.1. The polynya generated by this device at Menzies Lake near Merritt, B.C. is shown if Figure 1.1a. The size of the aeration equipment must be sufficient to ensure a large enough ice-free zone to allow adequate diffusion and turbulent entrainment of oxygen into the lake, but small

enough to avoid cooling the water to temperatures which threaten the resident aquatic life. The hardware generally consists of a compressor or axial flow pump fixed inside of a vertical draught tube, which is attached to a floatation device. The assembly is anchored as close to the deepest part of the lake as practically possible. A single 0.75 kW pump will produce an ice-free zone of 30-50 m in diameter, which is sufficient to prevent winterkill in lakes up to approximately 10 ha in surface area (Ashley, pers. comm., 1991).

Water is drawn up through the draught tube, which extends 0 to 3 metres into the lake, and is projected into the air. The fountain-like jet plunges back into the water and spreads radially. The area around the device remains ice-free out to a critical distance where the artificially-induced turbulence and thermal energy is insufficient to prevent freezing.

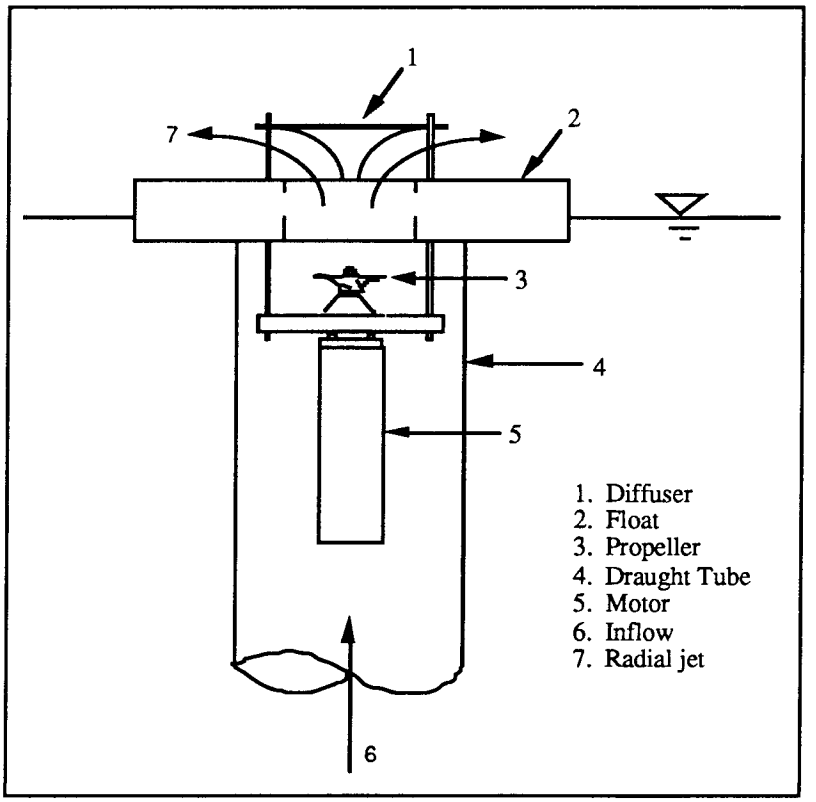

Figure 1.1 The Air-o-lator®

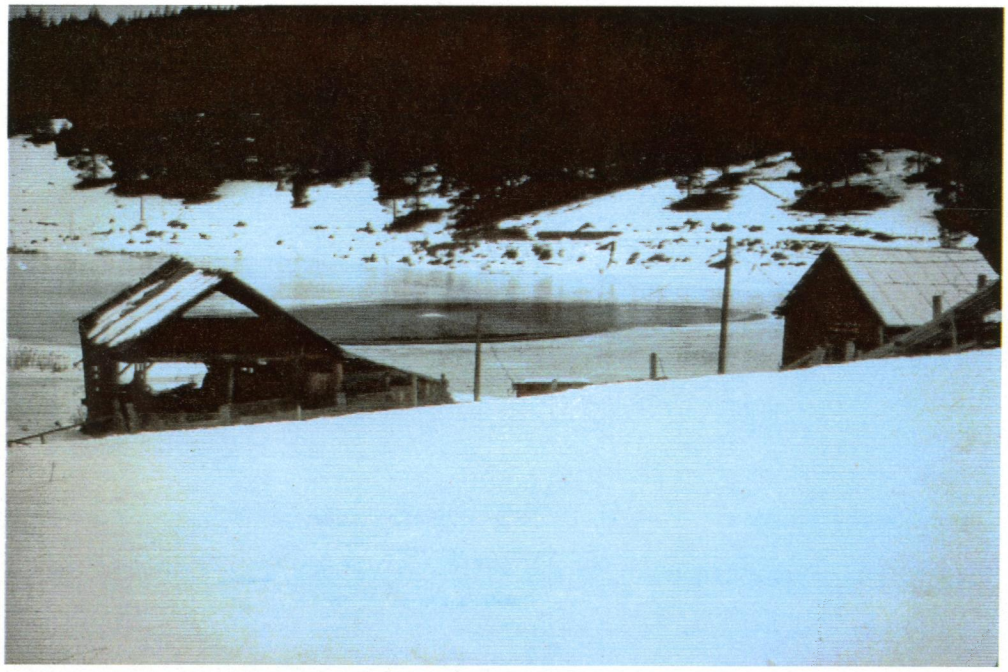

Figure 1.1a Polynya Generated by Air-o-lator® at Menzies Lake
(photograph taken from north end of lake)

1.1.3 Circulator Effectiveness

Field measurements at Menzies Lake near Merritt, B.C. in mid-February, 1991 indicated very effective reaeration due to artificial circulation. The weak inverse thermal stratification normally observed under the ice was mixed down to a depth of about 12 metres. The depth of the pycnocline is controlled by a 3 m draught tube and the lake morphometry as a result of its shallowness. As shown in Figure 1.2, no significant horizontal variations of oxygen or temperature were observed other than those caused by heat and mass transfer across the sediment-water interface (see Chapter 3). This indicates that a one-dimensional representation of the effect of the circulator is appropriate provided a sufficient rate of pumping is maintained. The top 12 metres contained 7 to 8 mg/l of dissolved oxygen and was isothermal at about 1°C. Below the thermocline, the water was anoxic (below 0.5 mg/l) and near the temperature of maximum density. In addition to aeration, the circulator has significant cooling effect on the lake. When ice-covered, a mid-latitude lake in its natural state will generally be close to 4°C over the entire water column below a relatively thin boundary layer which brings the water to 0°C at the ice-water interface.

1.2 PROJECT SCOPE

1.2.1 Importance of the Heat Budget

Oxygen concentrations depend on water temperature and ice cover characteristics in several ways. These dependencies include rates of decay of organic material, oxygen saturation concentrations, inhibition of photosynthesis through light attenuation, and duration of ice-cover. The first step in developing a comprehensive oxygen budget

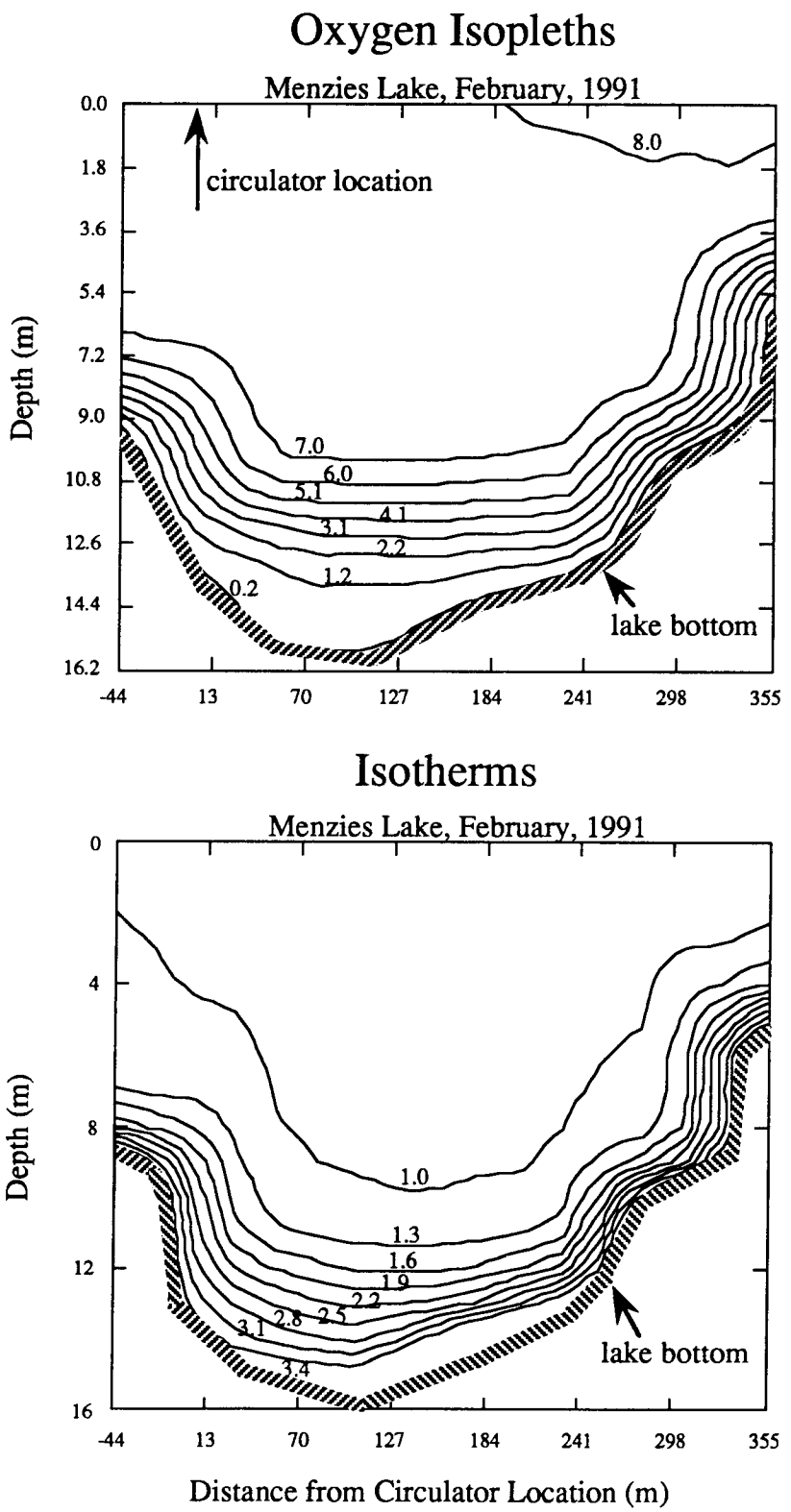

Figure 1.2. Oxygen and Temperature Isotherms: Menzies Lake, February, 1991

model for the artificially circulated lake is therefore a model which simulates the heat budget. The current investigation is limited to this first step.

1.2.2 Winter Stratification

An exhaustive treatment of the heat budget would require a numerical description of the internal hydrodynamics induced by the artificial circulation. It is suspected that selective withdrawal theory (see §3.2.4) may govern the fate of the winter pycnocline, but the continual operation, induced lake circulation, and radial jet behaviour make the problem unique. In addition, with the formation of a circulator-induced winter thermocline, the hypolimnetic water quickly becomes anoxic (this has been observed throughout the current study). The anoxia leads to the release of metals which are sensitive to oxidation-reduction potential (see Mortimer, 1941; 1942; Stauffer, 1987). The build-up of solids near the lake bottom may actually be greater than if the lake were not artificially circulated because diffusion is restricted by the density gradient associated with the thermocline above. The resulting increase in solids concentration serves to stabilize the circulator-induced stratification.

The circulation equipment, however, is generally sized in B.C. winterkill applications to cause the lake to overturn continually over the winter period, without disturbing the lake sediments. Furthermore, the winter hypolimnion at Menzies Lake is of almost negligible volume, compared with the mixed region above (this fact is illustrated by the morphometric data given in Chapter 3). In order to simplify the heat budget problem, complete mixing will be assumed, and the internal hydrodynamics ignored.

1.2.3 The Natural State

Before examining the effects of artificial circulation, a model must first be developed to predict the thermal behaviour of the ice-covered lake in its natural state. In spite of the

existence of many hydrodynamic lake models, few have tackled the ice-cover problem. Those that have are highly simplified and/or do not deal with the particularities associated with mid-latitude lakes. For this study, an existing ice and snow-cover model was selected and improved to account for these particularities. The product is called MLI (Mixed Lake with Ice cover). It is applied here to Harmon Lake which is situated in the same geographical region as Menzies Lake (see §3.1). The improved version was then modified to account for artificial circulation. This modified version is called MLI-C, and is applied to Menzies Lake.

Chapter 2

BACKGROUND PHYSICS & RELEVANT LITERATURE REVIEW

2.1 EXISTING HEAT BUDGET MODELS

2.1.1 A Brief History of Lake Simulation

A number of water quality simulation models have been developed to address the need to manage the quality of water stored in reservoirs. Most are fashioned after the WRE (Water Resources Engineers) model originally developed by Chen and Orlob (1975). Thermal stratification is of primary importance to water quality and therefore much effort has been focused on its prediction. As temperature variations in small to medium sized lakes and reservoirs is for most purposes, only significant in the vertical direction, the one-dimensional horizontal slab concept first advanced by Raphael (1962) is basic to most of these models. The heat budget of most lakes with high retention times are basically a function of meteorological forcing, and for simplicity, bulk aerodynamic formulae, such as those given by the Tennessee Valley Authority (TVA, 1972) are generally applied.

The incorporation of ice-cover routines into existing models, however, is only in the early stages of development. Recently, two independent research teams have make this attempt using DYRESM (see Imberger & Patterson, 1981), a commercially available stratification model which has been thoroughly tested and proven for temperate climates. Both models, however, were developed for lakes at high latitude, and have been insufficiently tested (Patterson & Hamblin, 1988; Gosink, 1987). They are also similar in

that they involve a solution to the heat conduction equation which includes a depth dependent heat source to account for the penetration of solar radiation through the ice and snow. The Patterson & Hamblin (1988) model is superior, however, to the Gosink (1987) model in at least two ways. In the latter model, the heat flux through the entire ice and snow cover is assumed constant and equal to the balance of meteorological forcing. Secondly, the short wave radiation is assumed to consist of only one spectral band characterized by a single attenuation coefficient for each medium through which it passes. In the former model, however, the heat flux through the cover is a function of depth, and two spectral bands are used. Consequently, the Patterson & Hamblin (1988) model (DYRESMI) was selected and modified for application to this investigation. The formulation will be described in detail following a brief overview of the development of their model.

2.1.2 The Development of DYRESMI

The definitive thermodynamic model of surface ice formation and ablation, according the Patterson & Hamblin (1988), is that of Maykut and Untersteiner (1971). It is a 1-D unsteady heat transfer model through a two component ice and snow cover, developed for sea ice, but not linked to oceanic mixing. As such, the heat flux across the ice-water interface is left unknown and must be specified by the user in order to arrive at a solution. As an alternative to the same model, Semter (1976) showed that a quasi-steady state solution to the heat transfer equations is reasonable if the ice is thin. The approach implies that the temperature distribution in the ice-snow cover has reached a steady state before a time step has elapsed. It has been shown that a quasi-steady state solution will be within 5% of a transient solution if the Stefan Number, S, is less than 0.1 (see Hill & Kucera, 1983):

$$S = \frac{C_{pi}\,\Delta T}{L} \tag{2.1}$$

where C_{pi} = specific heat of ice
ΔT = characteristic temperature difference across ice thickness
L = Latent heat of fusion

For the above condition to hold, ΔT must be less than about 15°C. This restriction is more likely to be satisfied at mid-latitude lakes than at those at high latitudes. The Stefan condition may be violated, however, provided that the ice (or snow) layer is thin. If it is assumed that the temperature gradient through the is ice cover is small compared with that through the snow cover, then the time scale for heat conduction through the snow must be short compared to the time scale of changes in meteorological forcing. This limiting time scale is of order h_s^2/κ_s, where h_s = snow thickness, and κ_s = thermal diffusivity of snow (see Patterson & Hamblin, 1988). Given a time step of one day (as is the case for DYRESM and DYRESMI), the snow thickness must be less than about 20 cm for the steady-state solution to be reasonable. Since the maximum snow thickness over lake ice is limited due to the low buoyancy of ice (see §2.3.3), it is relatively uncommon to observe thicknesses in excess of 20 cm, especially during mild winters. For a snow-free ice surface, the equivalent limiting ice thickness is about 30 cm.

Patterson and Hamblin (1988) developed two main improvements to the Maykut & Untersteiner (1971) model. First, a thermodynamic link with DYRESM was established, negating the need to specify the ice-water heat flux. Secondly, the effect of partial ice cover was incorporated into the model.

The thermodynamic link with DYRESM is interactive; DYRESM determines the heat flux at the ice-water interface, thereby affecting the ice cover, which in turn provides a boundary condition for the mixing model. Partial ice cover is dealt with by assuming that ice will not persist below a minimum thickness, but will be transported by wind stress and accumulate elsewhere at this specified thickness. This thickness has been observed to be about 10 cm for medium-sized lakes (Hamblin, pers. comm., 1992). During periods

of partial cover the heat transfer will be non-uniform over the lake surface. Horizontal temperature gradients are instantly relaxed, however, so that the model remains one-dimensional.

2.1.3 DYRESMI Formulation

Provided that freezing conditions persist over the winter period, both a layer of ice and a layer of snow will usually be observed on a lake. The distribution of temperature in the ice and snow is governed by the heat conduction equation which includes the absorption of solar radiation as a distributed heat source. The conductivity and attenuation characteristics of ice and snow are significantly different, and this must be reflected in the governing equations. A two term absorption law was adopted to account for the dependence of attenuation on wavelength. The absorption of radiation is assumed to follow Beer's Law, which for one spectral band is given as follows:

$$I_z = I_o \, e^{-\lambda z} \tag{2.2}$$

where, I_o = incident (non-reflected) radiation
= $(1 - \alpha) \cdot Q_o$, where α = albedo; Q_o = total incoming radiation
I_z = radiation remaining at depth z below the surface
λ = attenuation coefficient

The attenuation coefficient is dependent on the radiation wavelength and the transparency of the medium through which the radiation passes and the radiation wavelength. The appropriate form for radiation characterized by two spectral bands is:

$$I_z = I_o \, (A_1 \, e^{-\lambda_1 z} + A_2 \, e^{-\lambda_2 z}) \tag{2.3}$$

where, A = fraction of total radiation in a given spectral band ($A_1 + A_2 = 1$)
subscripts 1 and 2 refer to the two spectral bands

Patterson & Hamblin (1988) set $A_1 = 0.7$, the fraction associated with visible radiation, and $A_2 = 0.3$, that associated with infrared radiation, in accordance with Kirk (1983) and Boër (1980). It has been found that an increase in the number of spectral bands beyond two does not result in significant change in the distribution of heat below the ice and snow cover (Patterson & Hamblin, 1988).

The steady-state one-dimensional heat flow equation for a material with a uniform heat source is:

$$K \frac{\partial^2 T}{\partial z^2} + \dot{q} = 0 \tag{2.4}$$

where, T = material temperature
K = material conductivity
$\dot{q}$ = heat generated per unit volume

For an ice and snow cover with a depth-dependent solar heat source (see Figure 2.1), the equivalent equations are:

$$K_s \frac{\partial^2 T_s}{\partial z^2} + A_1 \lambda_{s1} I_o \exp[-\lambda_{s1} (h_i + h_s - z)] + A_2 \lambda_{s2} I_o \exp[-\lambda_{s2} (h_i + h_s - z)] = 0,$$

$$h_i + h_s \geq z \geq h_i$$

$$K_i \frac{\partial^2 T_i}{\partial z^2} + A_1 \lambda_{i1} I_o \exp[\lambda_{s1} h_s - \lambda_{i1} (h_i - z)] + A_2 \lambda_{i2} I_o \exp[-\lambda_{s2} h_s - \lambda_{i2} (h_i - z)] = 0,$$

$$h_i \geq z \geq 0 \tag{2.5}$$

where, λ = attenuation coefficient
h = material thickness
s = snow
i = ice

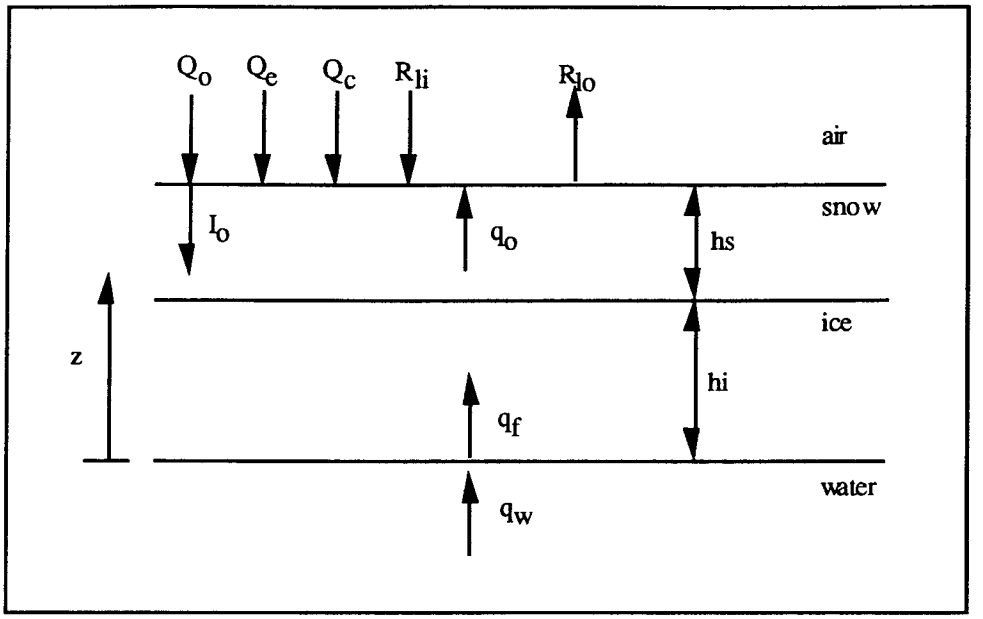

Figure 2.1. Heat Fluxes Across an Ice and Snow Cover

The appropriate boundary conditions for the above equations are:

$$T_i = T_f \qquad z = 0$$

$$\left.\begin{aligned} T_i &= T_s \\ K_i \frac{\partial T_i}{\partial z} &= K_s \frac{\partial T_s}{\partial z} \end{aligned}\right\} \qquad z = h_i$$

$$T_s = T_o \qquad z = h_i + h_s \tag{2.6}$$

where, T_o = the surface temperature of the top component of the cover
T_f = the freezing temperature

For the given equations to hold, the temperature distributions must stabilize on a time scale which is considerably shorter than that of variations in T_o and the snow and ice thicknesses. This condition is satisfied provided that the Stefan Number is less than 0.1 as previously described. The thermodynamic balances at the surface and ice-water interface can be treated independently, and an analytic solution is possible. As the

component temperatures are not required, the equations need only be solved for q_o, the conduction of heat at the air-snow interface:

$$q_o = -K_s \frac{\partial T_s}{\partial z}\bigg|_{z = h_i + h_s} \tag{2.7}$$

The solution can be written as:

$$\left(\frac{h_s K_i + h_i K_s}{K_i K_s}\right)(q_o - I_o) = T_f - T_o - A_1 I_o \left\{\frac{1-\exp(-\lambda_{s1} h_s)}{K_s \lambda_{s1}} + \frac{\exp(-\lambda_{s1} h_s)[1-\exp(-\lambda_{i1} h_i)]}{K_i \lambda_{i1}}\right\}$$

$$- A_2 I_o \left\{\frac{1-\exp(-\lambda_{s2} h_s)}{K_s \lambda_{s2}} + \frac{\exp(-\lambda_{s2} h_s)[1-\exp(-\lambda_{i2} h_i)]}{K_i \lambda_{i2}}\right\} \tag{2.8}$$

The solution reduces to the correct form in the absence of snow. It should be noted that there is a typographical error in this solution as given in Patterson & Hamblin (1988) (the correct form is in the DYRESMI code). The two terms representing the attenuation of short wave and infrared energy within the cover should result in an increase in q_o for an increase in any given attenuation coefficient. For this condition, the sign preceding these two terms must be negative, not positive as shown in Patterson & Hamblin (1988).

The components of the ice and snow cover heat budget are as shown in Figure 2.1. The thermodynamic balance at the surface depends on the meteorological forcing and on q_o, the flux of heat in the top component at the interface with the air. The surface temperature, T_o, will adjust itself so that a heat flux balance is achieved. T_o, however is bounded by T_m, the melting temperature. This provides the condition for surface melting. The surface condition may be expressed as:

$$\begin{aligned} q_o(T_o) + H(T_o) &= 0\,, & T_o < T_m \\ &= -\rho L \frac{dh}{dt}\,, & T_o = T_m \end{aligned} \tag{2.9}$$

where, $H(To)$ = net incoming meteorological flux
$= R_{li} - R_{lo}(To) + Qc(To) + Qe(To)$

R_{li} = incoming long-wave radiation
R_{lo} = outgoing long-wave radiation
Qc = sensible heat transfer between surface & atmosphere
Qe = evaporative heat flux

The above approach differs from that of Maykut and Untersteiner (1971) in that the solar radiation term enters the surface balance implicitly through the evaluation of the heat flux in the upper component, q_o. These authors specify a fraction of short-wave energy assumed to be available at the surface, which would produce a less accurate thermal profile in the cover. The model does not allow for ice growth at the surface. Snow thickening can only occur due to snowfall.

A criterion, based on a simple hydrostatic force balance, is given for the formation of snow-ice. If more snow falls than what the ice can support, the ice will bend and crack, resulting in flooding of the snow cover. In sufficiently cold conditions, this water will freeze, creating snow-ice. This phenomenon is discussed further in §2.3.3.

Ablation and accretion of ice may occur at the ice-water interface only. The flux of heat at this point, q_f, depends on T_f, the freezing temperature, and the surface conditions. It is obtained from the solution of Equation 2.5:

$$q_f = -K_i \left.\frac{\partial T_i}{\partial z}\right|_{z=0}$$

$$= q_o - A_1 I_o \{ 1 - \exp-(\lambda_{s1} h_s + \lambda_{i1} h_i)\} - A_2 I_o \{ 1 - \exp-(\lambda_{s1} h_s + \lambda_{i1} h_i)\} \qquad (2.10)$$

Independently, the heat flux from the water to the ice, q_w, depends only on the conditions in the water column. Any imbalance between q_f and q_w results in the freezing or melting of ice:

$$q_f - q_w = \rho_i L_i \frac{dh_i}{dt} \tag{2.11}$$

The flux of heat from the water to the ice may be due only to conduction if the water can be considered stagnant. In this case:

$$q_w = -K_w \frac{dT_w}{dz}\bigg|_{z=0} \tag{2.12}$$

where, w = water

The solution properties associated with the given formulation are described in Patterson & Hamblin (1988).

The above equations have been incorporated into DYRESMI to account for the transfer of heat across the ice and snow covered lake surface. Further investigation was required in order to tailor the given formulation to the small mid-latitude lakes with which this project is concerned. Areas of particular concern include the transfer of heat stored in the lake sediments over the summer, the effect of rainfall on the ice and snow-cover, and the formation of snow-ice due to excessive snow-cover. In addition, the great variability of albedo observed at mid-latitudes (see Strickland, 1982), required the incorporation of an appropriate albedo model, rather than the use of a constant value, as assumed in version of DYRESMI reported in Patterson & Hamblin (1988). (Another version of DYRESMI now exists which employs the empirical time dependent albedo relationships derived by the U.S. Army Corps of Engineers (Hamblin, pers. comm., 1992). These relationships are given in §2.3.2.)

2.2 HEAT TRANSFER FROM BOTTOM SEDIMENTS

2.2.1 Review of Observed Rates of Heat Transfer

Heat transfer from the lake bottom to the overlying water has been identified as being important in the circulation of small lakes over the winter period (see Birge et al., 1927; Mortimer & Mackereth, 1958; others). Considerable amounts of heat are stored below lakes during the warm season (Ashton, 1986). Thandertz (Ashton, 1986) computed heat fluxes at Lake Velen (59°N, mean depth, $\bar{z}$ = 6.5 m) in Sweden from measurements of lake water warming during periods of ice cover. Average heat fluxes of 1.0, 1.9 and 1.8 W/m^2 were computed over 3 consecutive years of observations. Maximum heat fluxes in the order of 4 W/m^2 were calculated for the month of January based on measured sediment properties and thermal profiles. This maximum flux decreased in a linear fashion throughout the winter period. The classic work of Birge et al. (1927) regarding the sediment heat budget of Lake Mendota in Wisconsin, U.S.A. (43°N, $\bar{z}$ = 12.4 m) produced results consistent with the Lake Velen findings. Sediment properties and thermal profiles were also measured at Mendota, and the investigation revealed a considerable range in heat transfer rates. The average winter period (December 15th to April 1st) heat transfer rate of 2.9 W/m^2, is considerably higher than the average rates calculated for Lake Velen due to higher summer temperatures. Mortimer & Mackereth, (1958) however, used the thermal profiles given in Birge et al. (1927) to estimate an average value of 1.6 W/m^2 for the actual ice covered period which began on January 1st. Welch and Bergmann (1985), for Methane (z_{max} = 14 m) and No-Fish (z_{max} = 13 m) Lakes (Canadian NWT, 63°N) estimated a heat flux of 1.5 W/m^2 based on average temperatures at and 2 cm below the sediment surface, assuming a thermal molecular diffusivity of 1.2 x 10^{-3} cm^2/s. The range in fluxes found in the literature is consistent

with the theoretical model by O'Neill and Ashton (1981) which computes heat transfer rates based on monthly average air temperatures.

Estimated rates of heat transfer in the Western Basin of Lake Torneträsk in Swedish Lapland (68°N, z_{max} = 169 m) were much lower, in the range of 0.2 to 0.4 W/m^2 (Mortimer & Mackereth, 1958). The lower rate is expected given the great depth of the lake, and the relatively cool summer temperatures (the maximum summer temperature at a depth of 1 m was 11.8 °C on average between 1921 and 1929, compared with about 26°C at Lake Mendota).

2.2.2 Methods of Estimating Sediment Heat Transfer

Quantitative sediment properties and thermal profiles are not available for the lakes investigated in this study. In order to estimate sediment heat transfer, use of published data and empirical equations are required.

In general, the shallower the lake, the more heat is stored in the sediments over the warming season. Morphometry, altitude and latitude are also factors which influence heat storage. As a rough estimate, however, Falkenmark developed an empirical relationship which predicts the ratio of sediment to lake heat budget based on the mean depth only (see Ashton's [1986] Figure 4.8). This relationship could be used to estimate sediment heat transfer rates.

A second method of estimating sediment heat transfer rates is available. Thermal profiles characteristic of lake sediments change markedly over the year in response to changing lake temperature and as a function of lake depth. Temperatures below about 2 m under the sediment-water interface remain, however, more or less constant over time (see, for example, Ashton, 1986). The temperature at 2 m is often close to the average annual temperature of the lake water above. As an approximation of the thermal gradient at the

sediment-water interface, it is reasonable to employ the following formula (Hamblin, pers. comm., 1992):

$$\frac{dT}{dz} \approx \frac{T_y - T_w}{z_{sed}} \tag{2.13}$$

where, T_y = the average annual whole lake temperature

Tw = the current water temperature

z_{sed} = distance over which sediment temperature (linearly) increases from T_y to T_w

= 2 m

The above formulation implies the use of the conduction equation to estimate sediment heat transfer. This necessitates an estimation of sediment conductivity based on data available in the literature. In most studies reported in the literature, only observations of thermal diffusivity have been made. In each of these cases, to determine conductivity, it is necessary to estimate the density and heat capacity of the sediments.

2.2.3 Sediment properties

Birge et al. (1927) made sediment temperature profile measurements which were consistent with the assumptions that heat was transported by molecular diffusion, and that the thermal diffusivity, κ, of the sediments equaled that of still water. Investigations by McGaw (O'Neill & Ashton, 1981) and Likens & Johnson (1969) are in agreement with these observations. Hutchinson (1957), however, reported values of 32.5 x 10^{-8} m^2/s for Lake Mendota, or almost 2.5 times that of pure water (κ_w = 13.6 x 10^{-8} m^2/s at 5°C). He also cited Neumann (1953), who determined a value of 40 x 10^{-8} m^2/s for sediments with some sand content.

Urban & Diment (1988) have reported conductivities in the range of 1 to 3 times that of water at Clear Lake California, the higher values being associated with the coarser-grained sediments. Likens & Johnson (1969) found that the gelatinous ooze consisting of

partly decomposed organic matter in the sediments at two Wisconsin lakes had the same conductivity as water. These latter two results suggest that the density and heat capacity of many water saturated sediments are comparable to water.

2.3 EFFECTS OF SNOW COVER

2.3.1 Snow Properties

The physical and optical properties of snow (density, conductivity, albedo, attenuation) are extremely variable especially at mid-latitudes. Because of the great importance of these properties on the heat transfer to the water, average values used as universal parameters (as is the case in the DYRESMI model) are not generally appropriate for the lakes in question. Here attention will be given primarily to density and albedo. A simple relationship is available which relates conductivity to density, and attenuation will be assumed constant owing to a lack of information.

Density

The density of snow varies widely depending on the following processes:

a) Heat transfer (convection, condensation, radiation, conduction)
b) The weight of overlying snow
c) Wind drifting and compaction
d) The temperature and variation of water content within the snow pack
e) The percolation of melt water

Snow density may vary from as little as 10 kg/m^3 for dry falling snow, to as high as 380 kg/m^3 for wind-toughened, well compacted snow. The presence of liquid water may increase the density of melting snow to as high as 500 kg/m^3 before it drains away (McKay, 1968). Patterson & Hamblin (1988) used a constant snow density of 330 kg/m^3

for DYRESMI. The density of the snow varies directly with depth, but layering leaves significant variations. Initially there is rapid settling following a snowfall. The highest rates of densification occur within the first few hours after deposition. Snow which has accumulated at an average of 46 kg/m^3 has been observed to increase to 176 kg/m^3 after 24 hours of drifting. (McKay, 1968). Changes in form and displacement of particles are responsible for the settlement (USACE, 1956). Much attention has been given to the density of newly fallen snow, because of its high variability. A simple air temperature dependent relationship has been derived from observations in the Rocky Mountains in Colorado (Grant & Rhea, 1973):

$$\rho_s = (0.0785 + 0.00219\, T_{air} + 0.00023\, T_{air}^2)\, \rho_w \tag{2.14}$$

In the range of 0 to -15°C, this equation, on average, predicts a density of about 80 kg/m^3.

Conductivity

The conductivity of snow increases substantially with density (Ashton, 1986):

$$K_s = 0.021 + 4.2 \times 10^{-3}\, \rho_s + 2.2 \times 10^{-9}\, \rho_s^3 \tag{2.15}$$

Furthermore, conduction of heat from the underlying ice to the air will also increase as densification proceeds because of the associated reduction in thickness of the snow layer.

Attenuation

Few data are available which quantify the attenuation of radiation through snow at mid-latitudes. Patterson & Hamblin (1988) use coefficients of 6 and 20 m^{-1} for visible and infrared radiation respectively. For the shortest wavelengths, however, Grenfell & Maykett (1977), found coefficients of about 18 m^{-1} for compact dry snow in the Arctic Basin.

2.3.2 Estimation of Snow Albedo

In DYRESMI, the snow albedo is set to 0.85 when the air temperature is below zero, and 0.6 when it is above zero. As described earlier, however, rapid and extreme weather variations should result in a wide range of snow albedos at mid-latitudes. A variable albedo should therefore be incorporated into the heat transfer model. Typical ranges and factors which determine albedo will now be described.

Albedo is commonly taken to decrease exponentially from about 0.8 for fresh snow, to about 0.4 for melting, late season snow (Gray, 1970). Grenfell, Perovish & Ogren (1981) report a significantly higher range, with values decreasing form 0.93 to 0.63. More recently, Henderson-Sellers (1984) tabulated a wide range of range of albedos for various lake surface conditions (Table 2.1).

A simple empirical relationship developed by the U.S. Army Corps of Engineers (see Petzold, 1977) accounts for the reduction in albedo due to compaction, fine flake destruction, accumulation of dust and debris, and, for melting conditions, the metamorphosis from powder to granular snow. Two equations, called the USACE decay functions, were derived; one for an accumulating snowpack, and the second for a melting snowpack. Both express the change in albedo only in terms of the number of days, d, since the last snowfall:

$$\Delta\alpha = \frac{-10^{(0.78-0.69d)}}{100} \qquad \text{(accumulating)}$$

$$\Delta\alpha = \frac{-10^{(1.05-0.07d)}}{100} \qquad \text{(melting)} \qquad (2.16)$$

With the exception of accumulation of impurities, the processes listed above all tend to

Table 2.1 Albedo Under Various Surface Conditions (Henderson-Sellers, 1984)

Surface Condition	Albedo
1. Freshly formed, snow-free black ice	0.02
2. Snow-free snow-ice	0.4-0.5
3. Freshly fallen snow	0.8-0.95
4. Old snow of moist wet snow	0.7-0.8
5. Wet snow	0.6-0.7
6. Slushy, gray melted snow layer	0.2-0.6
7. Completely wet top surface (ponding)	0.05
8. Water	0.06

increase the snow grain size. The following is a calibrated equation for albedo, α, in terms of grain size (Bohren & Beschta, 1979):

$$\alpha = 1 - 5.96 \cdot \sqrt{j_i \cdot d_g} \tag{2.17}$$

where, j_i = the wavelength dependent absorption coefficient for pure homogeneous ice

d_g = the average snow grain diameter

Robinson & Kukla (1984) monitored the albedo of a melting snowpack for over one month following an early February snow storm in the north-eastern U.S. For open farmland they found that the albedo dropped at an increasing rate from a maximum of 0.8. The opposite trend, observed for both urban and shrubland areas in the same study, is implicit in the USACE decay functions. Gray & Male (1981) explain that, for shallow snow cover, the albedo drops at an increasing rate due to the increasing influence of the relatively low albedo of the underlying ground or ice. The USACE functions were

derived from deep mountain snowpack data, and are not influenced by the optical properties of other materials below the snow. According to Choudhury (1982), the snowpack can be treated as semi-infinite when it is greater than only 10 cm in depth. This limiting depth, however, increases with snow grain size, and may be up to 50 cm for old melting snow (Wiscomb & Warren, 1980). This latter observation appears to be consistent with the results of Robinson & Kukla (1984).

Petzold (1977) found that USACE functions consistently under-predicted the actual albedo for the 1969 summer field season on Meighen Ice Cap, N.W.T. He derived the following quadratic correction function:

$$\Delta\alpha = \frac{3.86 + 0.380 \cdot d + 0.123 \cdot d^2}{100} \tag{2.18}$$

The above correction indicates that, as implied by Robinson & Kukla (1984), and Gray & Male (1981), a simple decay function may not be appropriate, at least for the data set to which the correction was applied.

In order to reduce the scatter produced when the USACE functions were applied to the data set used by Petzold (1977), further corrective functions were developed in order to account for cloud conditions and solar angle. It is commonly reported that albedo increases with increasing cloud cover, opacity and with decreasing cloud height. Albedo decreases, however, as the solar angle increases up to about 40 degrees, beyond which, it remains fairly constant. Strickland (1982) found that 14% of albedo variability in sunny non-melting conditions could be explained by solar angle. Diurnal or seasonal trends caused by changing solar angle, may, however, be obscured by variable cloud cover and aging snow (Bergen et al, 1983). The effect of solar elevation may be accounted for using Petzold's (1979) Figure 2a, to which the following expression has been fitted:

$$\Delta\alpha = \frac{-1.9 + 24.8 \cdot e^{-\beta/15.5}}{100} \tag{2.19}$$

where, β = solar noon angle

Petzold (1979) also performed a regression analysis, using data from four polar stations, to derive a simple relationship expressing the change from clear sky albedo to a value under a given cloud cover:

$$\Delta\alpha = \frac{0.449 + 0.0097 \cdot (10 \cdot C)^3}{100} \tag{2.20}$$

where, C = fraction of sky obscured by cloud

In general, he found that the greatest errors in the complete albedo model occurred on days with fresh snow. He suggested that rain mixed with the falling snow may have, on some occasions, resulted in lower than predicted albedos.

When applying the USACE functions it is generally assumed that the maximum possible albedo is 0.84. Petzold (1977) however, suggests that a new snowfall albedo between 0.84 and 0.89 is reasonable, and furthermore, this value is likely to vary between 0.90 and 0.95 at low sun angles. Strickland (1982) has observed natural snow albedos up to 0.95 at solar noon near Peterborough, Ontario over the 1980-81 snow season. Bergen et al. (1983) have also documented late winter albedos in excess of 0.96 on a level clearing in the White Mountains of Arizona, at an elevation of 3000 m. Over a one week period, the daily average albedo never dropped below 0.92. Snow purity also has a profound influence on albedo. Fresh, pure snow may reflect more than 95% of incident radiation (see Wiscomb & Warren, 1980).

Strickland (1982) observed a dramatic drop in albedo following mid-winter rainfall. The effect of rainfall is not considered in either the USACE functions or Petzold's (1977) computer model. Strickland (1982) found the accuracy of USACE functions to be a disappointing 48% for her data set. She implies that they may not be appropriate for

latitudes in the range of 40 to 50 degrees north, due to rapid and extreme weather variations. Better agreement with actual albedo may be expected at the lakes considered in the present study, however, given that the USACE equations were developed using data from high elevation snowpacks.

2.3.3 Snow-ice Formation

If the weight of the added snow is too great, the underlying ice will crack and flooding will occur. This results in the formation of snow-ice when the flood water freezes. A simple force balance, based on buoyancy theory, is used to determine the maximum thickness of snow that the ice will support (Patterson & Hamblin, 1988):

$$h_{sm} = \frac{h_i.(\rho_w - \rho_i)}{\rho_s} \tag{2.21}$$

In the DYRESMI formulation, the excess snowfall is reduced in thickness, according to the ratio of snow to ice density, and added to the ice layer.

The water which seeps through cracks in the ice caused by the weight of the overlying snow and into the snowpack constitutes a significant source of heat in the snow layer. Sensible heat is given up to the snow as the flood water temperature is cooled to the freezing mark. Under most weather conditions following snowfall, the water will then freeze, and snow-ice is formed. This latter process releases latent heat to the surrounding ice and snow.

2.3.4 Snowmelt Due to Rain Events

Snowmelt due to rain may be an important factor in the depletion of a snowpack. This possibility was ignored in the DYRESMI formulation because it is a rare event at high latitude lakes (Patterson & Hamblin, 1988). When rain falls on snow, the sensible heat associated with the rain water is given up to the snow. If the heat transferred is more than

sufficient to raise the snow temperature to 0°C, then the excess heat results in snowmelt. The heat released to the snow is given as follows:

$$Q_{rs} = C_{pw}\, \rho_w\, (T_{air} - T_m) \cdot P \tag{2.22}$$

where, Q_{rs} = sensible heat released to snow
P = total rainfall
C_{pw} = heat capacity of water

It is often assumed that when rain does occur, the snowpack is isothermal at 0°C and all of the heat associated with the rain is used to melt snow (USACE, 1956; Harr, 1981). Harr (1981) uses this assumption in illustrating that rain is only a significant contributor to snowmelt in forested watersheds when total daily rainfall is in the order of several centimetres. If a sub-freezing snow pack were assumed, melt due to rain would be shown to be even less significant. However, in this latter case, the rain water would freeze inside the snowpack, thereby releasing latent heat.

The relative importance of latent heat is illustrated by the following example: 46 mm of rain at 0°C will increase a 1.8 m snowpack (ρ_s = 400 kg/m^3) from a mean temperature of -10°C to 0°C. If, however, the same quantity of rain were at 8°C and fell on a snowpack at 0°C, less than 0.5 cm of meltwater would be produced. Although some snow is melted directly by the rain, the associated high humidity and air temperature results in heat transfer to the snow dominated by condensation of water vapour. When precipitation is less than 13 cm/day (less than 2 cm of rain falls on average between December and March in the B.C. Southern Interior Plateau), condensation is 4 times more important than the sensible heat released from rainfall (Harr, 1981). Condensation will occur in warm, humid conditions when the vapour pressure of the air above the snow exceeds the saturation vapour pressure at the temperature of the snow surface. Condensation is

handled by the bulk aerodynamic equations adopted for use in the DYRESMI heat budget (see Chapter 4).

2.4 EFFECT OF ARTIFICIAL CIRCULATION

2.4.1 Review of Systems Used Worldwide

Artificial circulation has long been used to prevent or remove ice cover in ports and marinas to facilitate their use year-round. These systems, in general, differ from that used at Menzies Lake in three ways:

a) the circulated water may be saline
b) the water is only a fraction of a degree above freezing
c) the system is open: there is effectively an infinite body of water on which to draw.

Very little quantitative information, however, is available regarding their behaviour or impact.

Eranti et al. (1983) describe the use of flow developers in Finnish ports where the average harbour temperature is 0.1°C above freezing. It was found that the thermal reserve was sufficient for the prevention of freezing when surface currents are greater than 0.6 m/s. This is consistent with the findings of investigations of ice cover on rivers (Stigebrandt, 1978). The polynyas generated, however, varied significantly in size depending on the local water temperature and ice conditions. Furthermore, the survey suggested that the presence of a warm water discharge may be more important in increasing the polynya size than the flow developer engine power. This latter point is illustrated in Table 2.2.

Table 2.2 Polynya Areas in Finnish Harbours (Eranti et al., 1983)

Engine Power (kW)	Ice-Free Area (m^2)
11	170
11	200
15	50
30	300
30	1000
30	3000 ‡

‡ warm water discharge (Q=0.13 m^3/s, T= 7°C)

Predictive models

The only known model which predicts the size of an artificially-generated polynya is that developed by Ashton (1979). The model predicts the flow induced by a point source bubbler system and the associated heat transfer to the ice cover. An earlier model (Ashton, 1974) deals with the problem of a line source bubbler. In the new model, air is discharged from a point at some depth below the water surface. Water is entrained as the plume rises to the ice-water interface at which point it is redirected and spreads radially. The temperature of the plume is of primary importance and is calculated by integrating the product of temperature and the rate of increase of flow over the vertical distance, z, through which the plume rises:

$$T_{wH} - T_m = \frac{1}{Q_{wH}} \int_0^H (T_w(z) - T_m) \frac{dQ_w(z)}{dz} dz \tag{2.23}$$

where, T_{wH} = temperature of the plume at height H above the bubbler
Q_{wH} = flow at height H
T_m = melting temperature

A coefficient is developed for the turbulent transfer of heat from the water to the ice using the results of Gardon & Akfirat (1966), who investigated the heat transfer associated with an axisymmetric air jet impinging on a flat plate. This coefficient, h, is given as a function of radial distance, r, from the point of impingement:

$$h_r = \frac{2.08\ K_w\ U_{cH}^{0.55}\ r^{-0.45}}{\nu^{0.55}} \tag{2.24}$$

where, U_{cH} = The centerline water velocity at the point of impingement
ν = kinematic viscosity

The variation with r is an empirical result from the work of Gardon & Akfirat (1966), and is not based on boundary layer heat transfer.

The actual melting of the ice cover is handled by employing a much cruder model than that of Patterson & Hamblin (1988). Ashton's (1979) model was applied to a mid-western location in the U.S. for a water temperature of 0.2°C. It is unclear whether this temperature is the mean ambient temperature, the mean plume temperature, or an initial condition. It is also unclear if buoyancy was of significance in the application. The model predicted a polynya which responded dramatically to changing air temperature. The polynya radius varied from 0 to 4 metres over a 24 day simulation.

Heat loss from a natural polynya in polar pack ice has been given a considerable amount of attention, but few studies have attempted to quantify rates of lateral ice growth in the open water. Den Hartog et al. (1983) have predicted heat loss from an Arctic polynya in the Canadian Archipelago. Good agreement was achieved when comparing net heat loss calculated using bulk aerodynamic formulae to heat flux tray measurements. No attempt, however, was made at predicting polynya size. Bauer & Martin (1983), however, have examined the growth of grease ice across polynyas in some detail. Grease ice, which consists of about 30% ice and 70% seawater by mass, grows in the upwind direction

under high wind conditions, from the downwind end of the lead. Ice forms as frazil discs which are advected downwind to pile up against the lead edge to depths of 0.05 to 0.3 m. The ice growth model developed by Bauer & Martin (1983) predict high rates of growth because the exposed water is at or very close to its freezing point. The ice pile up depth is given as functions of wind speed parameters and fetch. For a constant wind speed of 10 m/s and an initial fetch of 50 m, the average predicted grease ice thickness is 0.07 m. The predicted thickness increases with both wind speed and fetch.

Lake Aeration

Artificial circulation of lakes and ponds in winter can be an effective method of maintaining dissolved oxygen concentrations which are required to support fish life in winterkill lakes. This fact has been well established (see Ashley, 1987; Bandow, 1986; Lackey & Holmes, 1972), but little information regarding thermal impact, ice thickness, and polynya behaviour is available. It has frequently been observed, however, that average lake temperatures are lower than would be expected under natural conditions (Lackey & Holmes, 1972).

2.4.2 Heat Transfer Between Water and Air

The heat flux at the air-water interface of the polynya is determined in the same manner as that at the snow-air interface, with T_0 replaced by T_w, the water temperature, and the surface albedo changed to a value appropriate for the open water. Once this flux is known the net effect of the polynya on the lake heat budget can be calculated. In addition to short wave radiation, sensible and latent heat, and the balance of long wave radiation, the contribution of free convection, and cooling due to snowfall are required in the balance. A further consideration is the turbulence induced by the circulator at the air-water interface. Sensible heat transfer measurements made in the ocean, however, have shown that sensible heat transfer is a function of wind speed, but is independent of sea state

(Kraus, 1972). Given this finding, it is assumed that the turbulence generated by circulator is only important insofar as it increases the heat transfer to the ice cover (see §2.5.3).

Free convection due to unstable humidity profiles, is considered important in cooling ponds, Arctic leads and polynyas, where the air temperature is on average much less than the surface water temperature, and wind speeds are low (Ryan et al., 1974; Den Hartog, 1983). Its contribution to the evaporative heat loss is given as follows (Ryan et al., 1974):

$$Q_{fc} = \lambda \cdot (svp0 - svpd) \cdot \sqrt[3]{T_{wv} - T_{av}} \tag{2.25}$$

where, svp0 = saturation vapour pressure at the water temperature, Tw (mbars)
svpd = vapour pressure of the air (mbars)
T_{wv} = virtual surface water temperature (^oC)
T_{av} = virtual air temperature (^oC)
λ = 2.7 $Wm^{-2}mbar^{-1}(^oC)^{-1/3}$

Since water vapour is lighter than air, evaporation increases the driving buoyancy force driven by the temperature difference T_w - T_{air}. This effect is accounted for by employing the virtual temperature difference, T_{wv} - T_{av}. The virtual temperatures are calculated as follows:

$$T_v = \frac{T+273}{1 - \left(\frac{0.378svp}{P_{atm}}\right)} - 273 \tag{2.26}$$

where, P_{atm} = atmospheric pressure (mbars)

Reservoir operators have often observed a reduction in water temperature following snowfall over open water (Ashton, 1986). The following equation may be employed:

$$Q_{sp} = L\, \rho_w\, I_s - C_{pi}\, \rho_w\, (T_{air} - T_m)\, I_s \tag{2.27}$$

where, Q_{sp} = heat removed from the water (W/m^2)
I_s = snowfall (mm/hr, rain equivalent)

The first term accounts for the latent heat of fusion, and the second for the heat used in warming the snow to the melting temperature.

The net heat flux, H_p, at the air-water interface is calculated as follows:

$$H_p = I_{wp} + R_{li} - R_{lop} - Q_{cp} - Q_{ep} - Q_{ef} - Q_{sp} \tag{2.28}$$

where the subscript p refers to the polynya.

2.4.3 Heat Transfer Between Water and Ice

In present sea ice models, the transfer of heat between water and ice is often ignored or set to a constant value, even in the vicinity of polynyas where horizontal variations can be significant (Hamblin & Carmack, 1990). Gilpin et al. (1980) parameterized the turbulent vertical heat transfer using Newton's law of cooling:

$$q = h\,(T_b - T_\infty) \tag{2.29}$$

where, q = local heat transfer per unit area
h = convection heat transfer coefficient
T_b = boundary temperature
T_∞ = temperature of the free stream

A more useful form of this law is the bulk aerodynamic formulation, in which heat transfer is given as a function of a dimensionless coefficient, C_t, and the flow velocity, U, at some distance away from the boundary (Hamblin & Carmack, 1990):

$$q_t = C_t\,\rho\,c_p\,U\,(T_w - T_m) \tag{2.30}$$

where all other terms are as previously defined.

From Figure 13 in Gilpin et al. (1980) it can be found that, under experimental conditions, C_t varies from 0.6×10^{-3} to 1.0×10^{-3} depending on the ice roughness. As Hamblin & Carmack (1990) point out, however, the scales of turbulent motion associated with laboratory flow fields are generally not representative of lakes or oceans. Furthermore, the use of cross-sectionally averaged velocities in Equation 2.30, is not applicable to these water bodies.

To determine the appropriate depth where velocity measurements should be taken, Hamblin & Carmack (1990) make reference to the standard height above ground used in meteorological applications and scale the analogous distance below the ice-water interface by:

$$\left(\frac{\rho_{air}}{\rho_w}\right)^{0.5} \tag{2.31}$$

where, ρ_{air} = air density
ρ_w = water density

This factor is based on the following requirements:

a) stress continuity across the boundary
b) proportionality of boundary layer thickness to friction velocity.

Given a standard above-ground height of 10 m, the appropriate below-ice depth is about 1.0 m. Using under ice-current and temperature measurements in three large northern lakes with significant flow-through, Hamblin & Carmack (1990) found C_t to be in the range of 0.5×10^{-3} to 1.1×10^{-3}.

Boundary Layer Development

The details of boundary layer development may, in some applications, be of importance to the net turbulent heat flux between the water and the ice. Hirata et al. (1979) examined these details in their laboratory investigation of the steady state profile of an ice layer in a forced convection flow of water. It was found that the Nusselt Numbers throughout the turbulent regime were in the order of 35% larger than those given by the von Kármán correlation for turbulent flow over a flat plate. The von Kármán relationship is given as follows:

$$Nu_x = 0.0296\, Pr^{1/3}\, Re_x^{4/5} \tag{2.32}$$

where, Nu_x = Nusselt Number $= \frac{h_x\, x}{K_w}$

Pr = Prandtl Number $= \frac{C_{pw}\, \mu}{K_w}$

Re_x = Reynold Number $= \frac{U_\infty\, x}{\nu}$

x = distance from leading edge of plate

h_x = convective heat transfer coefficient at location x

U_∞ = free stream velocity

Therefore, from the results of Hirata et al (1979), the equivalent expression for an ice layer would be:

$$Nu_x = 0.039\, Pr^{1/3}\, Re_x^{4/5} \tag{2.33}$$

In terms of the convective heat transfer coefficient, h_x, the above formulation is expressed as:

$$h_x = 0.039\, \frac{K_w\, Pr^{1/3}}{x}\, Re_x^{4/5} \tag{2.34}$$

Assuming that U_∞ is equivalent to U in Equation 2.30, then C_t may be estimated using the above result:

$$C_t = \frac{0.039\ K\ Pr^{1/3}\ Re_x^{4/5}}{\rho\ C_{pw}\ U\ x} \tag{2.35}$$

This formulation implies that C_t is not constant unless $U = f(x^{-1})$. For laminar flow over an ice sheet, Hirata et al (1979) found that the ice thickness varies as $\sqrt{x}$. They did not provide a formulation for the ice thickness in turbulent flow, but from their Figure 3, it is clear that the ice thickness increases much more slowly than it would in laminar flow. This is consistent with the field observations made by Stigebrandt (1978). This latter investigator found that, downstream of a river inflow into an ice-covered Norwegian lake, the ice thickness increases gradually towards the lake proper.

Gilpin et al. (1980) explain that the heat transfer rates for forced convection over an ice layer are greater that those predicted by flat plate boundary layer theory because of irregularities that will develop in the ice layer profile as a result of variability in the heat transfer coefficient. Since heat transfer coefficients increase with surface roughness (Holman, 1990), it is clear that greater heat transfer rates would be expected across an irregular ice surface, than across a smooth plate.

2.4.4 Flow Field

The flow field generated by the Air-o-lator ® is complicated by the following conditions:

a) in lakes of sufficient depth, density stratification requires that the internal hydraulics be considered
b) fountain-like pumping of water into air
c) irregular lake morphometry
d) impingement of radial jet, in some directions, on the float used to support the circulation device.

As described in Chapter 1, the first condition may be ignored owing to the small depth of the lakes considered. Given that the flow field model will be based on near-surface velocity measurements, the mechanics of the second problem may be ignored. It is assumed that the near-surface velocities are proportional to the pumping rate Q, and therefore, an empirical formula based on measured velocities will apply for Air-o-lators® of various sizes. It is also assumed that the circulator operates in a semi-infinite body of fluid, and that the radial jet velocity is not dependent on the direction of flow.

The flow field generated by the circulator is modeled as two independent components. First, the radial flow to the intake at some distance below the water surface is assumed to be governed by potential flow theory. Applying the semi-infinite body assumption and the method of images, it can be shown that the intake velocities are small near the surface where the outflowing jet velocities are important. The circulator is considered to be important to the heat budget only in terms of the size of polynya generated and the transfer of sensible heat to the ice-sheet. This means that only the near surface velocities need be considered in the model, and the intake flow field can therefore be ignored.

This leaves the problem of modeling the outflowing radial jet produced by the circulator. The resulting flow field is assumed to be consistent with submerged, non-constrained, radial jet theory as described by Rajaratnam (1976) and Witze & Dwyer (1976). The velocity generated along the jet centerline varies as r^{-1}. This result is derived from the governing equations of motion. The standard semi-empirical relationships which give the centerline velocity as a function of the initial flow rate, are also dependent on the outlet geometry. Tolmeinn & Goërtler have also derived solutions that require empirical coefficients for the non-centerline flow (Rajaratnam, 1976).

2.5 PREVIOUS WORK AND THE MLI MODEL

The work of Patterson & Hamblin (1988) constitutes a major step forward in the area of ice-covered lake modeling. Their model will be utilized in this study and extended to address the issues which have been introduced in this chapter:

a) rainfall,
b) heating of the snowpack due to flooding of the ice-cover,
c) sediment heat transfer,
d) variable albedo,
e) variable snow density.

In addition to these factors which may be important with regard to the heat budget of the ice-covered lake in the natural state, the DYRESMI model will be extended to include the impact of the Air-o-lator®. The heat transfer associated with snowfall on open water and free convection (see §2.4.2) will be added to the list of bulk aerodynamic equations commonly used in lake modeling. A more difficult problem is that of predicting the polynya size and the turbulent heat transfer from the water to the ice. The predictive model developed by Ashton (1979) is particular to bubbler aeration systems and is based on empirical results involving an air jet impinging on a flat plate and not on boundary layer heat transfer considerations. Furthermore the ice melting formulation developed by Ashton (1979) is much cruder than that of Patterson & Hamblin (1988).

Given the lack of a satisfactory model for the prediction of polynya size, development of a new model is required. Ice melt in the vicinity of the circulator is a function of turbulent heat transfer from water to ice as described by Equation 2.30:

$$q_t = C_t \rho C_p U (T_w - T_m) \tag{2.30}$$

The velocity field associated with the radial jet produced by the circulator will be assumed to provide a reasonable measure of the dependency of turbulent heat transfer on radial distance from the circulator. The heat transfer coefficient C_t is expected to require calibration given the unique nature of the problem but should be of the same order as the range found by Hamblin & Carmack (1990) for river flow through ice-covered lakes.

The details of the modifications to DYRESMI are dealt with in Chapter 4. Verification of the new model and calibration of parameters requires a thorough field investigation of ice-covered lakes in a natural state and artificially circulated. This investigation is described in detail in the following chapter.

Chapter 3
FIELD INVESTIGATION

3.1 CHARACTERISTICS OF STUDY LAKES

The two lakes which were selected for this study are both located in British Columbia's Southern Interior Plateau, about 300 km north-east of Vancouver, and 15 km south-east of Merritt (Figure 3.1). Both are small, naturally eutrophic lakes which experience significant rates of oxygen depletion below the thermocline in summer and under ice-cover in winter. Harmon Lake is the centrepiece of a small provincial park and is very popular among recreational anglers. Menzies Lake, 5 km to the north of Harmon, has been set aside by the B.C. Ministry of the Environment for Fisheries Research purposes. Harmon, which is left in its natural state over winter, was selected as a control lake, for comparisons with Menzies Lake, which is artificially circulated.

3.1.1 Morphometry

As reliable morphometric information was only available for Harmon Lake, a survey of Menzies Lake was conducted in August 1991. This was accomplished by taking echo-soundings along 13 transects from a boat moving at constant velocity. Bathymetric maps for both lakes are shown in Figure 3.2. A summary of morphometric information derived from these maps is given in Table 3.1. Hypsographs for both lakes are given in Figure 3.2b. The wind sheltering coefficients were determined following USACE (1986). A transit was used to determine the average tree height at the end of each lake from which the dominant winds blow. For abrupt changes in relief at the water's edge, it will take a distance of roughly 8 times the height of the relief before the wind field and resultant

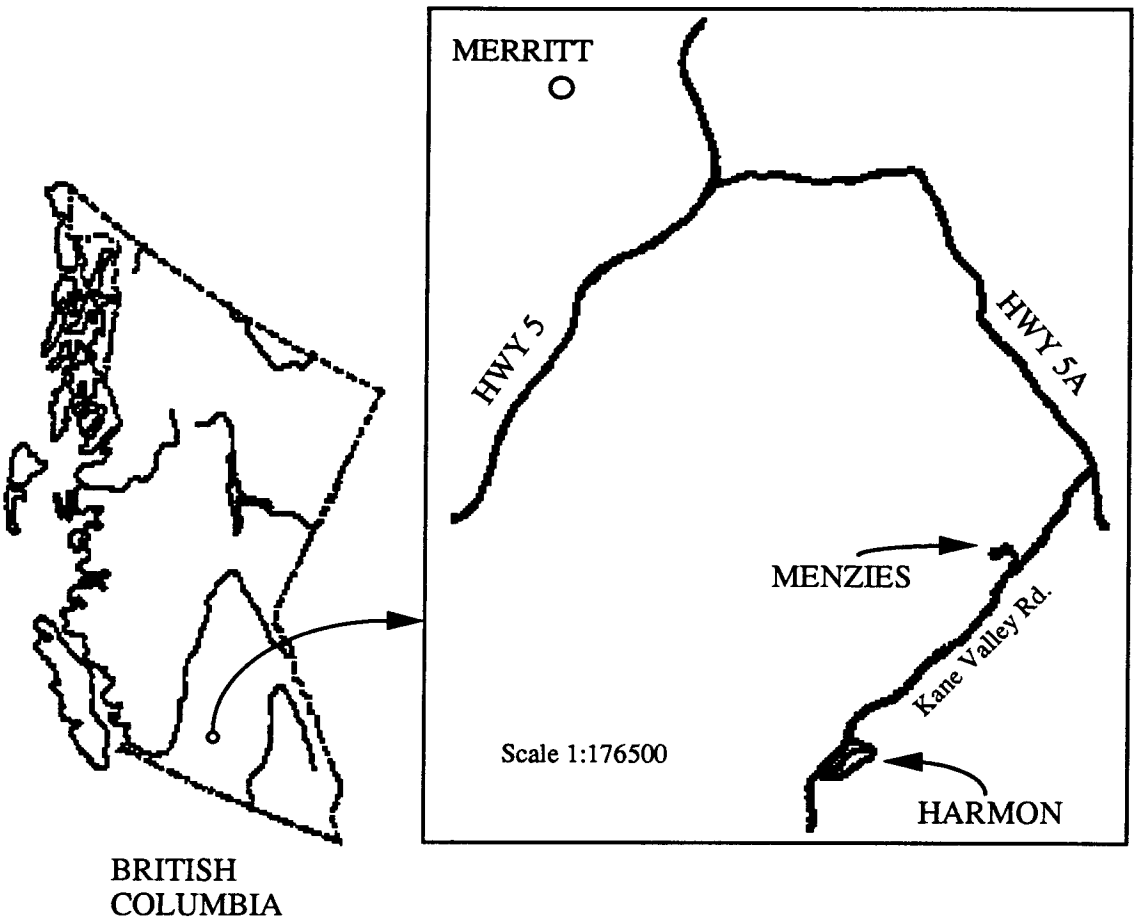

Figure 3.1 Field Study Location

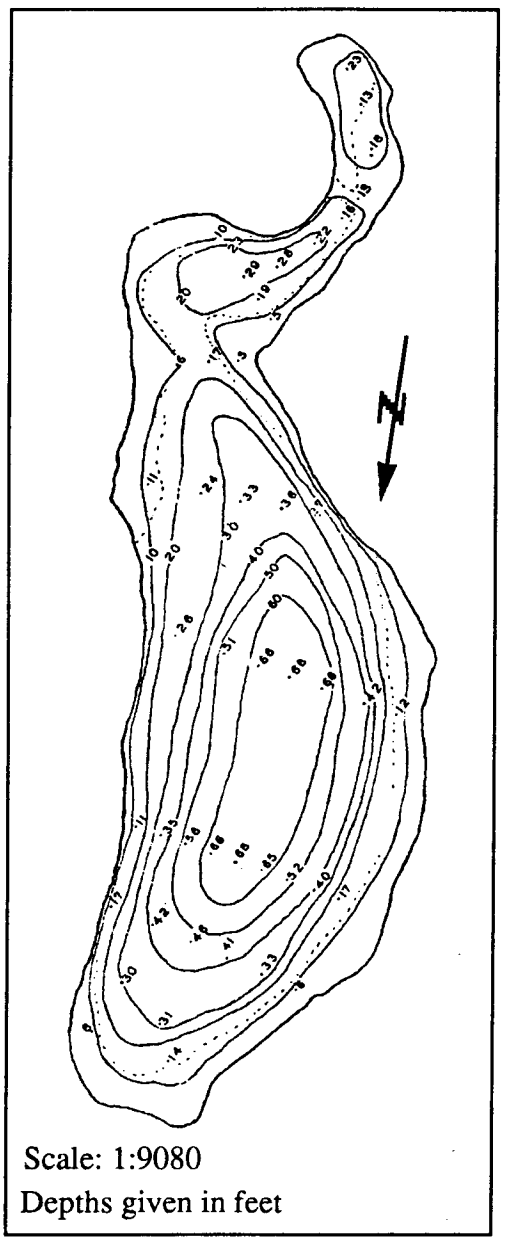

Harmon Lake

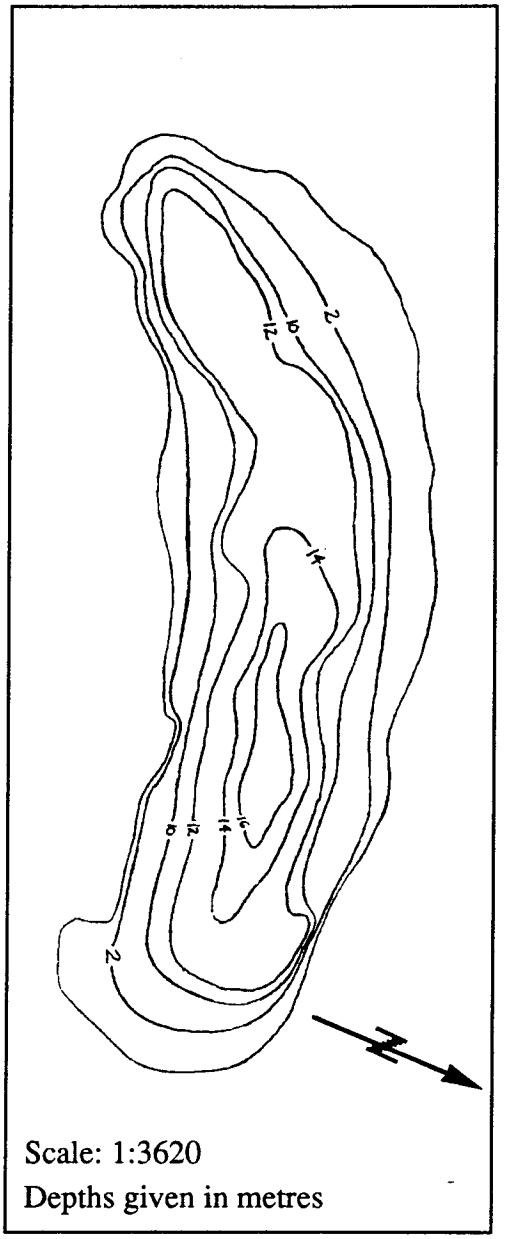

Menzies Lake

Figure 3.2 Bathymetry of Menzies and Harmon Lakes

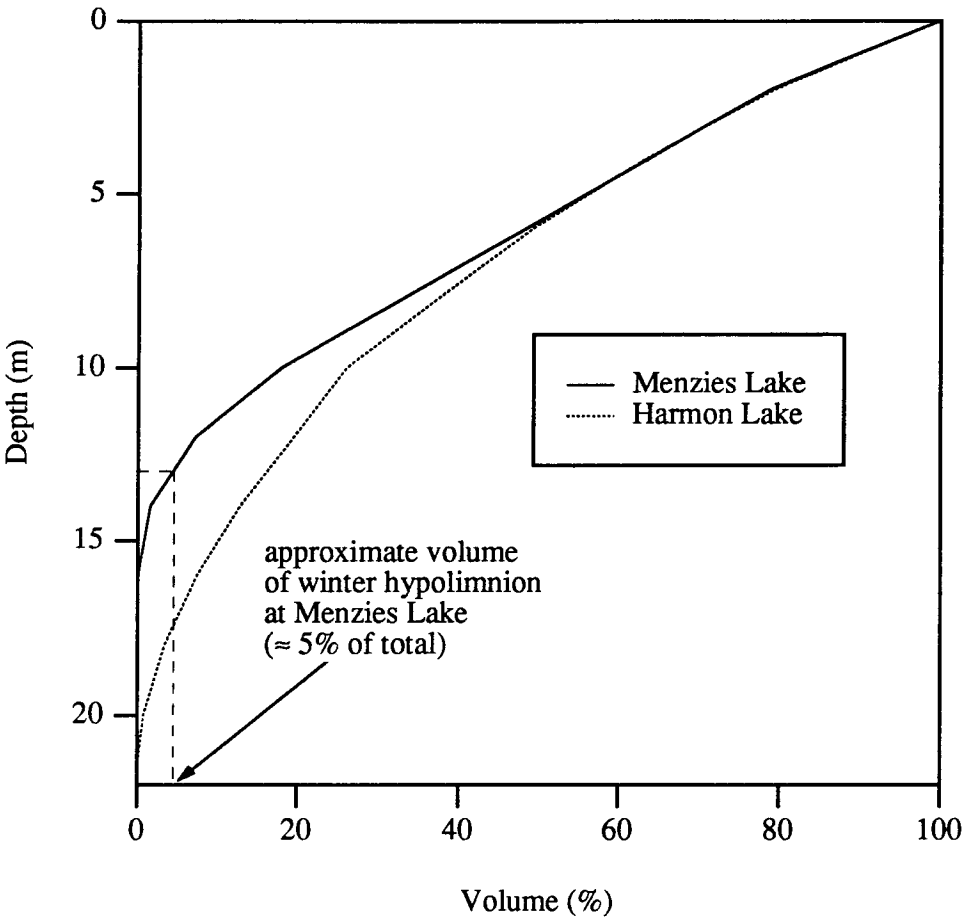

Figure 3.2b Menzies and Harmon Lakes Hypsographs

stress reattach to the lake surface (USACE, 1986). The coefficient was calculated as follows:

$$S_w = 1 - \frac{8\,\bar{H}}{L_f} \tag{3.1}$$

where, S_w = wind sheltering coefficient
$\bar{H}$ = average tree height at the water's edge
L_f = effective length of lake or fetch in dominant wind direction

The surrounding topography (along the dominant wind axes) is sufficiently flat as to have little influence on S_w.

Table 3.1 Morphometry of Menzies and Harmon Lakes

Parameter	Menzies Lake	Harmon Lake
Elevation (m)	1250	1150
$\bar{z}$ (m)	8.2	8.0
Volume (m^3)	390 000	2 480 000
Surface Area (m^2)	47 500	311 000
z_{max}(m)	16.5	22.0
S_w	0.68	0.82
Maximum Fetch (m)	500 (NE)	1100 (N)

3.1.2 Annual Temperature and Oxygen Budgets

Isopleths of oxygen and temperature for the period of June, 1991 to April, 1992 are given in Figures 3.3 and 3.4. As described below, these isopleths exhibit typical characteristics of dimictic eutrophic lakes. The maximum summer thermocline depths of about 9 m at

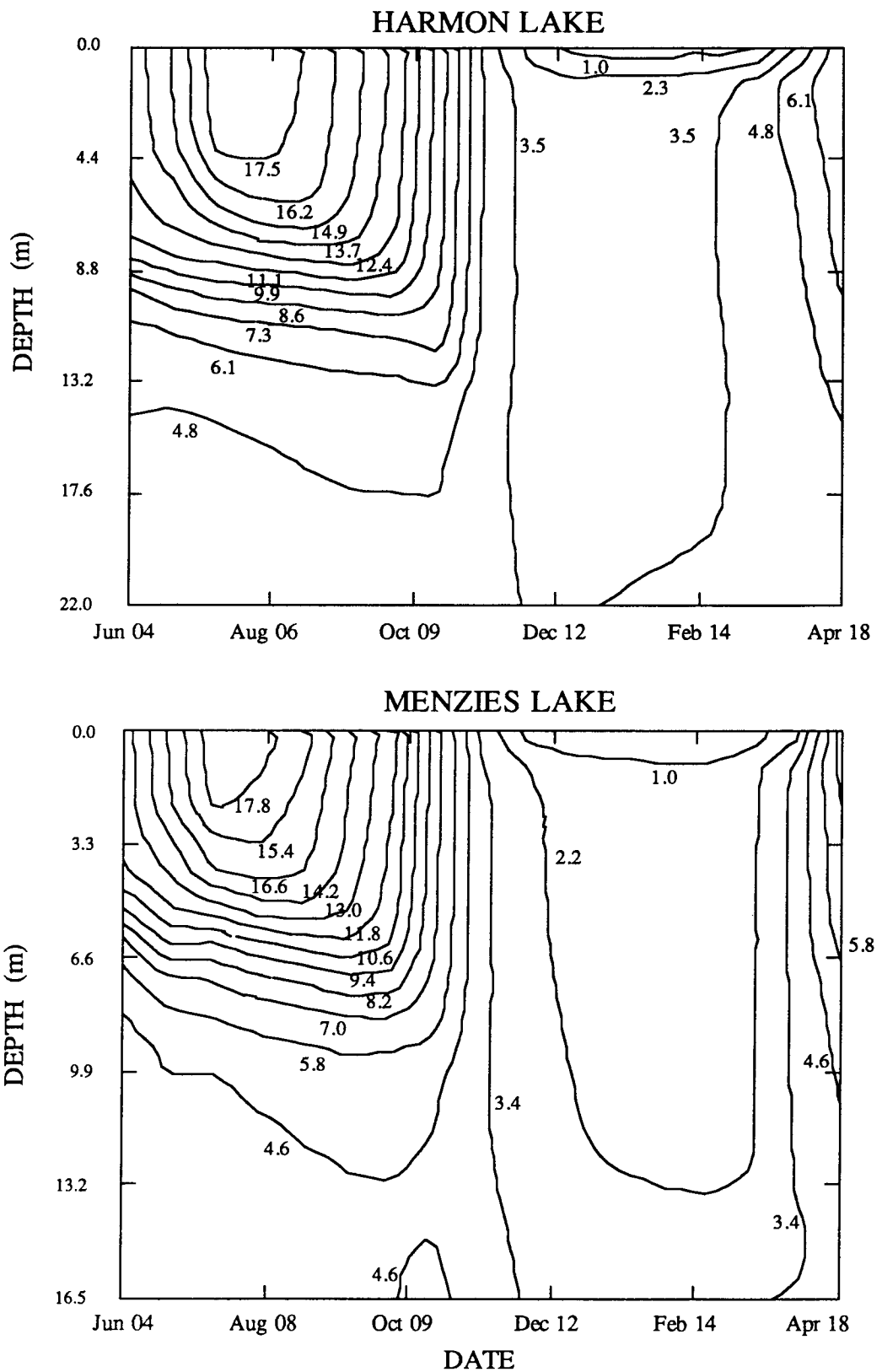

Figure 3.3 Isotherms at Menzies and Harmon Lakes, June 1991 - April, 1992

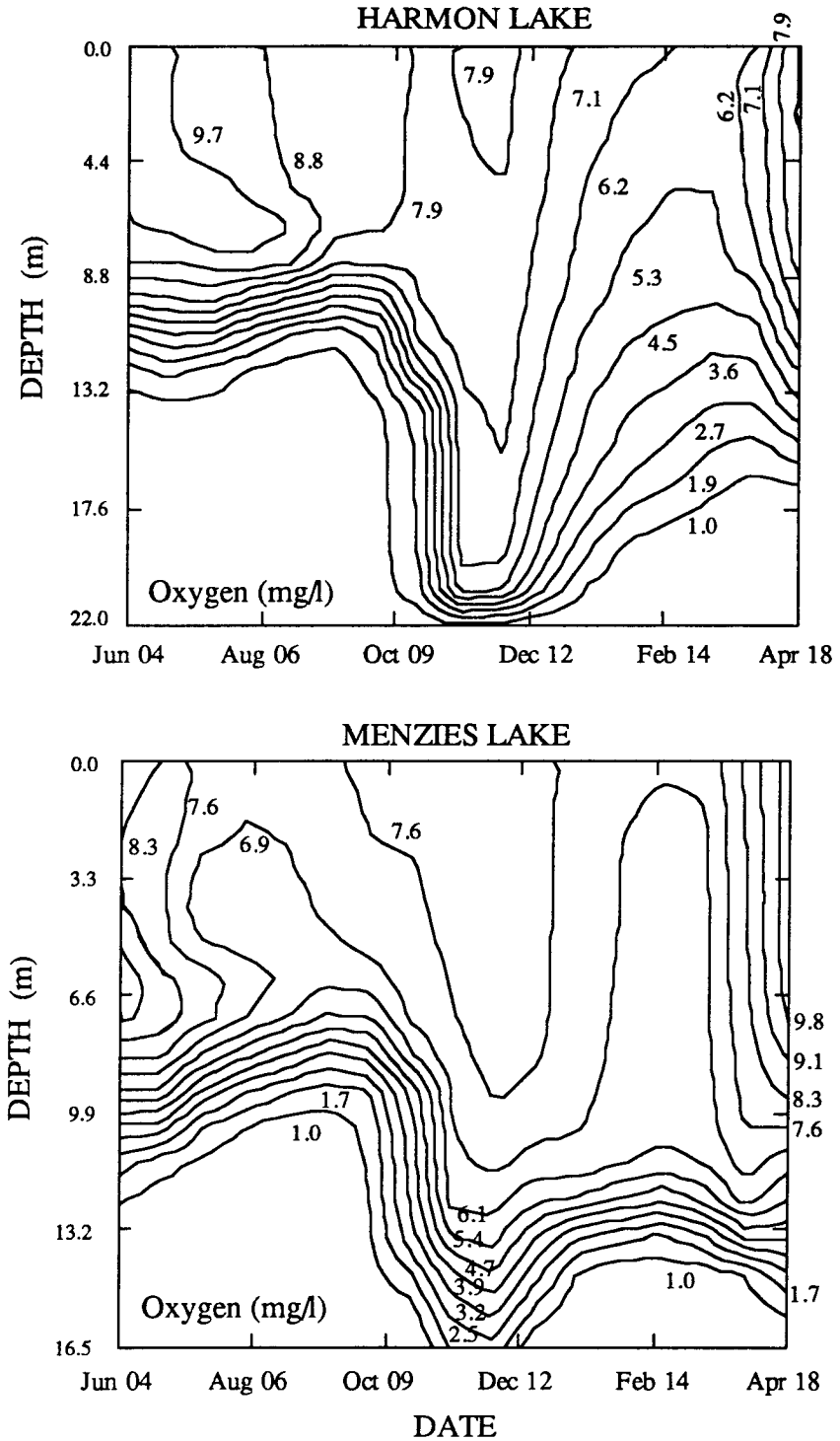

Figure 3.4 Oxygen Isopleths at Menzies and Harmon Lakes, June, 1991 - April, 1992

Harmon Lake and 6.5 m at Menzies Lake are evidence of greater fetch and wind exposure at Harmon Lake (§ 3.1.1).

The Oxygen Budget

Both lakes exhibit the typical clinograde oxygen profiles of productive lakes: as shown in Figure 3.4, there is a rapid drop in oxygen concentrations across the thermocline, mainly as a result of biological oxidation of organic material. This oxygen is not replaced because the hypolymnetic water is never exposed to the atmosphere over the course of the stratified period. By late June, an oxygen peak is observed above the thermocline. This is mainly due to the photosynthetic production of oxygen by phytoplankton. Phytoplankton commonly adapt to the low temperatures and dim light associated with this depth, where they take advantage of relatively high nutrient concentrations (Wetzel, 1983). Approaching the thermocline from above, there is an increase in oxygen solubility due to the drop in temperature which may contribute to this peak. The peak is further pronounced by the rapid decline in oxygen below the thermocline due to bacterial consumption. The peak subsides by early September, at the end of the summer algae bloom.

The oxygen budget at both lakes are similar up until a few weeks after the Menzies Lake circulator was activated in early November, 1991. Once ice had formed later that month, oxygen depletion began near the bottom of both lakes. Diffusion of oxygen towards the lake bottom where it was being rapidly consumed resulted in significant depletion throughout the entire water column at Harmon Lake. At Menzies Lake however, most of the water column was being re-circulated and replenished with oxygen by turbulent entrainment and diffusion across the air-water interface within the ice-free area.

Interactions at the Mud-Water Interface

Further evidence of oxygen consumption is available from the measurement of dissolved solids. Dead plankton which has settled onto the lake bottom decompose, thereby decreasing the oxidation-reduction potential. Once the potential reaches zero at the sediment-water interface, dissolved metals are released as described by Mortimer (1971;1941;1942) and Stauffer (1987). Dissolved solids concentrations were consistently higher in the hypolimnion than in the epilimnion over the summer period (suspended solids concentrations at both lakes were small compared with the dissolved fraction at all times). Over the winter, samples taken 1.0 m above the lake bottom also had a relatively high concentration of dissolved solids, most notably at Menzies Lake (Figure 3.5). This is a noteworthy point since it provides further evidence that Menzies Lake experienced

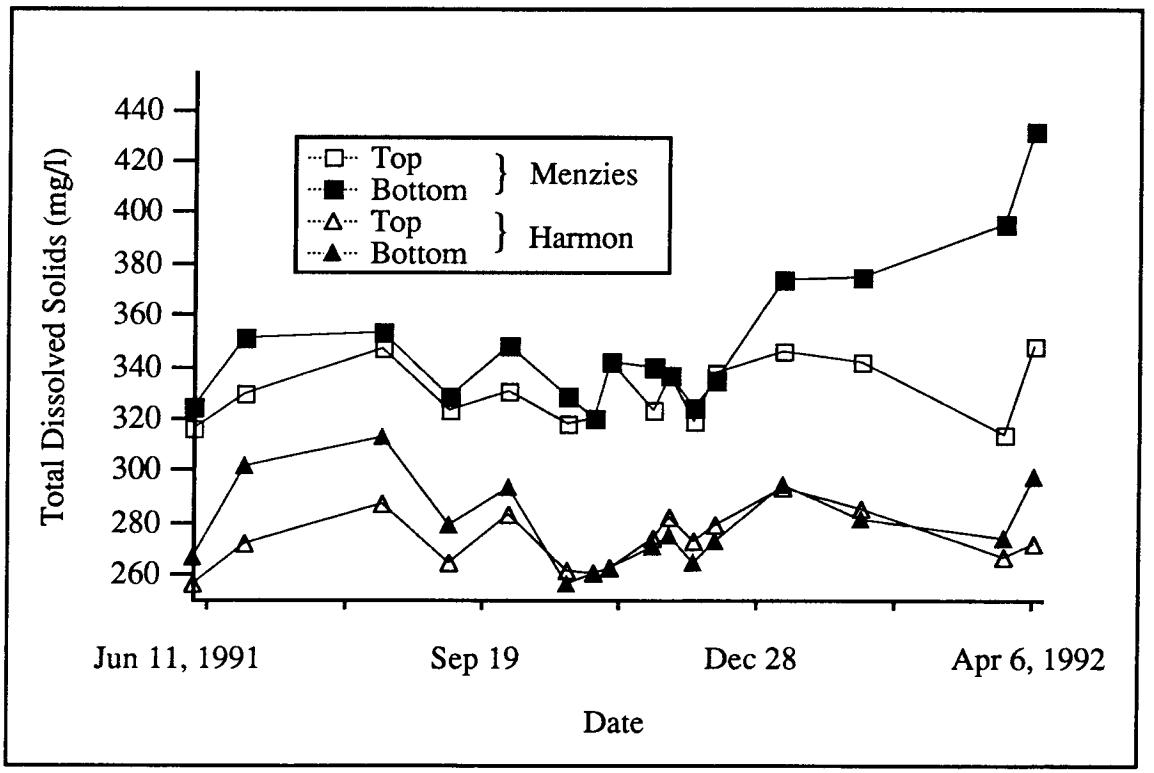

Figure 3.5 Total Dissolved Solids Near Lake Surface and Sediments

incomplete circulation due to the Air-o-lator®: the small volume of water below 13 m (approximately 5% of the total lake volume [see Figure 3.2b]) remained stagnant throughout the artificial circulation period. In addition to solids measurements (by evaporation of a known volume of lake water), a strong smell of hydrogen sulfide in the bottom samples indicated that reducing conditions prevailed at depth due to oxygen consumption.

3.2 DATA COLLECTION PROCEDURES AND OBSERVATIONS

3.2.1 Data Requirements

In order to utilize and verify MLI and MLI-C, a significant effort was required to acquire field data.

Input Data

As the model was designed for future compatibility with DYRESM, the input requirements are similar. The bulk aerodynamic equations suggested by the TVA (1972) and employed in MLI require the following meteorological data:

a) air temperature
b) wind speed
c) total daily solar radiation
d) vapour pressure
e) cloud cover
f) precipitation

All of the above data are daily averages except for solar radiation and precipitation. As described in § 3.2.2, meteorological sensors were installed in order to collect all of the data except precipitation and cloud cover. The latter variable enters into the calculation

of incoming long-wave radiation, R_{li}. No direct means was available of sensing R_{li}, but an empirical relationship exists which expresses cloud cover in terms of the observed and theoretical clear-sky solar radiation. This formula is given along with the bulk aerodynamic equations in Chapter 4. Snowfall depth was measured by the Menzies Lake resident using snow boards and a metre stick as described in § 3.2.2. Given that rainfall at the field location is rare over the winter months, no means for measuring rainfall was provided. (Less than 2 cm in total fall, on average, from December to March in the Southern Interior Plateau. Even less would be expected at the field location due to its high elevation.) In accordance with Murphy's Law, however, rainfall was a significant factor over the investigation period. Fortunately, the Menzies Lake resident noted all days on which rainfall occurred. For these days, the rainfall data from the city of Merritt, 500 m lower in elevation and about 20 km to the North, was used for snowmelt predictions as described in Chapter 4. Although rainfall was observed at Merritt on every day that it was noted at the lake, there was no significant correlation between the precipitation measurements at Menzies Lake and those at Merritt ($r = 0.37$). Therefore, no adjustments to the Merritt rainfall data could be justified for use in the MLI model.

Verification Data

In order to verify the model predictions, the following data were required:

a) average temperature of the unfrozen lake
b) ice thickness
c) snow thickness
d) snow-ice thickness
e) polynya radius

As described in § 3.2.2, sensors were installed to continuously measure the lake temperature at various depths. All of the remaining variables were only measured during field trips to the lakes.

3.2.2 Instrumentation

Meteorological data was collected using sensors connected to a multi-channel data acquisition unit. This unit was housed in an aluminum buoy which was anchored in the lake at the location of maximum depth prior to the onset of ice cover. An anemometer, pyranometer, humidity sensor and thermistor were installed on a 2 m tower which was fixed to the buoy (Figure 3.6). Light-gauge wire and surveyor pins frozen into the ice-cover were used to provide rigidity to the tower. In addition to this weather station, a temperature/dissolved oxygen meter was used to measure profiles of these two parameters during field trips. All of this instrumentation is described below.

Datalogger

A Multidata GNOME datalogger, developed by Terrascience Systems Ltd. was employed. This unit scans up to fifteen channels simultaneously and logs data while unattended. It runs under the control of a BASIC language interpreter that stores the collected data in non-volatile random-access memory. It also has a time-out feature which conserves power by switching to low-power between acquisitions. An external 12 V battery was used to power the unit, leaving the internal battery to act as a back-up. The scanning interval used was 0.5 hours. This interval was chosen to provide adequate data, while ensuring that enough memory would be available for field trip delays of up to one month beyond the scheduled field trip interval. The unit was new at the time of installation.

Portable Computer

A SHARP PC-6220 notebook computer was used to provide an interface for field communication with the datalogger via an RS232 serial port cable. The data acquired by the datalogger was downloaded in hexadecimal form to the computer using

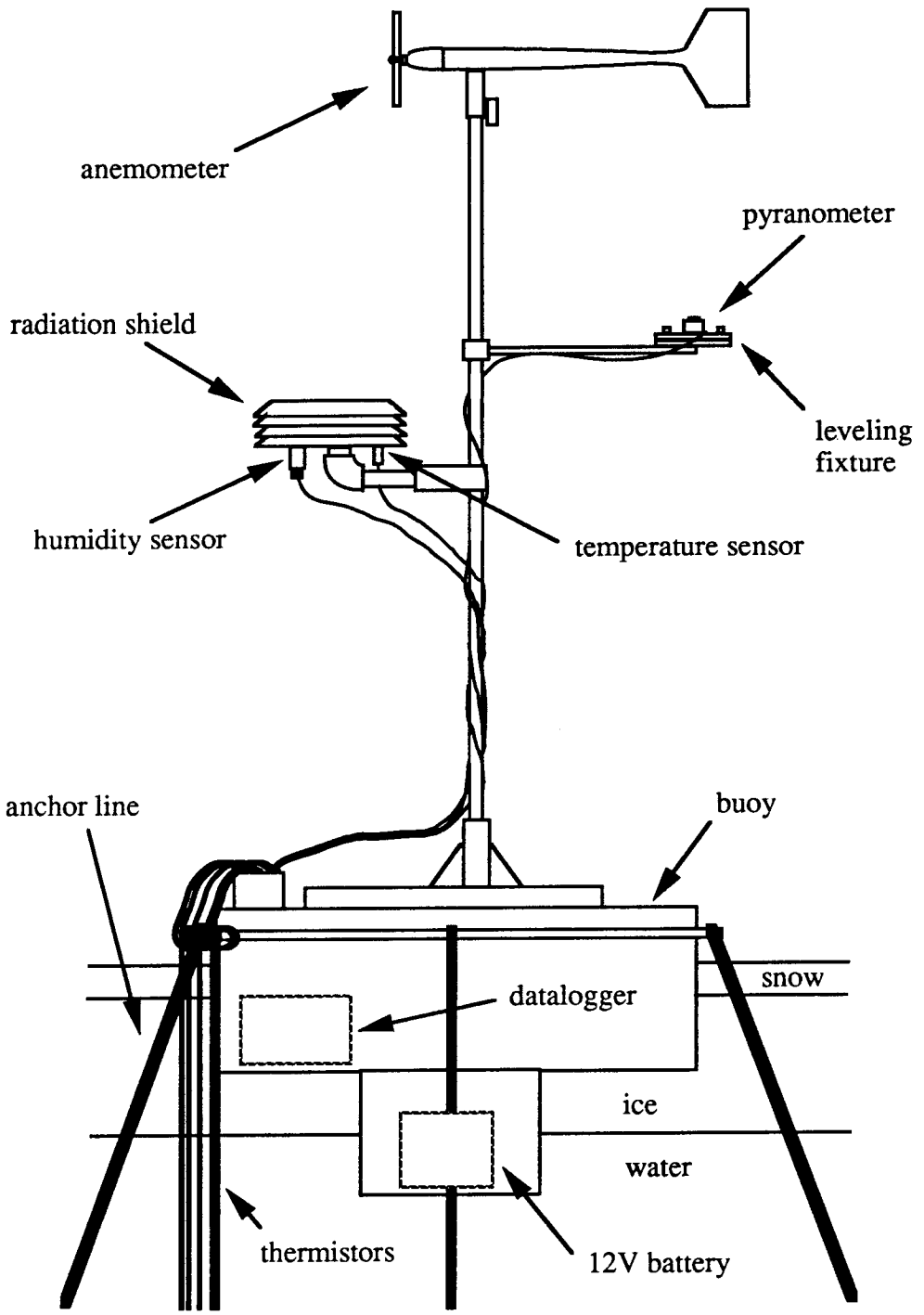

Figure 3.6 Menzies Lake Weather Station

interfacing software provided by Terrascience. This procedure required 5 to 10 minutes to complete. The software provided was also used to average and translate the data to a file which could by imported to commercial spreadsheet packages.

Sensors

All sensors provide reliable data under the field conditions observed at Menzies and Harmon Lakes over data collection period

Temperature Sensors: Thermistors were connected to eight of the analog channels. Two models were used (4 LM335 and 4 LM34), both producing an output voltage of which temperature is a linear function. In order to ensure accurate data, the sensors were field calibrated in the narrow temperature range characteristic of ice-covered lakes using the Y.S.I. temperature sensor. In this manner, any non-linearity in the voltage-temperature function would be minimized. One of the sensors was used to measure air temperature, and two were fixed at the same depth in the lake in order to provide further assurance of sensor accuracy. A hole was augered into the ice and the sensors placed at 3, 7, 8, 11, 12.5 and 15 metres below the water surface. The cables subsequently froze into the ice cover. Periodic checks following the installation of the weather station showed that the LM335/34 sensors were in agreement with the Y.S.I. sensor to within 0.1 ^{o}C. The LM34 sensors were new at the time of installation.

Solar Radiation Sensor: A LI-COR 200SA pyranometer was employed to measure direct and diffuse solar radiation. Although this sensor does not cover the full range of the solar spectrum, the absolute error involved in the measurement of total solar radiation is only ±5%, and typically ±3% under daylight conditions. The sensitivity of the sensor is about 80 μA per 1000 W/m^2, with a maximum linearity deviation of 1% to 3000 W/m^2. A millivolt adapter (LI-COR model 2220S) was required to amplify the signal for use with the datalogger. The sensor was mounted on a LI-COR

2003S leveling fixture which was bolted to a pipe that extended 0.3 m away from the anemometer post (see below) in order to avoid shading by other instruments. Stabilization of the anemometer post was required in order to ensure that the pyranometer remained level. Four lengths of light gauge wire were fixed to the post and tied back to surveyor pins frozen into the ice on the previous day. The unit was new at the time of installation.

Wind Monitor: An RM Young model 05305 anemometer was used to measure wind speed and direction. It has a working range of 0-40 m/s, and a propeller threshold of 0.4 m/s. The rotation of the propeller produces an AC sine wave signal with frequency proportional to wind speed. According to factory calibrations, the propeller is accurate to within 2% of the actual wind speed. The anemometer was fixed to a post which was bolted to the buoy. The approximate height of the propeller was approximately 2.0 m above the ice surface. The unit was new at the time of installation.

Relative Humidity Sensor: A VAISALA HMP 35A humidity and temperature probe was installed at a height of approximately 1.0 m above the ice surface and was protected from solar radiation using a shield made up of four aluminum pie plates. The HMP 35A probe contains a HUMICAP H-Sensor (model 0062). It is accurate to ±1% relative humidity against factory references at 20°C. There is a temperature dependence of ±0.04% / °C, and its long term stability is better than 1% per year. The unit was new at the time of installation.

Temperature / Dissolved Oxygen Probe

Temperature and dissolved oxygen measurements were made using a Y.S.I. (Yellow Springs Instruments) digital dissolved oxygen meter (model 58). The meter was checked using a precision mercury thermometer (accurate to better than 0.1 °C) in the

laboratory. Calibration for dissolved oxygen was performed in the field by wrapping the probe in a wet cloth and adjusting the reading to correspond to oxygen-saturated water at the local atmospheric pressure once the probe electrodes had polarized. In freezing conditions, polarization required up to 20 minutes.

Other equipment

Precipitation Gauges: Two snow boards were placed in locations where wind exposure was low and well away from tall obstructions such as trees and buildings. A local resident measured snow accumulation on the boards following each snow event using a metre stick. Following each measurement, the boards were cleared of snow and placed on top of the new snow. These measurements are considered accurate to ± 1 cm. Neither the duration of the snowfall, nor the time of measurement relative to the end of the snowfall event were recorded. Since much compaction can take place over the first 24 hours following a snowfall (see Chapter 2), and since the snow boards may not have been ideally placed with respect to exposure, the errors in estimating the actual depth of snowfall is probably much greater.

3.2.3 Field Procedure

Field trips were scheduled every 2 to 3 weeks, depending on expected rates of change in ice-cover, in addition to the availability of both equipment and assistants. The field trip schedule is given in Table 3.2. One full day (including travel time) was required to complete the observation procedure at Menzies and Harmon Lakes.

Basic Observations

All observations were made near the location of maximum depth at Harmon Lake. At Menzies Lake, additional measurements were made within the polynya and at a point near the opposite end of the lake. This was done to ensure that the circulation device was

never causing any significant horizontal density variations other than those caused by heat and mass transfer across the mud-water interface. Furthermore, examination of the temperature data from within the polynya was required in order to determine if there were any buoyancy effects in the behaviour of the radial jet.

Table 3.2 Field Trip Schedule

DATE
Dec. 12/13, 1991 ‡
Jan. 7, 1992
Jan. 19
Feb. 4
Feb. 27
Mar. 10
Mar. 27
Apr. 7

‡ meteorological sensors installed

One hole was augered into the ice at each station. Ice depths were measured in the following manner: a metal bar was submerged into the hole, and pulled back up along the edge of the hole until a metal plate welded to its end made contact with the ice. The distance between the top of the plate and the point on the bar corresponding to the top of the ice sheet was then measured. Flooding due to excessive snowfall (see § 2.3.3) was observed on February 4th, 1992. Snow-ice thickness was only measured for the first time on the following field trip, on February 27th. Total ice measurements are considered accurate to ±1cm, whereas snow-ice measurements are not considered reliable for the reasons outlined in § 3.2.4.

The Y.S.I probe was lowered through each hole, and measurements of both oxygen and temperature were made at 1 m intervals below the water surface.

Water samples were taken using a Van Doorn sampling bottle at 2.0 m below the surface and 1.0 m off the lake bottom. These samples were analyzed in the laboratory for total solids using the standard evaporation technique. The mixed layer sample was taken at 2

m in order to avoid the ice-water boundary layer stratification in which solids concentrations may be relatively high due to salt rejection. The deep sample was assumed to represent total solids in the stagnant layer, and was taken only 1 m above the sediments given the great depth of mixing induced by the circulator.

Additional Observations Made at Menzies Lake

Air temperature and relative humidity measurements were taken using a mercury thermometer and sling psychrometer. The psychrometer readings were only considered reliable when the air temperature was above the freezing mark. These measurements were compared with instantaneous readings from the humidity sensor on the weather station. The weather station thermistors were also checked irregularly to verify that readings were consistent with the Y.S.I. meter.

On each trip, the data collected by the weather station was downloaded to the portable computer. The datalogger was subsequently cleared of memory and re-initialized to immediately begin data collection.

Oxygen and temperature profiles were also observed from a boat within the polynya, as close to the circulator as possible. In addition, a surveyor's chain was used to supplement visual estimates of the polynya radius. The end of the chain was tied to the circulator. The chain was then permitted to unspool as the boat was moved to the polynya perimeter, where measurements were make in 2 to 10 directions, depending on the time available.

Radial Jet Velocity Measurements

In order to quantify the sensible heat transfer to the polynya edge, it was necessary to formulate an equation describing the velocity field induced by the radial jet of water produced by the circulator. This required field measurements of velocity as a function of

radial distance away from the circulator. This was carried out using a propeller-driven OTT® meter. Measurements were taken from the bow of a boat set inside the polynya such that the meter was always located upstream of the boat. This was done so as to avoid erroneous measurements due to disruption of the flow field. It was found that only surface measurements provided data which were reproducible and useful in terms of producing a reliable velocity field formula.

A surveyor's chain was fixed to the circulator at one end, and a tree on shore at the other. This produced no disruption to either the operation of the circulator, nor the induced velocity field. The boat was pulled along the chain and three measurements were taken at each station. The sampling interval was as short as 10 cm close to the circulator, increasing with radial distance to a maximum of 2 metres. At about ten metres from the circulator, the surface velocities were below the threshold of the current meter.

In addition, current velocities were estimated by timing drogues placed in the water at the raft, and allowed to float toward the edge of the ice-free zone. Although much less accurate, the velocities calculated from the drogue data were of the same order as the direct measurements. Wind speed was less than 0.5 m/s during all current measurements, and was therefore ignored.

3.2.4 Field Trip Observations

The Menzies Lake Polynya

It was found that the polynya radius varied only slightly over the entire winter period (see Chapter 5). Measurements were not of adequate quality or frequency to detect significant changes in size until spring when the ice cover retreated rapidly to produce completely ice-free conditions within 2 weeks. The radius remained at about 20 m on average. The shape of the polynya was elliptical rather than circular, with the upwind end tending to be

several metres shorter, and the downwind end several metres longer. When Menzies Lake was visited in the early morning in cold weather, there tended to be a very thin ice layer, about 1 m wide, around the perimeter of the polynya. This was the only clear evidence of polynya contraction due to cold weather. Frazil ice was never observed in the polynya because the average lake temperature never dropped below about 1.4 ^{o}C.

Since isothermal conditions (to an accuracy of +/- 0.1 deg C) were measured within the polynya over at least the top 3 m (the depth of the circulator intake) , buoyancy was dismissed as an important factor in the circulation pattern and heat transfer.

Lake Temperature

Isotherms based on the Y.S.I. probe data, for the period spanning December 13th and March 10th are given in Figure 3.7. The latter date is that of the last field trip during which full ice-cover was observed at Harmon Lake. Clearly, the impact of the circulation device on the heat content of Menzies Lake is substantial. While the water below ice-cover at Harmon Lake gradually but consistently heats up over the winter due to solar radiation and sediment heat transfer, the circulator at Menzies Lake cause the water to cool down at a relatively high rate. As early as late February, however, average air temperatures almost consistently above zero and increased solar heating rapidly drive the temperature of both lakes up (Figure 3.8). By early April, both lakes were completely ice free.

On March 10th, a reproducible unstable temperature profile was observed at Harmon Lake. Throughout most of the water column on this date, the temperature was near the point of maximum density. The vertical variation in solids concentration was insufficient to explain the instability. It is hypothesized that the lake was undergoing vigorous convective circulation. as solar radiation penetrated deep into the lake (the Secchi depth transparency on this date was 11 m, the greatest ever observed at Harmon Lake). At 4°C,

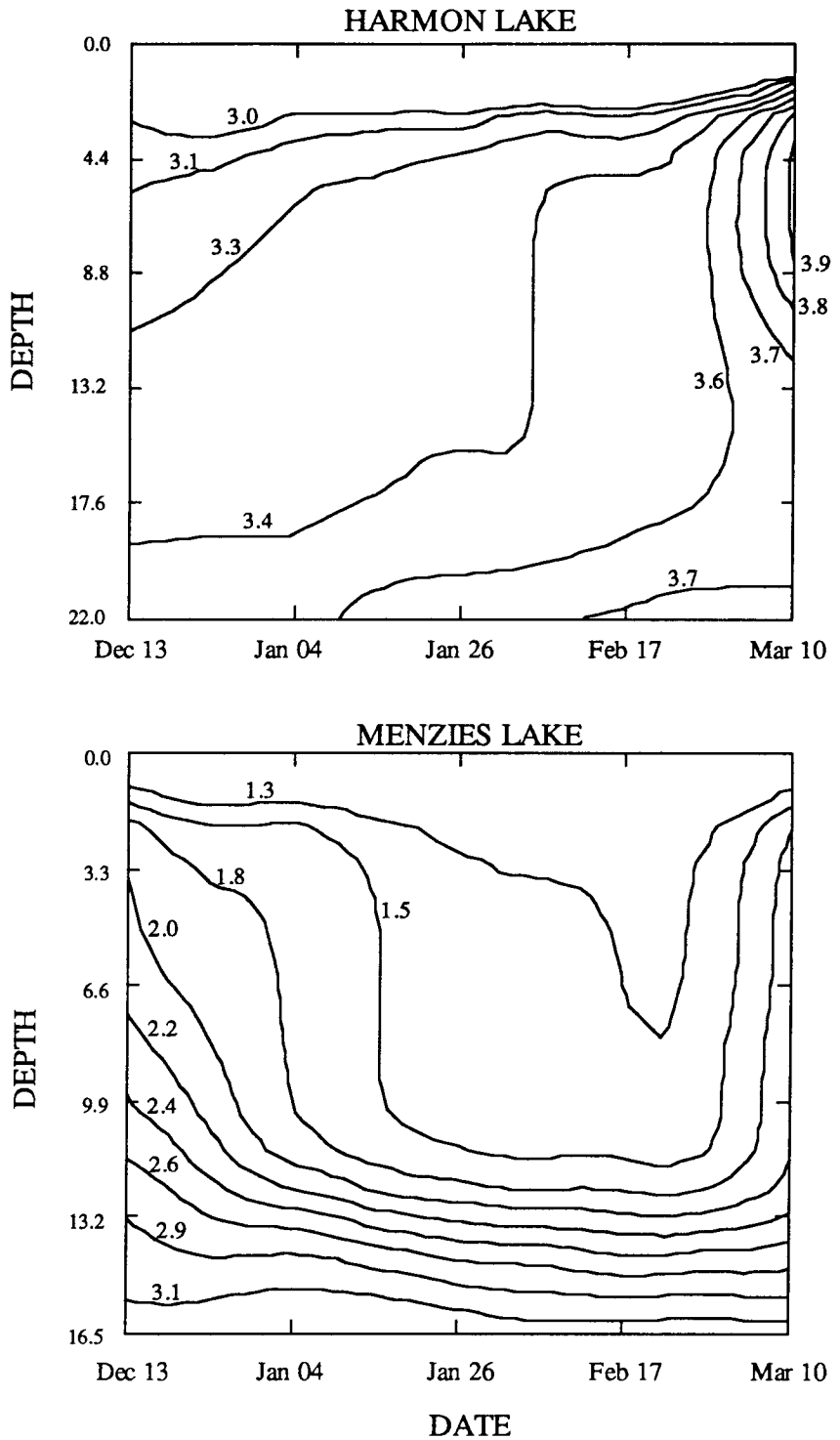

Figure 3.7 Isotherms at Menzies and Harmon Lakes, December 13th - March 10th

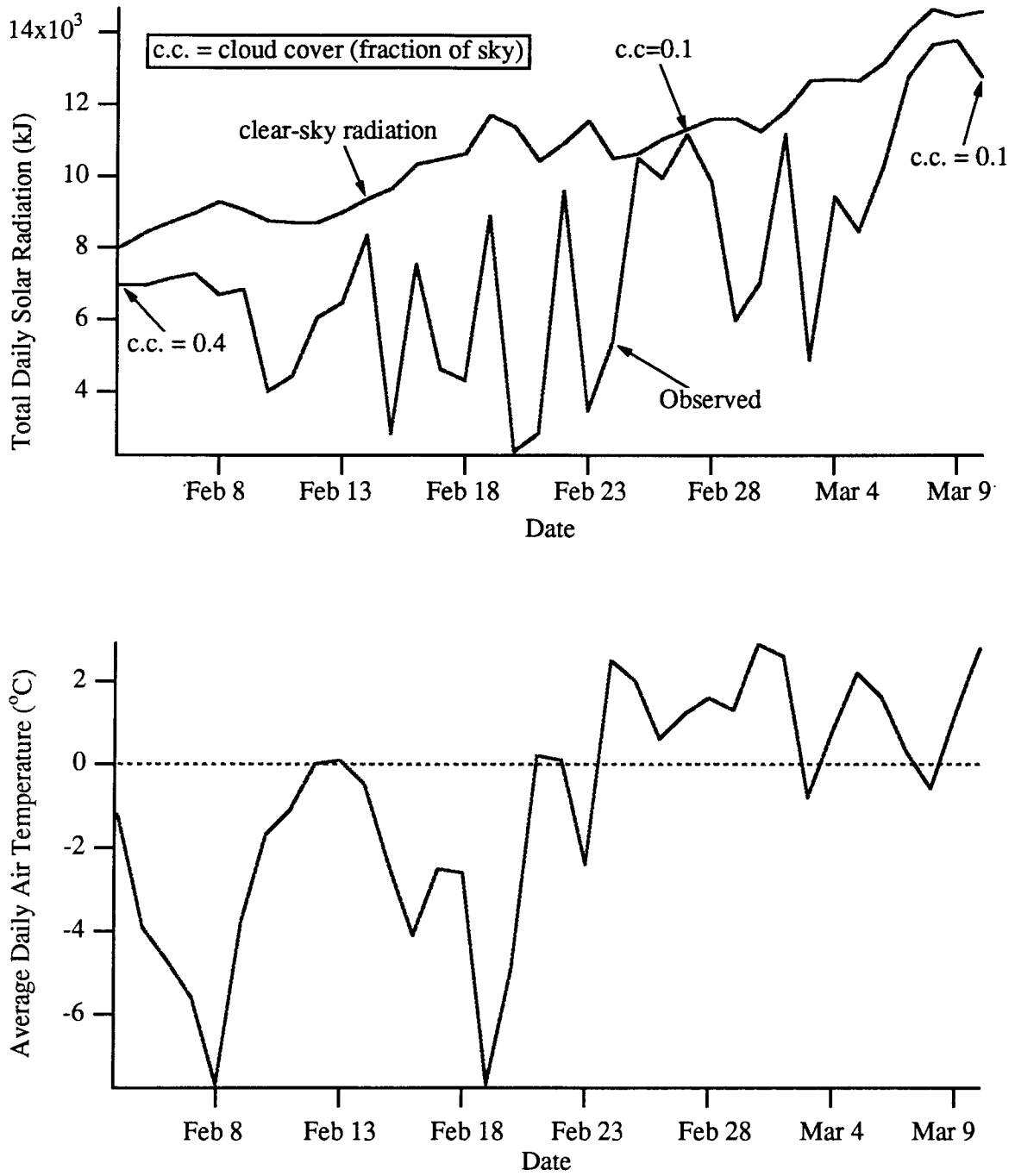

Figure 3.8 Air Temperature and Solar Radiation

any local changes in temperature (except at the surface) results in instabilities which cause convection. A re-circulation pattern may have developed as water heated by solar radiation rose up through the water column, only to be cooled near the thermal boundary layer at the ice-water interface. This water would then begin to sink again as it approached the temperature of maximum density.

Another potentially important factor in the heat budget during the melting period is the re-radiation of solar heat from the lake bottom in the littoral zone, which may have produced greater melting of the ice-cover in the near-shore area. In addition, the heat transfer assumed to be active at the ice-water interface may have increased due to an increased thermal gradient at the boundary and/or the development of much higher rates of turbulent heat transfer.

Comparison of the temperature profiles at the three Menzies Lake stations has revealed that there are no significant horizontal variations at any time over the winter period other than those caused by heat and mass transfer across the sediment-water interface (see §3.2.3).

Ice and Snow Thickness

Ice and snow thicknesses over the observation period are shown in Figure 3.9. Snow-ice thicknesses may not be reliable for several reasons. On January 19th, a flooded snowpack was observed, presumably as a result of a recent snowfall. (The most recent occurred the day before, according to the records provided by the Menzies Lake resident.) The thickness of flooded snow tended to increase towards the centre of the lake, with no observed flooding at the lake edge. The response of the ice sheet could be compared to that of a simply supported beam bending under a distributed load. The depth of flooding was observed, but snow-ice thickness was not, since the phenomenon was not previously evident as an important factor in the heat transfer problem. The

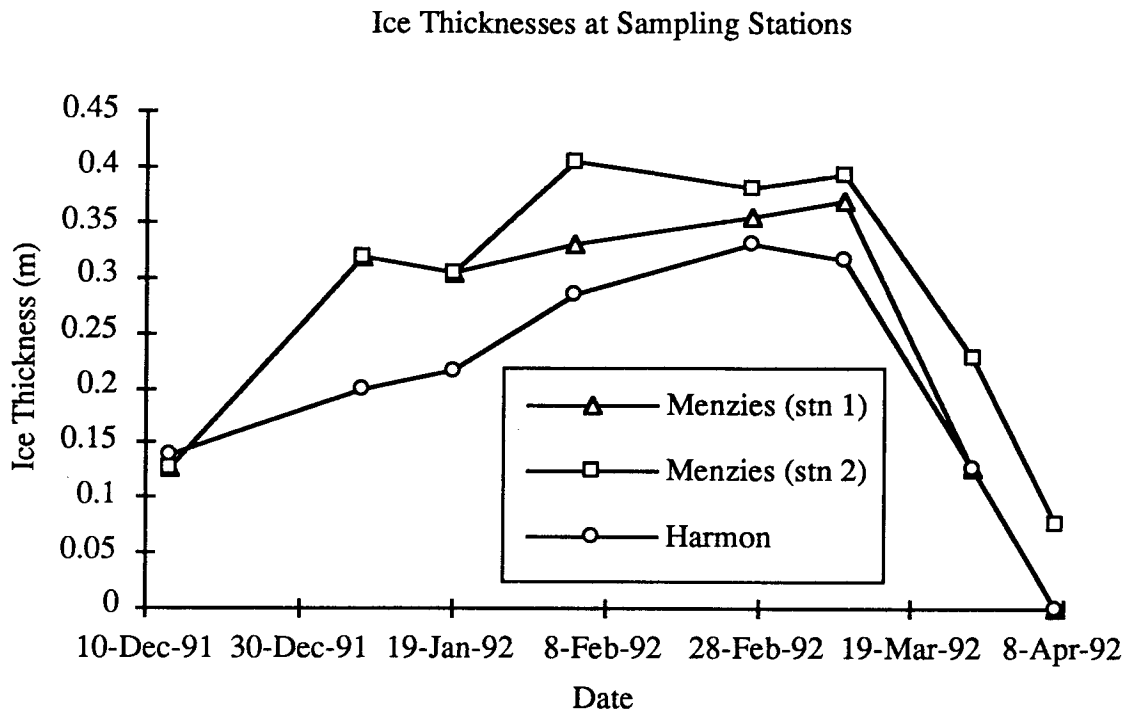

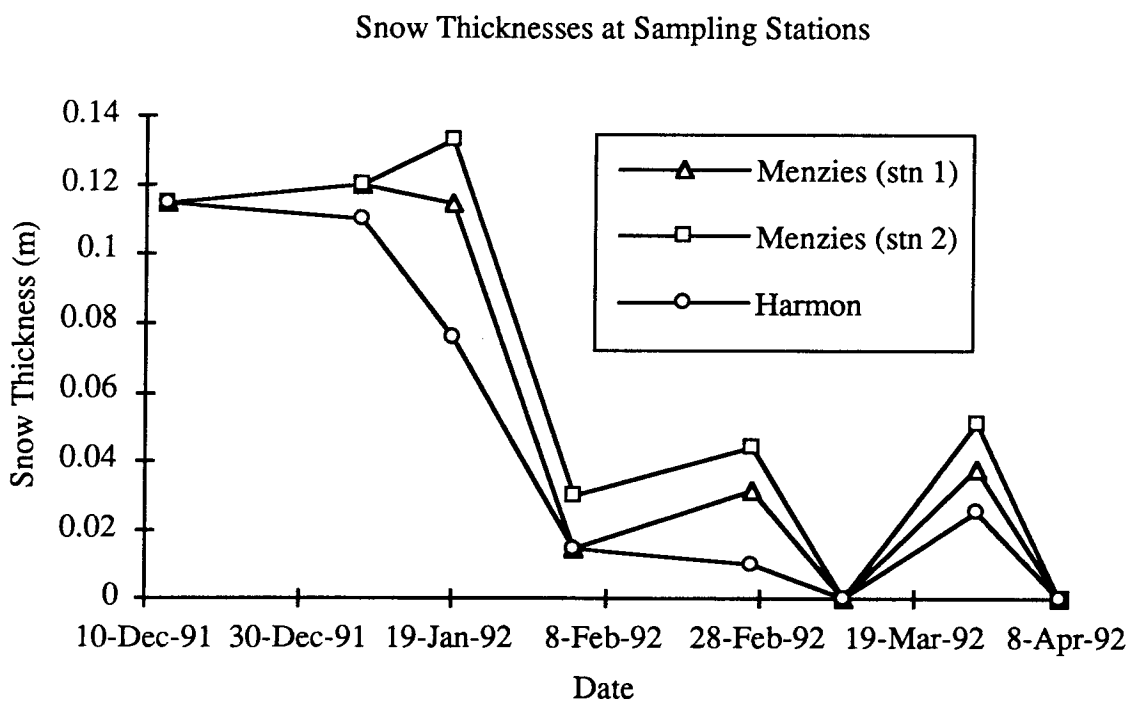

Figure 3.9 Ice and Snow Thicknesses

actual total thickness of snow-ice was only observed for the first time on February 27th. Furthermore, there was a subjective transition from snow-ice to pure ice which may have been interpreted differently during the proceeding field trips. Since the modeling period ends on the third trip which included snow-ice observations (March 27th : see Chapter 4), no snow-ice observations will be used for model verification purposes.

The Melting Period

Between the field trips of February 27th and March 10th, heating of both Menzies and Harmon Lakes increased significantly (Figure 3.7). Observations near the locations of maximum depth, however, indicate an insignificant decrease in total ice thickness at Harmon Lake, and even an increase of similar magnitude at Menzies Lake (Figure 3.9). Just over two weeks later, on March 27th, there was an ice-free zone 1 to 4 m wide around the main basin of Harmon Lake. This zone was substantially wider in the shallow basin at the south end of the lake. The ice at the sampling station, however, was 13 cm thick. At Menzies Lake, the polynya had reached the east end of the lake, and care was required to reach the weather station: it was clear that the maximum ice thickness in the littoral zone was barely sufficient to support the weight of an adult (during field trips in the late fall of 1991, it was found that an adult could be supported by as little as 5 cm of ice). However, the ice was 13 cm thick at Station 2, and 23 cm thick at Station 3. This was by far the most substantial spatial variation in ice thickness observed at either lake.

Judging by the changes in water column temperature, and the observed ice-free zone on March 27th, it is suspected that substantial thinning of the littoral ice would have occurred between February 27th and March 10th.

Boundary Effects at Menzies Lake

A closer inspection of the Menzies Lake isotherms as generated by the weather station sensors (Figure 3.10), indicates that the circulator's zone of influence extended down to the lake bottom by about December 18th, 1991. Without regard to morphometry, it would appear that a sudden increase in the rate of cooling occurred between December 15th and 17th. There is, however, neither consistent information in the meteorological data, nor is there conclusive evidence that a concurrent decline in the whole lake heat content occurred. The upper and lower heat content bounds using the weather station thermistor data and applying density considerations are shown in Figure 3.11. The information contained in this figure is insufficient to be conclusive, but when combined with the meteorological data, there is strong evidence that the sudden drop in the isotherms between 2.0 and 2.8 ^{o}C can be explained by examining the dynamics of circulation within the lake.

Laboratory investigations have been performed in which a fluid was injected at a constant rate on top of another fluid of greater density. This lower fluid being withdrawn at the same rate (see Wood, 1978; Jirka & Katavola, 1980). The interface which develops descends through the water column and is drawn down at some critical point above the withdrawal depth. The interface then continues to drop until it reaches a second critical point below the intake, where the denser fluid will no longer be withdrawn. It is hypothesized that the equivalent interface at Menzies Lake dropped from about 8 to 13 m between December 15th and 17th. Hence the rate at which the isotherms shown in Figure 3.10 drop is a function of pumping rate and lake morphometry, rather than the rate of cooling.

Given that the lake depth is approximately 13 m directly below the circulator and the lake is almost isothermal above this depth by the 18th of December, it is concluded that the

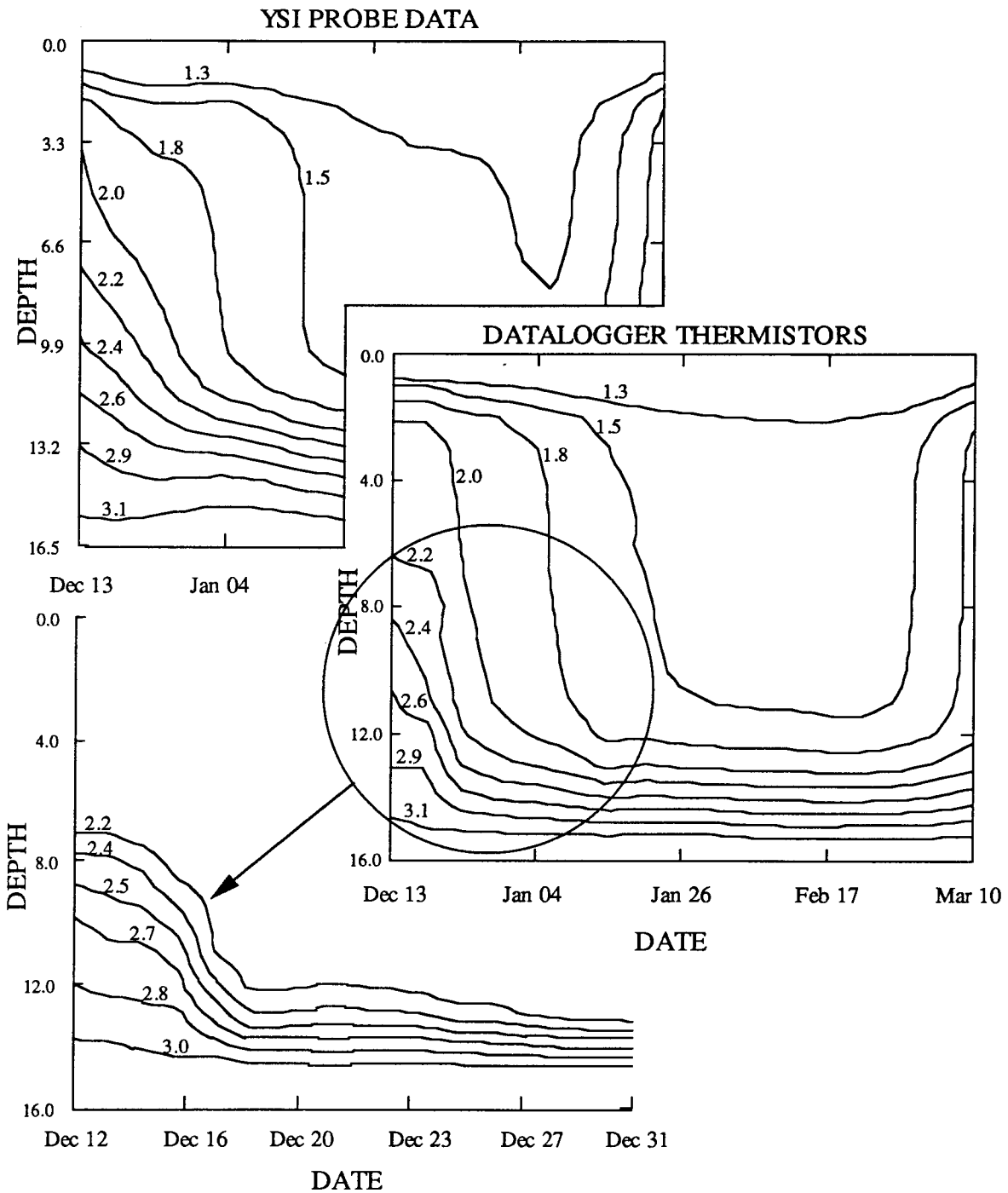

Figure 3.10 Isotherms Generated from Datalogger Data at Menzies Lake

maximum withdrawal depth of the circulator is limited by the lake bottom. A thermal boundary layer caused by the diffusion of heat from the sediments would account for the observation that purely isothermal conditions only existed above about 12 m after this date.

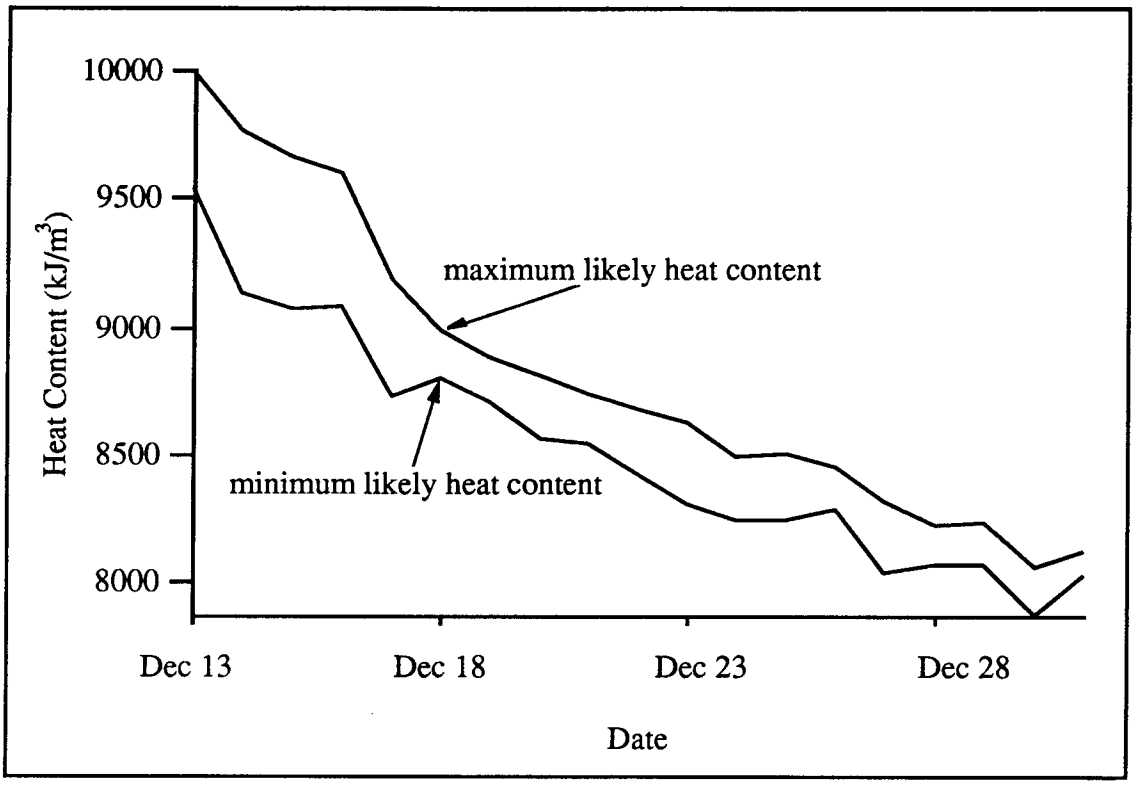

Figure 3.11 Maximum and Minimum Likely Heat Content at Menzies Lake (based on density considerations [temperature effects only])

Cloud Cover

Cloud cover was also observed from time to time during field trips. Estimates of daily average cloud cover, expressed in tenths of the celestial hemisphere, are given in Table 3.3. These observations will be compared with the estimates made in the model as described in the following sub-section.

Weather station

In the few weeks before and after the winter solstice, the tall trees on the south side of Menzies Lake cast a shadow over the pyranometer all day except for 3 to 4 hours starting in the late morning. Although the solar radiation data during this period, may be appropriate in terms of the heat transfer between the lake and the atmosphere, two problems are created by the shading. First, as described below, comparisons cannot be made with the theoretical clear-sky radiation. Second, the empirical formula expressing cloud cover in terms of the ratio of observed to clear-sky radiation cannot be considered accurate for use in the model (see Chapter 4). These problems apply from the start of the observation period (December 13th) to some time between January 7th and January 19th. No shading of the pyranometer was observed on the latter date.

Table 3.3 Observed Average Daily Cloud Cover

Date	Cloud cover
December 13	5
January 7	1
January 19	4
February 4	4
February 27	1
March 10	1
March 27	9
April 7	3

During a cold spell in the data collection period, the glass which encases the pyranometer leveling bubble cracked, and the alcohol inside evaporated. As a result, accurate leveling of the pyranometer could not be ensured for a significant portion of the data collection period.

As described in §3.2.3, the meteorological tower was anchored to the ice cover using light gauge wire and four surveyor's pins frozen into the ice. As melting of the top of the ice cover proceeded, however, the pins loosened, but at different rates depending on their

location and the depth and angle of penetration. In addition, melting of the ice around the circumference of the buoy occurred due to solar heating. As result of these two melting processes, the entire weather station became tilted to the west. This occurred at some time between February 27th and March 10th. The angle of tilt was not measured, but is estimated at 10°. Therefore, the deviation of the pyranometer from the horizontal may have been 10° or more for up to two weeks.

The impact of this tilt may have been considerable. From the cloud cover observations, the solar radiation should have been nearly equal to clear-sky levels on February 27th and March 10th (the theoretical clear-sky radiation is shown in Figure 3.8, and was computed as given in Appendix A. It should be noted that the clear-sky radiation does not increase monotonically after the winter solstice as a result of the influence of albedo on the indirect portion of the total incoming radiation.). On March 10th, however, the ratio of observed to clear-sky radiation is comparable to that on February 4th, when the observed average cloud cover was 0.4. No other observations of clear sky days were made during the period when there was insignificant topographic obstruction (tree shading) of the incoming solar radiation. Confidence in the clear-sky radiation calculations is limited by the lack of reliable comparisons between the observed and calculated cloud cover over the ice-covered period.

Anthropogenic Effects

Harmon Lake is a popular ice-fishing lake over the winter period. In the early spring, photosynthetic activity resumes under the ice-cover as a result of increased levels of solar radiation and reduced snow-cover. In response, the resident fish move up the water column to feed in the photic zone. Their presence near the lake surface makes the fish more susceptible to angling (Ashley, pers. comm., 1992). The anglers use snowmobiles extensively at this time of year, resulting in a significant impact to the ice surface. Snow

and snow-ice were melted in the snowmobile tracks, which were estimated to cover between one third and one half of the lake surface area. In some areas, ponding was observed in the depressions caused by these vehicles. The important consideration to be made here is the impact of this melting and ponding on the surface albedo.

The Radial Jet

The circulator is supported by a square raft and the jet strikes the raft at the corners (refer to Figure 1.1). The jet, however, extends beyond the raft, entering the water directly, along the sides. This results in the current being strongest in the NNW,WSW,ENE and SSE directions. Measurements were made in these directions, and any dependencies of velocity on the direction of flow have been ignored.

The surface velocities measured using the current meter (Figure 3.12) agree very well with turbulent radial jet theory (see §2.4.4). Measurements at 10, 15 and 20 cm below the water surface are, however, only qualitatively consistent with theory. The maximum depth at which velocities were large enough to measure increased with radial distance from the circulator. This is consistent with the concept that the jet thickness, or entrainment zone should thicken with radial distance. Furthermore, the velocities at a given depth reach a peak then decay, as would be expected as the jet continues to thicken with increasing radius. The vertical velocity gradient reduces rapidly and at a radial distance of 7 m, the velocity is nearly uniform over the top 20 cm.

The motion of the drogues was observed to be qualitatively similar to the velocity relationship shown in Figure 3.12. The average speed in the first 3 to 5 metres was estimated to be in the order of 0.25 m/s. These estimates are consistent with the direct measurements.

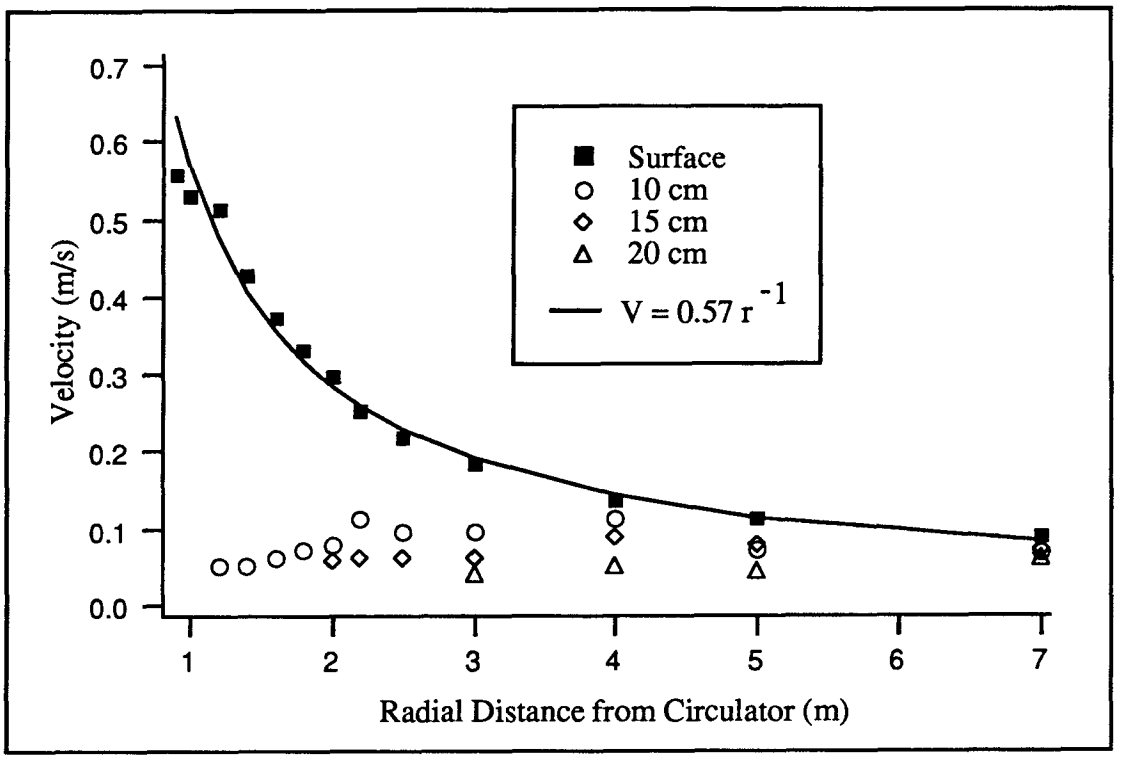

Figure 3.12 Velocity Measurements in Vicinity of Circulator

Chapter 4
NUMERICAL MODEL

In this chapter, the development of MLI and MLI-C is given, along with a discussion on the choice of the many parameters required to run the model.

The ice cover component of the model developed by Patterson & Hamblin (1988) has been extended and adapted to a bulk representation of the lake heat budget (in other words, it is assumed that the small lakes considered are of uniform temperature under ice-cover). The formulation, as described below, is based on the same basic assumptions and equations as those presented in Chapter 2. Improvements to the model include the addition of the following features:

a) a snow-ice component in the heat conduction equation
b) a heat source distributed over the top component of the cover to account for the heat associated with snow-ice formation
c) an extra term in the surface heat budget to account for rainfall
d) sediment heat transfer
e) a variable albedo.
f) a variable snow density and conductivity

In addition, routines were added to account for the impact of artificial circulation in the MLI-C model. These routines feature the following algorithms:

a) an estimate of polynya size based on the balance struck by the meteorological conditions and turbulent heat transfer as caused by the radial jet
b) an estimate of the net turbulent heat transfer between the water and the ice-cover
c) free convection between the atmosphere and the water in the ice-free area
d) cooling due to snowfall on the open water.

Also considered in this chapter are the following issues and parameters:

a) thermal characteristics of the lake sediments,
b) the turbulent heat transfer coefficient, C_t,
c) the area over which turbulent heat transfer to the ice cover is influenced by the radial jet,
d) the thermal gradient at the ice-water interface,
e) the attenuation of solar radiation through the ice and snow cover

4.1 MLI FORMULATION

Patterson & Hamblin (1988) applied a two-band radiation absorption law to the steady state conduction equations for an ice and snow cover. These equations can be extended to include snow-ice as a third component in the cover:

$$K_s \frac{\partial^2 T_s}{\partial z^2} + A_1\lambda_{s1}I_o\exp[-\lambda_{s1}(h_i+h_e+h_s-z)] + A_2\lambda_{s2}I_o\exp[-\lambda_{s2}(h_i+h_e+h_s-z)] + Q_{si} = 0,$$

$$h_i+h_e+h_s \geq z \geq h_i+h_e$$

$$K_e \frac{\partial^2 T_e}{\partial z^2} + A_1\lambda_{e1}I_o\exp[-\lambda_{s1}h_s-\lambda_{e1}(h_i+h_e-z)] + A_2\lambda_{e2}I_o\exp[-\lambda_{s2}h_s-\lambda_{e2}(h_i+h_e-z)]=0,$$

$$h_i+h_e \geq z \geq h_i$$

$$K_i \frac{\partial^2 T_i}{\partial z^2} + A_1\lambda_{i1}I_o\exp[\lambda_{s1}h_s-\lambda_{e1}h_e-\lambda_{i1}(h_i-z)] + A_2\lambda_{i2}I_o\exp[-\lambda_{s2}h_s-\lambda_{e2}h_e-\lambda_{i2}(h_i-z)]=0,$$

$$h_i \geq z \geq 0, \qquad (4.1)$$

where the subscript e refers to the snow-ice layer and all other terms are as previously defined.

The heat source, Q_{si}, accounts for the heat supplied by lake water flooding the ice cover following a heavy snowfall (see §4.3.2). This source of heat, which is assumed to be distributed over the entire snow thickness, includes the sensible heat given up to the snow layer as it cools to the freezing mark, and the latent heat which is produced when this water freezes to form snow-ice. Although it would be more appropriate to add a fourth medium to the lake cover to reflect that this heat is not distributed over the entire snow thickness, the data available are not of a sufficient quality to justify further complicating the governing equations. This process is described in greater detail in Chapter 2.

The appropriate boundary conditions for the above equations are:

$$T_i = T_f \qquad z = 0$$

$$\left.\begin{aligned} T_i &= T_e \\ K_i \frac{\partial T_i}{\partial z} &= K_e \frac{\partial T_e}{\partial z} \end{aligned}\right\} \qquad z = h_i$$

$$\left.\begin{aligned} T_e &= T_s \\ K_e \frac{\partial T_e}{\partial z} &= K_s \frac{\partial T_s}{\partial z} \end{aligned}\right\} \qquad z = h_i + h_e$$

$$T_s = T_o \qquad z = h_i + h_e + h_s \tag{4.2}$$

Again, qo is defined as the conductive heat flux between the ice-cover and the atmosphere:

$$q_o = -K_s \frac{\partial T_s}{\partial z}\bigg|_{z = h_i + h_e + h_s} \tag{4.3}$$

The solution can be written as:

$$\left(\frac{h_i}{K_i}+\frac{h_e}{K_e}+\frac{h_s}{K_s}\right)(q_o-I_o) = T_f - T_o - A_1 I_o \left\{\frac{1-\exp(-\lambda_{s1}h_s)}{K_s\lambda_{s1}} + \frac{\exp(-\lambda_{s1}h_s)[1-\exp(-\lambda_{e1}h_e)]}{K_e\lambda_{e1}} + \frac{\exp(-\lambda_{s1}h_s-\lambda_{e1}h_e)[1-\exp(-\lambda_{i1}h_i)]}{K_i\lambda_{i1}}\right\}$$

$$-A_2 I_o\left\{\frac{1-\exp(-\lambda_{s2}h_s)}{K_s\lambda_{s2}} + \frac{\exp(-\lambda_{s2}h_s)[1-\exp(-\lambda_{e2}h_e)]}{K_e\lambda_{e2}} + \frac{\exp(-\lambda_{s2}h_s-\lambda_{e2}h_e)[1-\exp(-\lambda_{i2}h_i)]}{K_i\lambda_{i2}}\right\}$$

$$+Q_{si}\, h_s\left(\frac{h_i}{K_i}+\frac{h_e}{K_e}+\frac{h_s}{K_s}\right) - \frac{Q_{si}\, h_s^2}{2\, K_s} \tag{4.4}$$

The extension to any number of components is obvious. The surface condition may be expressed as given by Equation (2.9).

Ablation and accretion of ice at the ice-water interface is modeled as given in Chapter 2. The heat flux, q_f, is again obtained from the solution of the heat conduction equation:

$$q_f = -K_i \left.\frac{\partial T_i}{\partial z}\right|_{z=0}$$

$$= q_o - A_1\, I_o\{\, 1 - \exp-(\lambda_{s1}h_s+\lambda_{e1}h_e+\lambda_{i1})\}$$

$$- A_2 I_o\{\, 1 - \exp-(\lambda_{s1}h_s+\lambda_{e1}h_e+\lambda_{i1})\} - Q_{si}\, h_s \tag{4.5}$$

4.2 Bulk Aerodynamic Formulae

The heat balance at the interface between the ice cover and the atmosphere is dependent on meteorological conditions. The components of the balance may be computed using bulk aerodynamic formulae such as those given in TVA (1972), Imberger & Patterson

(1981) and the DYRESM User's Manual. These formulae are given here. Adjustment of the meteorological data for use in the bulk aerodynamic formulae is discussed in §4.5.

The net incoming meteorological flux is given as:

$$H = R_{li} - R_{lo}(T_o) + Q_c(T_o) + Q_e(T_o) + Q_r(T_o) \tag{4.6}$$

The heat supplied by rainfall, Q_r, includes sensible heat as described in §2.4.4 and latent heat as described in §4.3.1. All other terms are as defined in §2.1.3. It is important to note that the heat generated both by solar radiation and ice cover flooding are not included in the balance since they appear in Equation 4.4.

Long-wave radiation is governed by black body radiation principles, and is therefore dependent on the temperature and emissivity of the body in question. The incoming radiation, R_{li}, depends on the characteristics of the sky and is thus more difficult to determine than the outgoing radiation from the lake surface, R_{lo}. R_{li} may be estimated using the Swinbank (Equation 3.7) or Anderson (Equation 3.8) relationships (TVA, 1972):

$$R_{li} = 9.37 \times 10^{-6}\, \sigma\, (T_{air} + 273)^6\, (1+0.17C^2) \tag{4.7}$$

$$R_{li} = (0.74+0.0049\ \text{svpd})\, \sigma\, (T_{air} + 273)^4\, (1+0.17C^2) \tag{4.8}$$

where, R_{li} = incoming long-wave radiation
C = cloud cover (fraction of sky)
svpd = vapour pressure at T_{air}
σ = Stefan - Boltzmann Constant
T_{air} = air temperature

Hamblin (1990), in a study involving a meteorological data set for the Yukon River basin, found that the former relationship was more accurate when the air temperature, T_{air}, is above freezing, while the latter is superior below freezing.

The vapour pressure of the air is calculated from the relative humidity (RH) data and the air temperature (TVA, 1972):

$$svpd = \frac{RH}{100} \exp\left(2.303 \left(\frac{a\ Tair}{Tair+b} + c\right)\right) \tag{4.9}$$

where the constants a,b,c depend on whether open water or ice-covered conditions prevail.

The cloud cover, C, was not directly observed on a daily basis but may be estimated using the solar radiation data. The following relationship is one of three recommended by the TVA (1972) and was found to provide reasonable estimates in Hamblin's (1990) study:

$$C = \sqrt{\frac{\left(1 - \frac{SW}{SWCS}\right)}{0.65}} \tag{4.10}$$

where, SW = observed total daily solar radiation
SWCS = theoretical total daily solar radiation under clear sky conditions.

The theoretical clear sky total includes indirect radiation and depends on the Julian day, latitude, atmospheric attenuation and the local albedo. Details of its calculation are given in Appendix A.

The outgoing radiation, R_{li}, is given as:

$$R_{lo} = \varepsilon\, \sigma\, (T_o + 273.15)^4 \tag{4.11}$$

where, ε = emissivity of the lake surface = 0.97

The sensible heat flux between the lake surface and the atmosphere is governed by forced convection heat transfer principles, and is thus a function of the temperature difference and the wind speed:

$$Q_c = \rho_{air} C_p C_h U_w (T_o - T_{air}) \quad (4.12)$$

where, ρ_{air}= density of air
C_p = heat capacity of water
C_h = dimensionless empirical coefficient
U_w = wind speed

For wind speed measured at 10 m above the lake surface, Imberger & Patterson (1981) recommend $C_h = 1.5 \times 10^{-3}$. Equation 4.12 should be multiplied by the sheltering coefficient described in Chapter 3.

The evaporative heat flux, Q_e, is dependent on the difference between the vapour pressure of the air, svpd, and the saturated pressure, svp0, at the temperature of the lake surface, T_o. In a vacuum, vaporization from the surface would continue until the vacuum reaches saturation pressure. Under atmospheric conditions, however, a vapour blanket at the surface approaches saturation and turbulently diffuses into the air above. The rate of evaporation is therefore also dependent on wind speed:

$$Q_e = C_e U_w (svp0 - svpd) \quad (4.13)$$

where, C_e = a dimensionless empirical coefficient. The saturation vapour pressure, svp0, is given by Equation 4.9, with RH = 100% and T_{air} replaced by T_o, the lake surface temperature. Equation (4.13) also applies in the case of condensation when svpd > svp0. The evaporative flux should also be reduced by the wind sheltering coefficient.

The only variable appearing in the above formulae which was not measured directly or estimated using techniques found in the literature, is T_o, which is provided in the solution to Equation 4.1.

4.3 MLI: Lake in the Natural State

4.3.1 MLI Main Routine

The MLI flow chart is given in Figure 4.1. Once the initial conditions and parameters have been set, the daily loop commences. Within this loop, the daily averages of the measured meteorological variables are read into memory. If snow is present on the ice cover, control is passed to SNOWDENS, the subroutine in which the snow density and conductivity are calculated, and then to SNOWICE where it is determined if flooding of the ice cover occurs.

Subroutine SOLAR is then called, where both SWCS and C are estimated. Since SWCS depends on the local albedo, the ALBEDO subroutine is called from SOLAR.

Control is returned to the main programme where the sub-daily time step begins. Since the internal hydraulics, which can cause rapid changes to thermal structure are ignored, the short sub-daily time steps used in DYRESM are not required. Without resorting to the requirement of sub-daily averages of the meteorological data, a sub-daily time step is only considered appropriate to reflect that solar heating is not distributed over the entire day. The time over which solar heating is active will vary over the ice-covered period but, for simplicity, two 12 hour time steps have been incorporated into MLI, with all of the observed solar radiation applied to the first sub-daily step.

Within the sub-daily time step, the surface temperature, T_o, and the heat fluxes at the surface-atmosphere interface are calculated. Newton's iterative method is used to find T_o from Equation 4.4, with T_{air} used as the initial estimate of T_o. If it is found that T_o is greater than T_m the melting temperature, it is set equal to T_m and subroutine MELT is called to quantify the amount of surface melt. In this case q_o, the flux in the surface

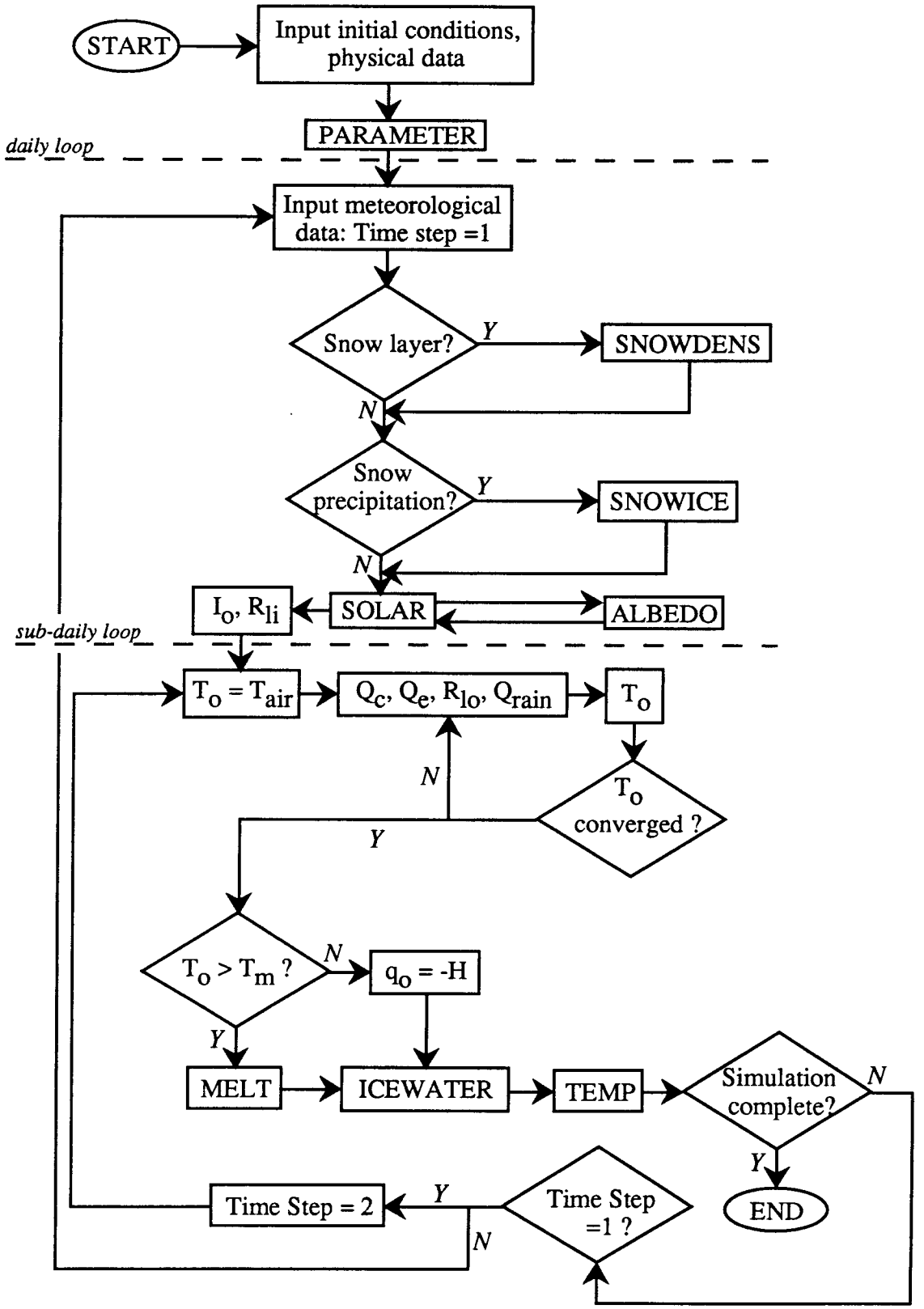

Figure 4.1 MLI Flow Chart

component at the atmospheric interface, is determined from Equation 4.4, with $T_o = T_m$. If T_o is less than T_m, then q_o is set equal to the net meteorological flux, H.

The heat source, Q_{si}, is required in the calculation of T_o described above. It is assumed that the heat is added to the cover at a uniform rate over the entire day. Q_{si} is calculated in Subroutine SNOWICE (§4.3.2).

It has been found that snowmelt due to rainfall is only important compared with condensation melt when total daily rainfall is greater than about 13 cm/day (Harr, 1981). Rainfalls of this magnitude were not observed at Merritt at any time over the winter of 1991-92 (rainfall was observed but not measured at Menzies Lake). However, the rain on snow events of late January may have been significant in increasing the snow-cover temperature from sub-freezing temperatures due to the latent heat of fusion, Q_{rl}, produced upon freezing of the rainwater:

$$Q_{rl} = L \rho_w P, \tag{4.14}$$

where all terms are as previously defined. This heat will increase the temperature of the snow pack and may result in melting if the surface temperature reaches 0 °C. Both the sensible (Equation 2.22) and latent heat (Equation 4.14) associated with rainfall are included in the surface meteorological balance as given by Equation 4.6. It would likely be more realistic to treat the latent heat as an additional internal source of heat in the snow cover. The use of daily meteorological averages, however, results in under-estimation of both condensation melt and sensible heat transfer from the rainfall to the snow. Ideally, the average humidity and air temperature associated with the rainfall period would be used in calculating Q_{rs} and Q_e, not the average daily values. Without the latent heat term in the surface balance, the model would incorrectly predict very little snowmelt. This issue is discussed further in Chapter 5.

From the main programme, subroutine ICEWATER is invoked, where the fluxes q_f and q_w are calculated using Equations 4.5 and 2.12 respectively. These fluxes are used in ICEWATER to determine the change in ice thickness at the ice-water interface as given by Equation 2.11. Finally the net heat transfer to the unfrozen lake is computed in subroutine TEMP. The change in lake heat content is determined by the balance of residual solar energy, I_w, sediment heat transfer, q_{sed}, and the conductive heat flux from the water to the ice, q_w. The formulation of these variables, as applied to MLI, is described in §4.3.2 and §4.3.3. Once the new lake temperature is computed, the time step is incremented. If the new time step is the second of the day, then the procedure is repeated starting from the calculation of T_o and the net meteorological flux, this time with the solar radiation set to zero in Equation 4.4.

4.3.2 MLI Subroutines

SNOWDENS

The SNOWDENS flowchart is given in Figure 4.2 First, the number of days since the last snowfall, is incremented. If no snow has fallen that day, then densification of the snowpack will proceed as follows:

If there are two layers of snow (that is, if there have been two or more snowfalls over the simulation period), then the lower layer is assumed to be at a pre-set maximum. This maximum density is increased to a second pre-set value if the surface temperature T_o is greater than 0^oC. A maximum density which is higher still is assigned if rainfall occurs. Once any accumulated snow has been assigned to a higher maximum density, only newly fallen snow may be characterized by a lesser maximum. The upper layer of snow is assumed to settle according to an exponential decay function:

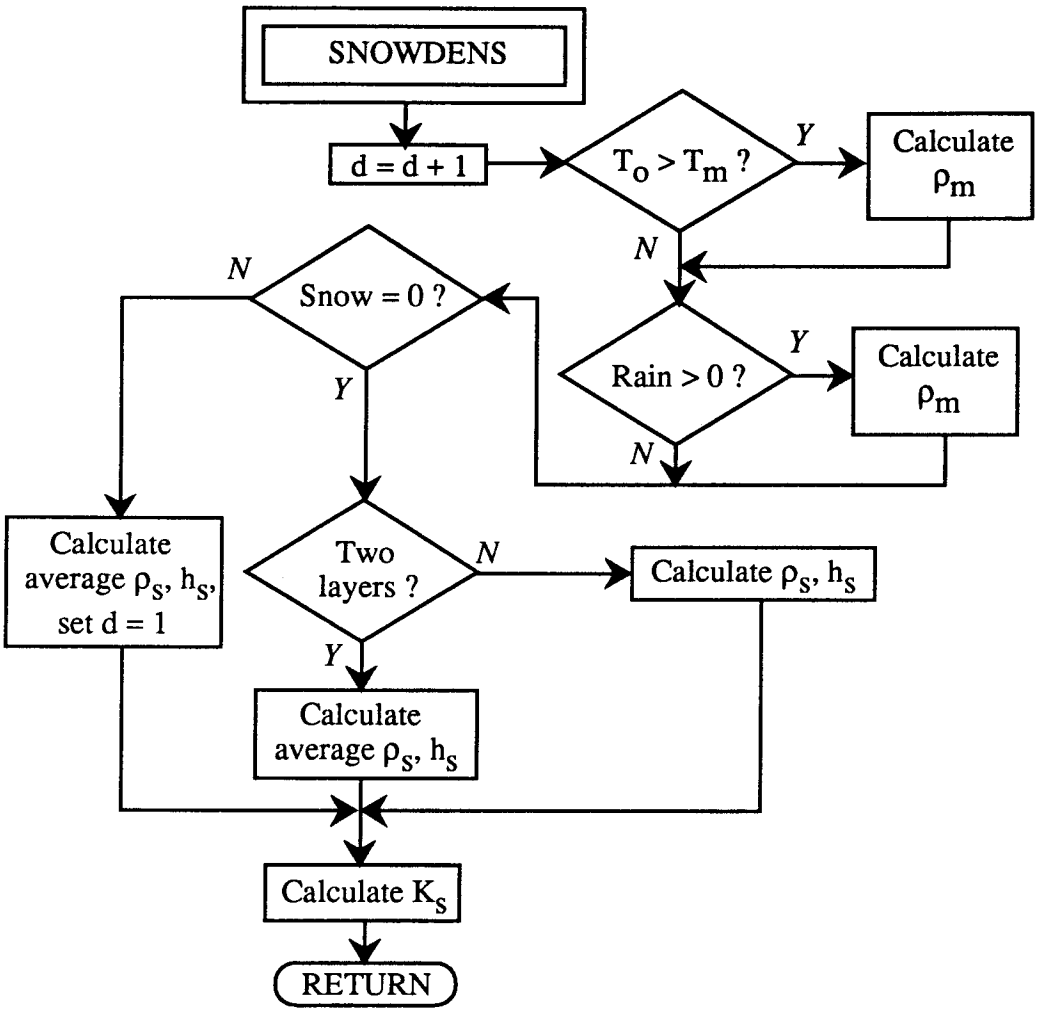

Figure 4.2 SNOWDENS FLOW CHART

$$\rho_s = \rho_n + (\rho_m - \rho_n)(1 - e^{-kd}) \tag{4.15}$$

where, $k = -\ln\left(\frac{\rho_m - \rho_1}{\rho_m - \rho_n}\right)$

ρ_n = density of fresh snow

ρ_1 = density of snow 24 hours after falling

ρ_m = maximum density of snow

d = number of days since the last snowfall

If there is one layer of snow, it is assumed to settle in accordance with the above equation. Although somewhat arbitrary in form, this function will predict densities within the appropriate ranges given in the literature (see §2.3.1), provided that reasonable values for ρ_n, ρ_1 and ρ_m are chosen.

In the case where snowfall occurs, then all of the underlying snow is assumed to be at ρ_m, the fresh snow is set to ρ_n, and d is reset to 1.

The empirical equation given by Grant & Rhea (1973) was specifically considered in choosing an initial density, ρ_n, of 80 kg/m^3 because it is based on observations at an altitude which is comparable to that of Menzies and Harmon Lakes. The density after 24 hours, ρ_1, was set to 100 kg/m^3, and the maximum density, ρ_m, was set to 200 kg/m^3 for $T_o < 0^oC$, or 300 kg/m^3 for $T_o > 0^oC$. These values may be altered somewhat in the testing of MLI in order to produce results which conform with the observations.

It should be noted that the ice cover observed on December 13th, 1991 at Menzies Lake would have been insufficient to support the observed fresh snow cover if the snow density had been greater than about 90 kg/m^3. Hence the assumed fresh snow density of 80 kg/m^3 is unlikely to be too low. On January 19th, for the observed 7.5 cm of snow which was saturated with flooded water, the snow density should have been in the order of 250 kg/m^3. Although fresh snow had fallen on the previous day to cause flooding, at

least two-thirds of the snow cover was old snow. According to the model described above, the average density of the entire snowpack would have been in the order of 230 kg/m^3 which is in good agreement with the first estimate (the maximum density of the underlying snow layer would have been at the highest maximum density on this date due to the rain which fell about a week earlier).

The final steps in SNOWDENS include the calculation of the average density of the entire snow thickness, which is used in Equation 2.16 to determine the conductivity.

SNOWICE

The SNOWICE flowchart is given in Figure 4.3. Equation 2.21, which provides an estimate of snow-ice production, must be modified for the case where a snow-ice layer already exits in the cover:

$$h_{sm} = \frac{h_i (\rho_w - \rho_i) + h_e (\rho_w - \rho_e)}{\rho_s} \tag{4.16}$$

where the subscript e refers to the snow-ice.

The density of snow-ice is generally in the range of 880 to 900 kg/m^3. Lower densities result from finer snow grains (Ashton, 1986). A constant value of 890 kg/m^3 is assumed here.

If h_{sm} is less than the total snow thickness, h_s, including the most recent snowfall, then flooding will occur. The calculations are complicated by the possible existence of two snow layers of different densities. First, Equation 4.16 may be applied using the average snow density to determine if flooding will occur. If so, then the depth of flooding may be calculated in one of several ways depending on the thickness of each snow layer. If two snow layers exist then Equation 4.16 is modified so that the depth of flooding is calculated based on the existence of 4 mediums. Otherwise Equation 4.16 is applied as

shown to determine the maximum snow thickness which can be supported by the ice. The new snow-ice produced, h_{en}, is equal to the difference between h_s and h_{sm}, and is added to the total snow-ice thickness, h_e. Q_{si}, the sensible and latent heat added to the snow layer by virtue of the flooding, is calculated as follows:

$$Q_{si} = (T_w c_{pw} + L)\, \rho_w \frac{h_{en}}{h_s}\left[1 - \frac{\rho_s}{\rho_w}\right] \tag{4.17}$$

where, Q_{si} = heat generated per unit volume of snow
T_w = water temperature
L = latent heat of fusion

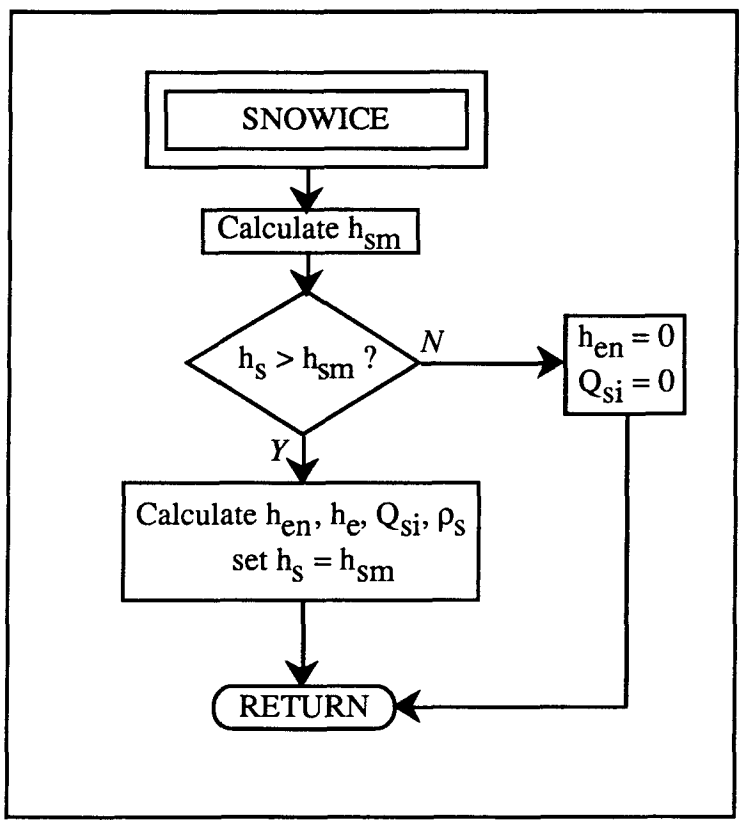

Figure 4.3 SNOWICE FLOW CHART

The factor h_{en}/h_s appears in Equation 4.16 to account for the fact that, although it is assumed that Q_{si} is uniformly distributed over the new value of h_s, in reality it is only distributed over h_{en}. The $(1-\rho_s/\rho_w)$ term is added in recognition of the fact that the water

which seeps into the snow layer must be distributed throughout the snow pore structure (i.e. the thickness h_{en} is composed of both snow and water, but only the water constitutes the heat source). Q_{si} is assumed to be distributed over the entire day.

SOLAR

The SOLAR flowchart is given in Figure 4.4. This subroutine begins with the calculation of, q_s, the total solar radiation at the top of the atmosphere for the given day and atmospheric attenuation. The ALBEDO subroutine is called at this stage, as it is important to the total amount of reflected or indirect solar radiation which could be measured near the lake surface. Hence it is required for the calculation of the theoretical short wave radiation under clear sky conditions, SWCS. The cloud cover, C, is then estimated using Equation 4.10. Since albedo is a function of C however, reiteration of the above steps starting from the call to ALBEDO is required until convergence of C is achieved. Once the first iteration is complete, then a flagging variable is set equal to 1 so that only the cloud dependent calculations are performed in Subroutine ALBEDO. This flag is reset to zero after convergence is achieved. The details involved in the calculation of SWCS is given in Appendix A.

ALBEDO

The ALBEDO flowchart is given in Figure 4.5. In the case where there is no snow layer, the albedo, α, is determined as given in Table 4.1

Table 4.1 Snow-Ice and Pure Ice Albedo (Henderson-Sellars, 1984)

Surface Condition	α
pure ice	0.02
snow-ice	0.45

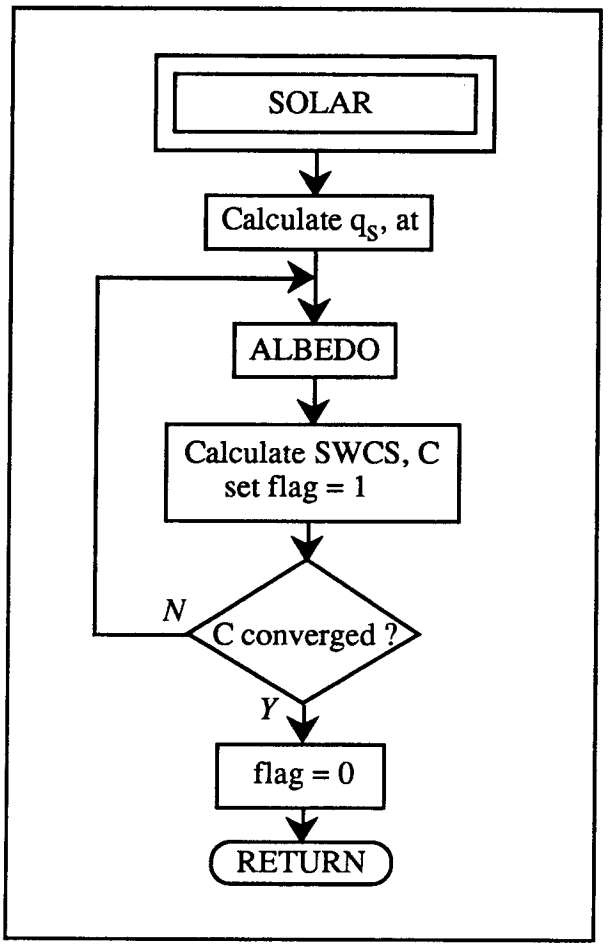

Figure 4.4 SOLAR FLOW CHART

Given the lack of grain size and snow quality data, it would appear that the USACE functions and Petzold's (1977) equations are the only quantitative means of altering the snow albedo for the Menzies and Harmon Lake data set. Tabulated lake albedo information (see §2.3.2) were referenced, in order to determine the applicability of the model.

If new snow has fallen, then d, the number of days since the last snowfall, is set to zero, and the base albedo, α_b, is set to 0.84 as is customary when using the USACE albedo decay functions. This base value is modified in accordance with the sky conditions to produce α. If no snow has fallen, α_b is modified using the aging functions (Equations

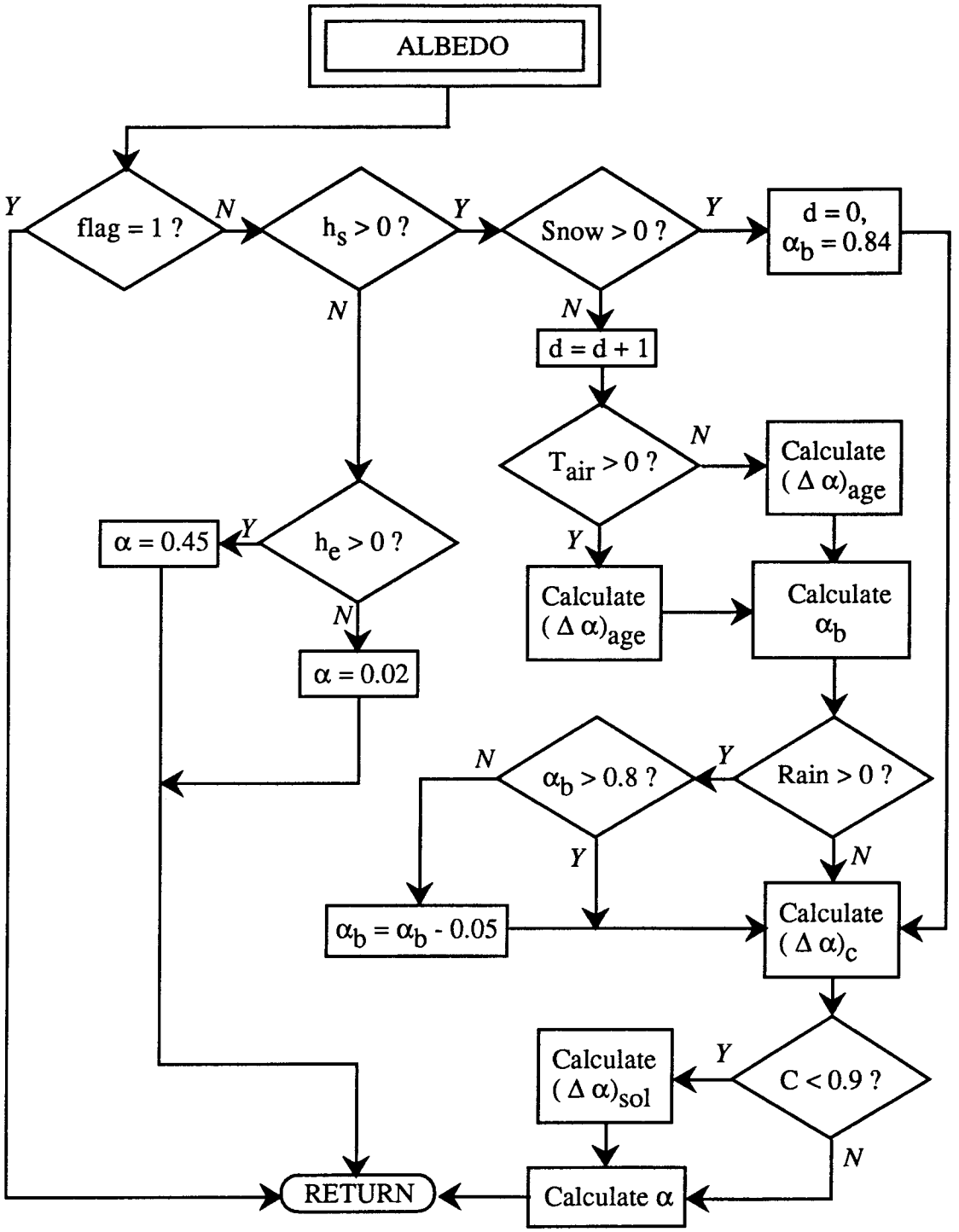

Figure 4.5 ALBEDO FLOW CHART

2.16) prior to the sky condition adjustments. In the case of rain, 0.05 is subtracted from α_b provided that it is not already less than 0.8. These latter adjustments, to account for solar angle and cloud cover are given by Equations 2.19 and 2.20.

Given that Menzies and Harmon Lakes are both remote and well over 1000 m above sea level, snow purity should be high. The solar angle is also low over much of the simulation period. It would therefore be reasonable to suspect that the albedo was often in excess of 0.9 following snow accumulation events. Although the reduction in albedo in the case of rain is arbitrary, albedos which are consistent with this expectation are produced. In addition, results for the full spectrum of observed conditions are within the range given by Henderson-Sellars (1984). Furthermore, a significant reduction in albedo following rain events is justifiable given that an increase in average grain size will result due to fine flake destruction and metamorphosis to granular snow (see Chapter 2). Both Petzold (1977) and Strickland (1982) attributed lower than predicted albedo observations to rainfall.

MELT

The flowchart for MELT is given in Figure 4.6. Since surface melting is taking place, the heat fluxes at the surface, H and q_o, are calculated using $T_o = T_m$. All melting proceeds according to Equation 2.9, with the density set to the value which is characteristic of the surface component whether it be snow, snow-ice or ice. Heat derived from rainfall is included in the surface balance as described in §4.3.1. If the entire top component is melted then the excess heat is used to melt the layer(s) below.

ICEWATER

The flowchart for ICEWATER is given in Figure 4.7. The fluxes, q_f and q_w, at the ice-water interface are calculated using Equations 4.5 and 2.12 respectively. The melt or

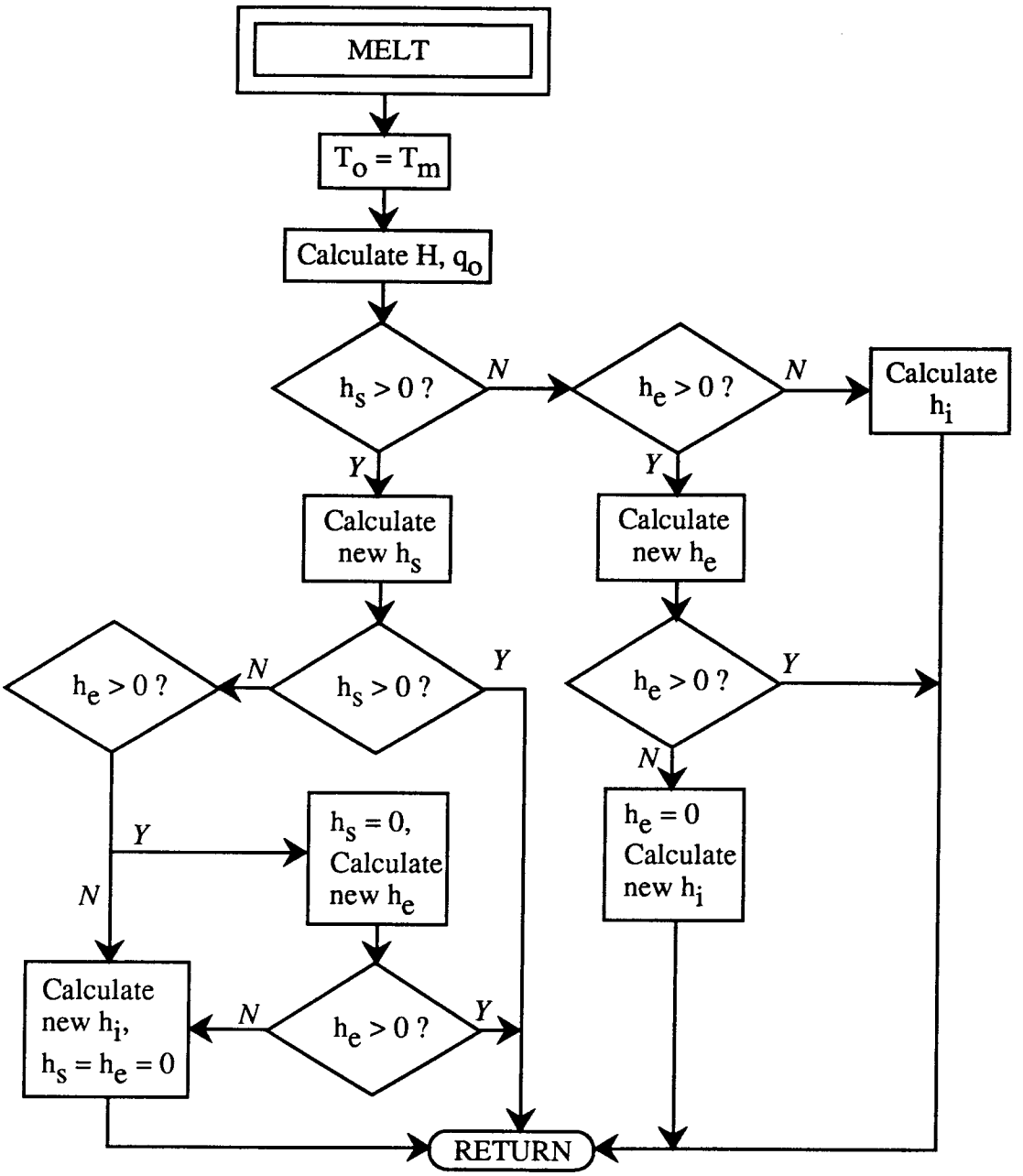

Figure 4.6 MELT FLOW CHART

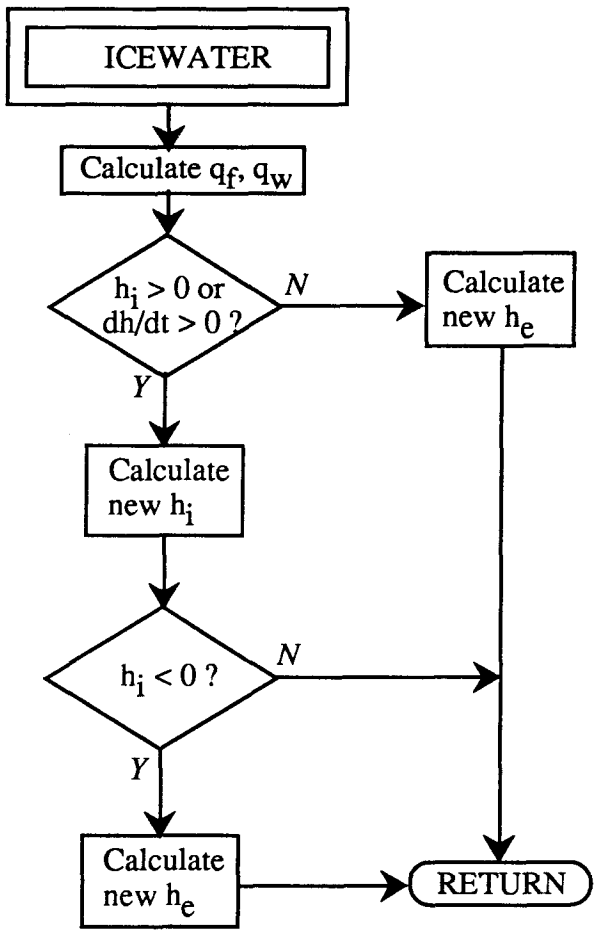

Figure 4.7 ICEWATER FLOW CHART

accretion of ice proceeds in a manner similar to that of subroutine MELT using Equation 2.11. Although melting of either pure or snow-ice may occur, only pure ice may be formed at the ice-water interface. Turbulent heat transfer is assumed to be of importance only in the case of artificial circulation since there is no significant flow-through at the lakes considered. This process is treated in §4.4.

In order to calculate q_w, information regarding the thermal boundary layer at the interface is required. Detailed measurements are not available, but a maximum layer thickness may be estimated from the field data. The shape and thickness of this layer is assumed to be constant over the entire ice-covered period for both Menzies and Harmon Lakes. Temperature measurements made 1 m below the water surface at both lakes (usually about 0.8 to 0.9 m below the ice-water interface, although this distance was not measured) indicated that the boundary layer did not extend to this depth. On March 10th, measurements were made at 0.5 m. At Menzies Lake there was an indication that the boundary layer was just intersected, but the data are inconclusive since the temperature at this depth was only 0.1°C less than at 1.0 m. At Harmon Lake, however, it is clear that the boundary layer had been intersected. Nonetheless, the temperature at 0.5 m (3.3°C) was still much closer to the temperature at 1.0 m (4.1°C) than T_m. In light of this very limited data, a linear decrease from T_w to T_m over a thickness of 0.5 m is considered a reasonable model. The equation for q_w is therefore:

$$q_w = -K_w \left.\frac{\partial T}{\partial z}\right|_{z=0} = -K_w \frac{T_w - T_m}{0.5} \tag{4.18}$$

TEMP

The water temperature, T_w, is calculated in TEMP and control is returned to the main programme where the time step is incremented. Intermediate steps include the calculation of I_w, the energy available to heat the water following reflection at the surface

and absorption in the cover, and Q_{sed}, the sediment heat transfer. The net heat is given by:

$$q_{net} = I_w + Q_{sed} - q_w, \tag{4.19}$$

and the change in temperature in one time step, Δt, is:

$$\Delta T = \frac{q_{net} A_L \Delta t}{V C_{pw} \rho_w} \tag{4.20}$$

where, A_L = lake area
V = lake volume

From §4.1, it can be seen that I_w is calculated as:

$$I_w = A1\ I_o \exp(-\lambda_{s1} h_s - \lambda_{e1} h_e - \lambda_{i1} h_i) + A2\ I_o \exp(-\lambda_{s2} h_s - \lambda_{e2} h_e - \lambda_{i2} h_i) \tag{4.21}$$

The term Q_{sed} is considered in detail in the following section.

4.3.3 Sediment Heat Transfer Estimates

Using Falkenmark's empirical relationship (Ashton, 1986; see Chapter 2) as a guide, the sediment heat budget at both Menzies and Harmon Lakes should constitute roughly 25% of the heat budget of the water compared with only about 8% at Lake Mendota. Since the effect of latitude and altitude may be considered to be reflected in the annual heat budget, average sediment heat transfer rates for both Menzies and Harmon Lakes may be estimated using data available for Lake Mendota and the following formula:

$$(q_{sed})_H = \left(\frac{25}{8}\right) \cdot \frac{(q_{sed})_M \cdot (\theta_L)_H}{(\theta_L)_H} \tag{4.22}$$

where, q_{sed} = sediment heat transfer rate
θ_L = annual heat budget
H = Harmon and Menzies Lake

M = Lake Mendota

The inherent assumption made here is that the sediment heat transfer is proportional to the sediment heat budget.

First it is necessary to determine the appropriate period over which q_{sed} applies at Lake Mendota. All three lakes reach maximum epilimnetic temperatures in mid-August. Data from 1908 (Hutchinson, 1957), however, indicate that fall turnover at Mendota may sometimes occur several weeks before turnover at Menzies and Harmon. With the onset of ice-cover in January, Mendota may often turn over for up to 3 months compared with about 1 month for Harmon and Menzies as observed in 1991. This information suggests that a greater proportion of stored heat is released during turnover at Mendota, and that the flux of 2.9 W/m^2 calculated by Birge et al. (1927) may be appropriate in spite of the two weeks of ice-free conditions that the associated period includes. Furthermore, data for use in the MLI model is available starting only two days before the beginning of the period considered by Birge et al. (1927).

Estimates of the annual heat budget, θ_L, are also required. For small lakes it is important to include the latent heat required to melt the maximum observed ice thickness, in addition to the heat needed to bring the ice to the melting temperature (Hutchinson, 1957) Excluding heat absorbed by the sediments, $(\theta_L)_M$ is 924 MJ/m^2 (Birge et al., 1927). Using the data collected in 1991-1992, $(\theta_L)_H$ is estimated at 562 MJ/m^2 for Menzies Lake, and 549 MJ/m^2 for Harmon Lake. It has been assumed that the maximum heat content associated with the hottest summer is 110% of the maximum heat content observed in the summer of 1991. Similarly, a factor of 90% was applied to the minimum heat content observed over the winter period. It is interesting to note that in spite of the severe winter cooling due to artificial circulation at Menzies Lake, the annual heat budget, and therefore the expected sediment heat transfer rate is almost equal to that at

Harmon Lake. This is a reasonable result, however, given that the two lakes are about 5 km apart, are at approximately the same elevation, and are similar with regard to chemistry and sediment type. Using Equation 4.22, the expected average sediment heat transfer rate is 5 W/m^2.

For comparison, the sediment heat transfer rate can also be estimated using Equation 2.13 and an appropriate sediment conductivity. T_y was estimated using the temperature data collected from June 4, 1991 to April 18, 1992. The temperatures measured over the depth of the water column were weighted in accordance with the lake morphometry in order to compute the whole lake average temperature, T_{avg}, on the date of each field visit (field visits varied in frequency from once a week to once every three weeks). The annual average T_y was approximated by weighting T_{avg} in accordance with the sampling frequency. From the literature, an average conductivity of 1.2 W/m^oC produces a heat transfer rate of about 2.8 W/m^2 at Harmon Lake, if an average T_w of 3^oC is assumed. This is only about half the rate estimated using Falkenmark's (Ashton, 1986) empirical result.

The average rate could very well be even lower than the second estimate, however, given the qualitative similarity between the lake sediments of this study and the Wisconsin Lake sediments for which Likens & Johnson (1969) reported conductivities equal to that of water (about 0.6 $W/m/^oC$). The deep sediments at Menzies and Harmon Lakes are soft and highly organic. A spherical 25 kg anchor lowered from the water surface was observed to penetrate over 0.5 m into the sediments. No qualitative observations, however, were made of the shallow (epilimnetic) sediments from which the bulk of the heat transfer would be expected to originate. Since finer grained material would not be expected to settle out in the littoral zone as readily as in the relatively quiescent hypolimnion, it would be reasonable to expect coarser, more conductive sediments in the shallow regions of the lakes. Furthermore, as suggested in Chapter 2, low level

turbulence under the ice cover may lead to greater heat transfer rates than predicted by the conduction equation.

Clearly, further work is required to better quantify sediment heat transfer. As a first estimate, however, the second method (Equation 2.14), using an average conductivity of 1.2 W/m^{o}C, was selected for use in MLI since it is based on theoretical considerations.

4.4 MLI-C: Artificially Circulated Lake

The MLI model is a one-dimensional balance of heat flux across an ice and snow cover. All fluxes are assumed to be uniformly distributed over the entire lake area. It has been modified, however, in order to account for the non-distributed effect of the Air-o-lator® device. The procedure for calculating the net heat transfer across both the polynya and the ice-covered area is similar to that used by Patterson & Hamblin (1988) to account for the effect of a partial ice cover. The modified version, MLI-C, is described here.

The new key variables which must be calculated at each time step is the radius of the polynya generated by the circulator, and the turbulent heat flux from the water to the ice in the vicinity of the polynya. It is assumed that the polynya is circular at all times, with the circulator at the centre. Beyond its importance with respect to sensible and evaporative heat loss, the wind is neglected as far as the shape of the polynya and the surface currents are concerned. This is reasonable given that, upwind of the circulator, surface currents are impeded while downwind they are assisted by the wind. The lake morphometry may also play a role in the polynya shape and size, but this possiblity has also been ignored.

Little information is available regarding the shape and other characteristics of the transition region between the open water and full ice and snow cover. This region may

be of significant importance to the flow regime, and hence the heat transfer at the ice-water interface. The lack of information described above, however, is such that prediction of the shape of the transition region is not justified. Instead, a simple model, based on the assumption that there is an abrupt change from open water conditions to some minimum ice thickness, will be employed to calculate the polynya radius, and an average turbulent heat transfer from the water to the ice.

All heat fluxes across the lake surface, including the polynya and the ice at the polynya edge, are shown in Figure 4.8. Details are given in the sections that follow.

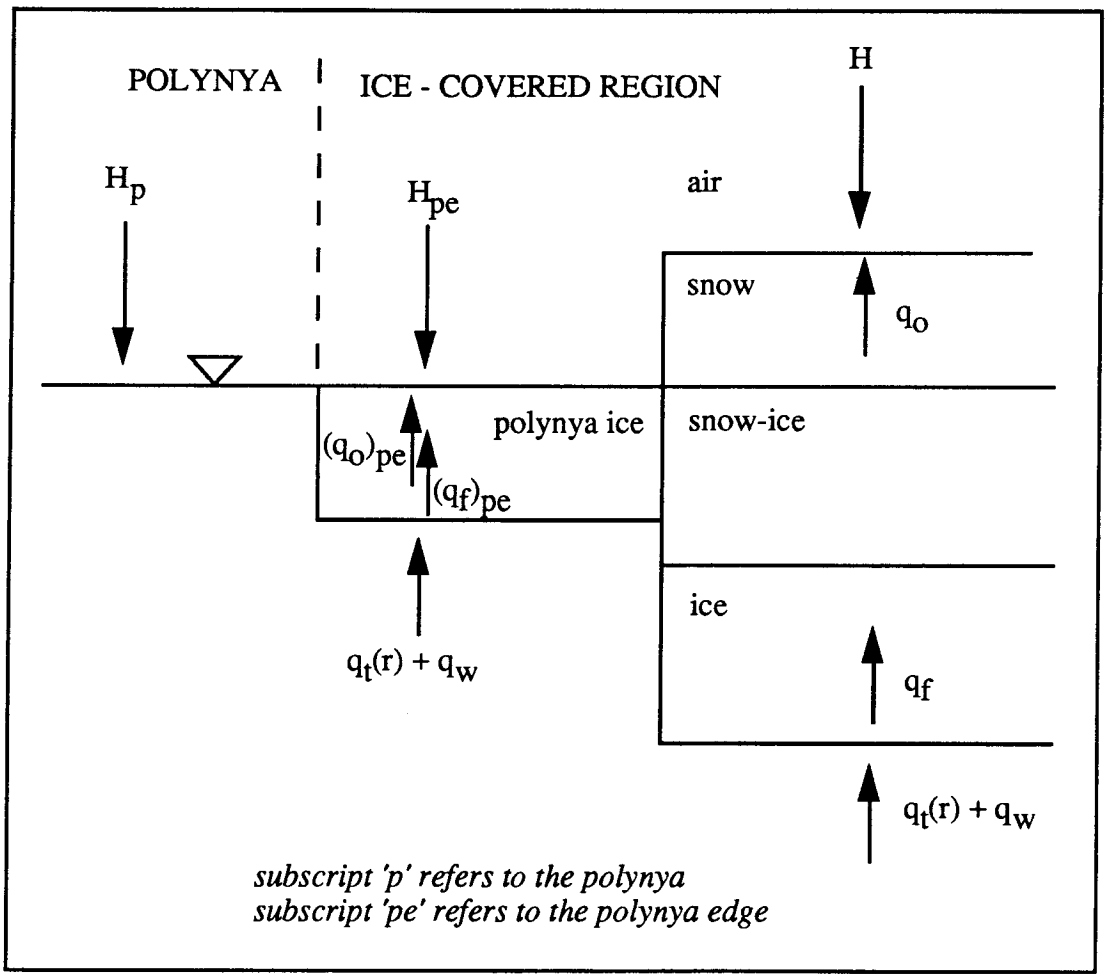

Figure 4.8 Heat Fluxes Across Ice-covered and Ice-Free Zones of Lake

Just as MLI requires the input of initial non-zero ice cover conditions, MLI-C requires input of an initial polynya radius (although a radius equal to the average lake radius should work as well, under ice-free conditions). The second input parameter required is the flow rate, Q, of the Air-o-lator®. Here it is assumed that the surface velocities produced are proportional to Q and inversely proportional to r, the radial distance away from the centre of the device. Detailed measurements were made of the surface velocity at Menzies Lake, which clearly varies as r^{-1} as shown in Figure 3.12. These measurements are consistent with the theoretical centerline velocity for an unconstrained radial jet (see §2.4.4). From these measurements the following relationship was derived:

$$U = \frac{6.13\,Q}{r} \tag{4.23}$$

It should be noted that the above relationship is only appropriate for the Air-o-lator® device complete with flow deflector, as shown in Figure 1.1 (item #1).

4.4.1 MLI-C Subroutines

Three new subroutines are added to MLI to account for the effect of the circulator. The POLYNYA subroutine is called just before the average lake temperature is calculated in subroutine TEMP. From POLYNYA, where the heat fluxes between the atmosphere and the open water are calculated, subroutine NEWAREA is called to compute any change in the polynya radius. If, in this latter routine, it is determined that surface melting of the ice should occur at the polynya edge, the quantity of melt is determined in subroutine MELTPE.

POLYNYA

Subroutine POLYNYA is responsible for the calculation of the heat fluxes across the air-water interface and the turbulent heat flux, $\bar{Q}_t$, from the water to the ice. In general, Equations 4.6 to 4.13 are employed with T_o replaced by T_w, the mean water temperature. Further modifications include recalculation of the non-reflected solar radiation to account for the much lower albedo of the open water and re-evaluation of the saturated vapour pressure (Equation 4.9) using the appropriate coefficients for water. In addition to these modifications, two additional fluxes are included in the surface heat balance to account for cooling due to snowfall on the open water (Equation 2.27) and the increase in the evaporative heat flux due to free convection (Equations 2.25 and 2.26). This latter flux is only applied when the water temperature is greater than the air temperature. The net heat transfer across the polynya, H_p, is given by Equation 2.28.

The heat loss from the lake across the polynya area is insufficient in explaining the low water temperatures observed at Menzies Lake. In addition to conduction of heat through the ice cover, the remaining heat loss is due to the turbulent heat transfer, $\bar{Q}_t$, from the water to the ice in the vicinity of the polynya. The extent of the zone in which turbulent heat transfer is important is unknown. This significant heat transfer mechanism may only be of importance over a small area in the vicinity of the ice-free patch. An important consideration which has not been dealt with is the profile of the ice edge. The steady state profile may be such that the flow is deflected downwards to such an extent that, beyond a short transition zone, the velocities at the interface may be negligible. At the other extreme, the transition to full ice thickness may be so smooth that, outside a thin boundary layer the interface velocities continue to vary as r^{-1} with no discontinuity at the ice edge. The average heat transfer, $\bar{Q}_t$, will be estimated by integrating q_t as defined by

Equation 2.30 (see Subroutine NEWAREA) from the ice edge to some radial distance, r_∞ away from the edge:

$$\bar{Q}_t = \frac{2\pi}{A_L - A_p} \int_{r_p}^{r_\infty} q_t \, r \, dr = \frac{12.26\pi \, C_t \, \rho_w \, c_p \, Q \, (T_w - T_m) \, (r_\infty - r_p)}{A_L - A_p} \tag{4.24}$$

where A_p = polynya area
r_p = polynya radius

The radial distance, r_∞, will be determined by calibration of the model. It is assumed that this parameter varies with the size of the polynya. If friction dissipates the velocity to a negligible value over the same distance under the ice, regardless of r_p, then the calibration parameter becomes Δr. Therefore $r_\infty = r_p + \Delta r$. The value of C_t, the turbulent heat transfer coefficient, is discussed in the section on Subroutine NEWAREA which follows.

NEWAREA

The flowchart for Subroutine NEWAREA is given in Figure 4.9 (note that most variables shown in the figure are modified by the subscript 'pe' in the model to indicate values associated with the polynya edge). The polynya size is determined at each time step in NEWAREA in a manner similar to the calculation of the ablation and accretion of ice at the ice-water interface for a lake with full ice cover. In this case, the change in ice thickness at the polynya edge is determined as follows:

$$\frac{dh}{dt} = \frac{(q_f)_{pe} - q_w - q_t}{\rho_e \cdot L} \tag{4.25}$$

where, $(q_f)_{pe}$= the flux of heat through the ice at the ice-water interface of the polynya edge,

and all other terms are as previously defined.

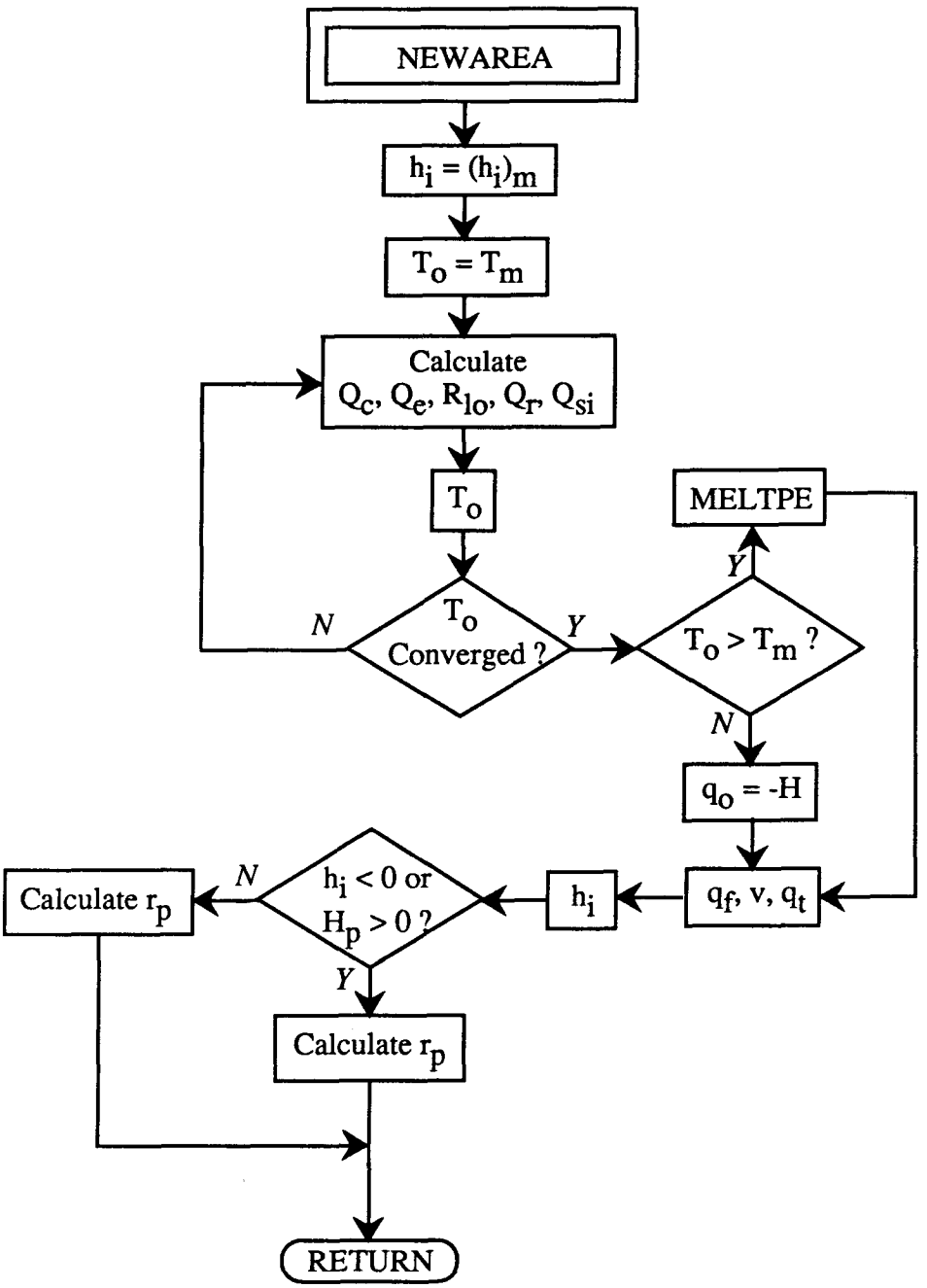

Figure 4.9 NEWAREA FLOW CHART

* *hi, To, Qc, Qe, Rlo, Qr, Qsi, qo, Hp and qf should be modified by the subscript 'pe' to indicate values associated with polynya edge*

The molecular heat flux from water to ice, q_w, is calculated using Equation 4.18. More difficult is the evaluation of q_t which is expected to decrease rapidly with distance from the circulator, possibly in accordance with the empirical surface velocity relationship (Equation 4.23). The turbulent heat flux, q_t, will be assumed to be dependent on the surface velocity, U, and the difference between the water temperature and the melting temperature. The appropriate equation will have the same form as that given in Hamblin & Carmack (1990):

$$q_t = C_t \rho_w Cp\, U(T_w - T_m) \tag{2.30}$$

As described in Chapter 2, the velocity used in Equation 2.30 should be measured 1.0 m below the ice-water interface. In all probability, a velocity at 1.0 m is inappropriate given that the sensible heat transfer equation was developed for a flow which can be considered uniform with depth as in the case of an inflowing or outflowing river (see Hamblin & Carmack, 1990). Similarly, the coefficient C_t is possibly only appropriate for these types of situations. Here C_t must account for the turbulence generated by the circulator and the shape of the boundary layer at the ice-water interface. This value of C_t may require adjustment in order to achieve good agreement with observations. However, a unique value for C_t is conveniently available using the information given in §2.4.3 and the flow field observations of §3.2.4. As can be seen in Figure 3.12, the velocity over the top 20 cm tends to uniformity as the jet moves towards the polynya edge. Right at the edge it is likely that uniformity exists over a much greater thickness. It may therefore be reasonable to treat the extrapolated radial velocity given by Equation 4.23 as the free-stream velocity, U, in Equations 2.30 and 2.35. Given that the radial jet velocity varies as r^{-1}, Equation 2.35 may be used to calculate a constant value of C_t, if x is set equal to r. By inserting Equation 4.23 into Equation 2.35, this value is 5.9×10^{-4}. This number is at the low end, but within the range given by Hamblin & Carmack (1990).

This value of C_t, however, cannot be considered reliable since it is based on experimental work using a laminar, uniform and uni-directional free velocity field. It is more likely that C_t is at the high end or above the range given by Hamblin & Carmack (1990) given that the radial surface jet produces maximum velocities which are less than 1 m from the ice-water interface. In the river flow examples by Hamblin & Carmack (1990), the velocities decreased monotonically from 1 m to meet the no-slip condition at the interface. In any event, it is reasonable to suspect that the velocity profile within 1 m of the interface is unique for this problem and C_t must be determined by calibration.

The heat flux through the ice at the ice-water interface, q_f, as calculated for the ice-covered area of the lake, is inappropriate for the polynya edge. First, to be consistent with field observations, the snow layer is removed in the vicinity of the edge. Furthermore, the minimum ice thickness, h_{min}, concept employed by Patterson & Hamblin (1988) to account for partial ice cover is assumed to apply to the ice at the polynya edge. This minimum thickness should, based on observations, be less than the 10 cm employed by Patterson & Hamblin (1988). It will, however, be used as an additional calibration constant for the model (see Chapter 5). In addition, this thickness will be assumed to consist entirely of white ice, as field observations have indicated. This latter assumption is supported by the fact that lake surface agitation (such as that produced by the circulator) will lead to granular white ice during freeze-up (Gray & Male, 1981). (It is assumed that the properties of white ice are the same as snow-ice). A new value of T_o is calculated for this white ice layer in order to determine if melting will occur at the surface. For the polynya size to increase, the entire ice layer must be melted at the radius defined by the location of the polynya edge. Here, an average value of q_f could be employed to reflect the ice thickness over the course of the time step as it reduces to zero. However, given that the model requires calibration using three constants (Δr, C_t, and h_{min}), calculation of an average value using an integration technique is

unjustified. It is therefore only important that the value of q_f reflect the relative day to day changes in meteorological fluxes. This will be achieved for q_f defined at any reasonable value of h_{min}.

In the above procedure it is assumed that there is an immediate transition from open water to full ice cover. This being said, it should be noted that it is also assumed that the ice cover has no effect on the surface velocity as given by Equation 4.23.

The computational procedure begins with calculation of the heat fluxes at the surface in the same manner as for the fully covered ice region. T_o, here the temperature of the white ice surface at the polynya edge, is again determined using Newton's iterative procedure. The heat associated with flooding, Q_{si}, is included in the polynya ice model, and, in this case, is assumed to be distributed over the entire ice thickness. Melting may occur at the surface just as it does for the rest of the lake. This process is quantified in Subroutine MELTPE.

At this stage, the change in ice thickness at the polynya edge is calculated using Equation 4.25. If the new ice thickness is less than zero, then the polynya is assumed to be undergoing expansion, and Equations 4.23, 4.25 and 2.30 are solved for r, the radius at which the polynya edge ice thickness is completely melted over the time step. If Equation 4.25 produces an ice thickness which is greater than zero, contraction of the polynya occurs and these equations are again solved simultaneously. In this case however, q_f and q_w are replaced by H_p, the net meteorological flux between the open water and the atmosphere, in Equation 4.23:

$$\frac{dh}{dt} = \frac{-H_p - q_t}{\rho_e L} \tag{4.26}$$

This is done to reflect the fact that accretion is assumed to be occurring on the face of the ice edge, where it is exposed to H_p. Melting, on the other hand, is assumed to occur at the bottom of the ice cover. This point is discussed further in Chapter 5.

MELTPE

Subroutine MELTPE is equivalent to Subroutine MELT, except that it is only applicable to the polynya edge. It is much simpler than MELT because of the assumption that only white ice exists in this region. The surface temperature, T_o, is set to T_m, and the net meteorological flux, H, and the flux through the ice at the air-ice interface, q_o, are calculated. The imbalance between these fluxes determines the amount of ice which is melted (Equation 2.9). The modified ice thickness at the polynya edge is calculated and control is returned to Subroutine NEWAREA.

Modifications to Subroutine TEMP

Subroutine TEMP must be modified to include the heat transfer terms related to the circulator. To Equation 4.17 must be added the turbulent heat flux from the water to the ice, $\bar{Q}_t$ and the net heat transfer across the polynya, H_p:

$$q_{net} = H_p + I_w + q_{sed} - q_w - \bar{Q}_t \tag{4.27}$$

The components of q_{net} are scaled appropriately to equivalent values which all apply over the same area.

4.5 Data Preparation

Some of the data retrieved from the datalogger must be adjusted and transformed in units of measurement required by MLI-C. Wind data is required for a point 10 metres above

the lake surface. Following the National Research Council of Canada (1985), a power relationship describing wind speed profiles was used to transform wind speed at 2.0 m to wind speed at 10.0 m. The appropriate correction factor is 1.25. Although the air temperature was not measured at the correct height for strictly proper use in the bulk aerodynamic equations, a simple correction factor is not available. The development of thermal inversions is extremely important in determining the nature of the boundary layer above the surface. Strong inversions would have occurred and persisted over more than half the average day in mid-winter. These inversions would become weaker and shorter in duration as melting conditions began to predominate (Geiger, 1965). Therefore, a characteristic daily average thermal profile which is applicable to the entire ice-covered period does not exist. Furthermore, the coefficient C_h in Equation 4.12 was determined using data for ice-free conditions and may not be appropriate for a lake with ice cover. As these difficulties are beyond the scope of this investigation, the raw temperature data will remain unmodified for use in the model.

The solar radiation data required integration to give daily totals. The radiation is assumed to remain constant over the half hour period surrounding the time of measurement. The total, therefore, is equal to the sum of the products of each measurement and the sampling period. For all other meteorological data, daily averages were calculated using the 48 half hour readings.

4.6 Summary of Parameters

A summary of the values chosen for the parameters required for MLI and/or MLI-C are given in Table 4.2. Some of these parameters will be varied to determine the sensitivity of the model to their values or adjusted for calibration purposes (Chapter 5). With regard to solar attenuation, it is clear from the literature (and intuition) that λ_e should lie

between λ_i and λ_s. Therefore an average of λ_s and λ_i as given by Patterson & Hamblin (1988) was selected as an appropriate first estimate of λ_e. Similarly, the conductivity of snow-ice should lie in between that of snow and that of ice. Since the voids in the snow are filled with water and subsequently frozen, it is reasonable to expect K_e to be closer to K_i than K_s. A value of 2.0 W/m°C was selected.

Table 4.2 Summary of Parameters

Parameter	Value	Comment
λ_{i1}	1.50 m^{-1}	see Patterson & Hamblin (1988)
λ_{s1}	6.00 m^{-1}	see Patterson & Hamblin (1988)
λ_{e1}	3.75 m^{-1}	see text above
λ_{i2}	20 m^{-1}	see Patterson & Hamblin (1988)
λ_{s2}	20 m^{-1}	see Patterson & Hamblin (1988)
λ_{e2}	20 m^{-1}	see text above
K_s	Equation 2.16	see §2.4.1
K_i	2.3 W/m/°C	see Patterson & Hamblin (1988)
K_s	2.0 W/m/°C	see text above
K_s	1.2 W/m/°C	see §4.3.3
ρ_i	917 kg/m^3	see Patterson & Hamblin (1988)
ρ_e	890 kg/m^3	see Ashton (1986)
ρ_i	Equation 4.15	see §4.3.2
C_t	***	*** calibration constant (see §5)
h_{min}	<0.10 m	see §4.4.1
Δr	***	*** calibration constant (see §5)
α_s	variable	see §4.3.2
α_i	0.02	see §4.3.2
α_{si}	0.45	see §4.3.2
α_w	0.06	see §2.4.2
ρ_n	80 kg/m^3	see §4.3.2
ρ_1	100 kg/m^3	see §4.3.2
ρ_m	200 - 300 kg/m^3	see §4.3.2

Chapter 5
RESULTS AND DISCUSSION

The models described in Chapter 4 were written in BASIC and run on an 80386 DX (25 MHz) PC equipped with an 80387 math co-processor. For 105 days of data, less than 10 seconds were required to produce results for either MLI or MLI-C.

5.1 LAKE IN NATURAL STATE

The results produced by MLI for Harmon Lake using the default parameters given in §4.6 are shown in Figure 5.1. Given the approximations made in the development of the model, the results are very good. The estimated errors in the observations account for most of the difference between the observed and predicted variable. It will be shown that reasonable variations in some of the default parameters provide an improved fit to the observations. The model continues to provide good predictions even in late March when an ice-zone 1 to 4 metres in width around the perimeter of Harmon Lake was observed. This observation emphasizes the fact that, although assumed to be uniform, the ice thickness can be highly variable over the lake surface. Results using the DYRESMI formulation are also given in Figure 5.1. A detailed analysis of the results follow the proceeding discussion on the observation errors, which are needed in order to assess the model's success in deciphering nature's work.

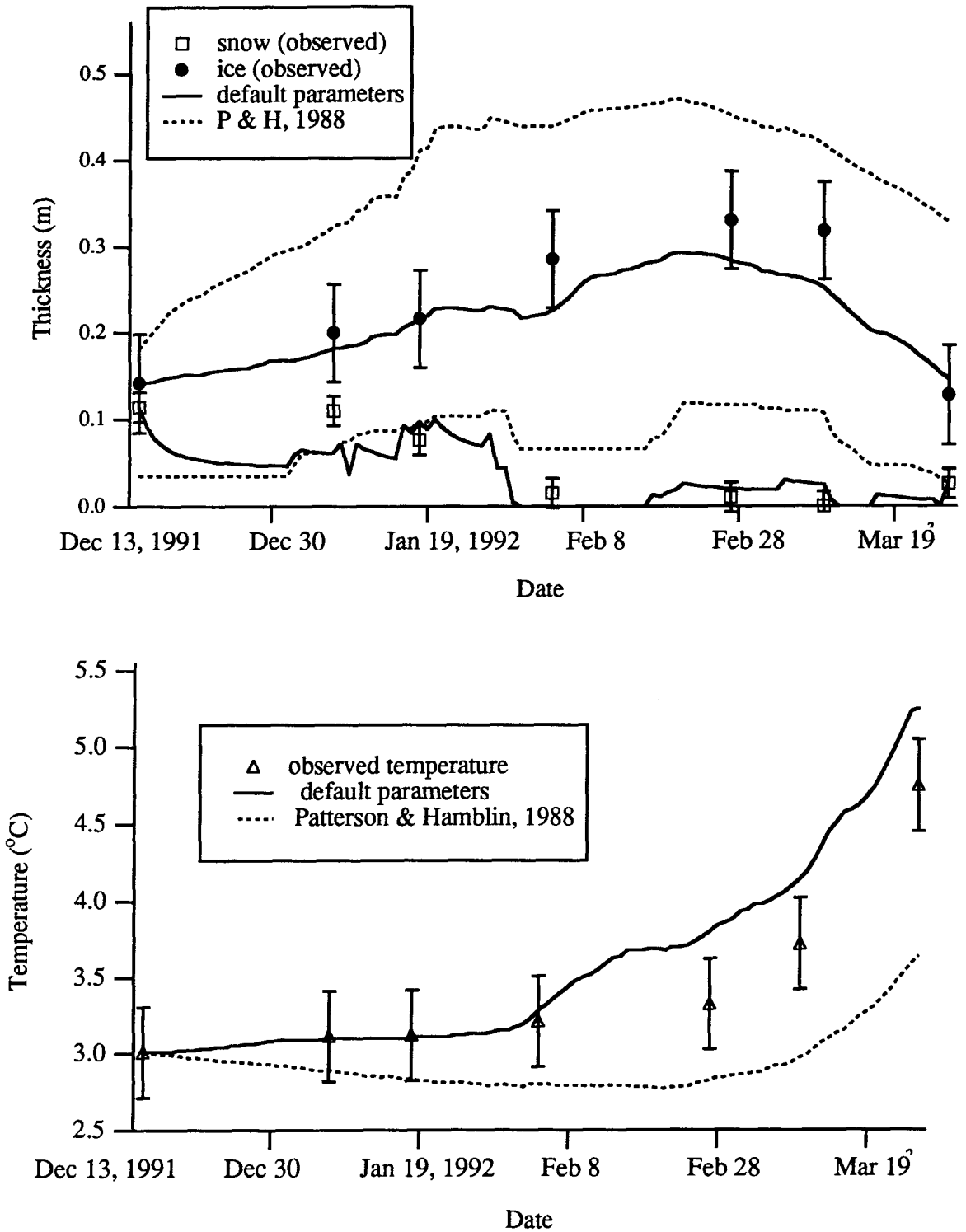

Figure 5.1 Ice and Snow Thickness and Whole Lake Temperature at Harmon Lake: A Comparison of Results Using MLI and Patterson & Hamblin's (1988) Model

5.1.1 Observation Errors

The error in the ice and snow observations were estimated using all of the thicknesses observed at the two Menzies Lake stations over the simulation period. The thicknesses observed at Station 1 were plotted as a function of the thicknesses at Station 2, and a linear regression was performed. The error bars shown in Figure 5.1 represents ± 2 standard deviations from the regression line. With regard to the ice thickness, this error was assumed to be applicable to both lakes. At Harmon Lake, the expected error would be larger given that measurements were only taken at one station. However, there is also less expected variability over the entire lake surface because there is no circulation device in operation which may be responsible for horizontal variability at a scale that is comparable to the lake length. It is assumed that the impact of the first factor on the standard error negates the second. Turning to snow thickness, the standard error for the measurements at Harmon Lake must be greater than that at Menzies Lake given that these measurements were only made at one station. If it is assumed that the variance of the regression is equal to the variance of the sample mean from the population mean (this is reasonable for the almost uniform distribution of snow thickness), and that the true population variance is the same at both lakes, then the sample variance for the Harmon Lake snow thickness data may be estimated by the Law of Large Numbers:

$$\sigma_x^2 = \frac{\sigma^2}{N}$$

where, σ_x^2 = variance of the sample mean from the population mean
σ = population mean
N = number of samples

Since N=1 at Harmon Lake, and N=2 at Menzies Lake, a reasonable estimate of the sample variance at Harmon Lake would be twice that at Menzies Lake.

With regard to whole lake temperature observations, the temperature probe is considered accurate to ±0.3°C by the manufacturers. This error may be considered too large given the following reasons:

a) periodic checks with a precision mercury thermometer indicated ±0.1°C accuracy
b) whole lake temperature data is based on 16 measurements

However, given the following additional sources of error, an accuracy of ±0.3°C is considered reasonable:

a) there is error in the morphometric data used to calculate the whole lake temperatures
b) interpolation between measurement depths was required
c) horizontal variations in temperature due to sediment heat transfer were not considered.

5.1.2 Analysis of MLI Predictions

A Comparison with DYRESMI

The MLI model provides an improved prediction of a mid-latitude lake winter heat budget over the DYRESMI model. Considering the latter model first, the initial predicted total ice and snow thicknesses do not match with observations because the initial ice thickness could not support the weight of the observed snow (Figure 5.1). This is explained by the high snow density assumed to be appropriate for the lakes considered by Patterson & Hamblin (1988). Hence DYRESMI predicts instant flooding of the ice cover from the initial conditions. Furthermore, DYRESMI predicts ice thicknesses almost 50% greater than the observations throughout most of the modeling period. This is primarily due to the relatively high snow conductivity associated with the assumed density. Using Equation 2.15 and the range of densities considered in this investigation,

MLI predicts snow conductivities of about 20% to 60% of the constant value of 0.31 W/m°C assumed in DYRESMI.

In addition, the DYRESMI model generally over-predicts the snow thickness for two principal reasons. First, it is assumed that no settling or wind transport of snow occurs, and secondly, rain melt is ignored. Some surface melt is predicted by DYRESMI at the end of January, when most of the rain fell, because the meteorological flux balance produces a surface temperature of 0°C on several consecutive days. Neglect of heat released to the snow cover due to flooding may also contribute to the inadequate snowmelt predicted by DYRESMI.

It should be noted that, in spite of the deficiencies of DYRESMI, the trend in ice thickness is very well predicted from mid-January until the end of the modeling period. Although the rate of ice melt is somewhat under-predicted in March, the predicted rates are only marginally less than MLI predictions, and furthermore, explanations involving the quality of the meteorological input data are available (see Chapter 3). This is in spite of significant discrepancies in snow thickness prediction. This is, for the most part, due to the fact that excess snow is converted to pure ice in DYRESMI, not snow-ice. This results in much less attenuation of solar energy through the total ice thickness, thereby offsetting the effect of the thick snow layer. Also, as stated earlier, the conductivity of the DYRESMI snow is much greater than that of the relatively thin MLI snow layer, which tends to increase the heat flux into the lake during the melting phase. The same may be said of the pure ice which DYRESMI produces as a result of ice cover flooding. Furthermore, DYRESMI predicts a much lower albedo ($\alpha = 0.6$) than MLI for a brief period due to above zero air temperatures immediately following the mid-March snowfall.

Turning to lake temperature, DYRESMI predicts cooling over the first two month of the simulation because of the neglect of sediment heat transfer. Less solar heating is also predicted during some periods when over-prediction of snow and ice thicknesses occur. DYRESMI also under-predicts the rapid increase in lake temperature in March. This can only be explained by an under-prediction of solar penetration. There are two major factors which lead to this result. First, MLI, on average, predicts a lower albedo than DYRESMI over the latter period of the simulation. Secondly, there is high solar attenuation through the thick snow and ice cover which is not completely offset by the lack of snow-ice as described above.

Where Improvement is Needed

The MLI predictions are almost always within the observations of total ice and snow thickness, as well as temperature. Consideration will now be given to where possible problems lie, and how results could be improved. The most notable deviation from observation is the snow thickness prediction in early January. As described in Chapter 4, the initial snow density could have been no more than about 90 kg/m^3 to be supported by the observed ice thickness. The Merritt precipitation data indicates that most of this snow was probably deposited over the previous two days. Unless snowfall events were not recorded between the first and second observation dates, or the two early January snowfalls were grossly under-estimated by the Menzies Lake resident, then very little densification and wind transport of the existing snow must have occurred. Clearly, more work is required in order to derive a physically based model of snow densification and wind transport. In spite of this problem, all of the remaining predictions are within the observation errors. This may be partially a result of the snow load restriction, but it is also possible that a meteorological event such as the freezing rain of January 9th may have increased the average snow density to within the range of the snow density formula used in the model. Furthermore, following the rainy period at the end of January (see

Figure 5.2), the snow is so thin that the model is not well tested as far as snow cover predictions are concerned.

It would also appear that the rate of snowmelt due to rain is over-predicted. MLI produces completely snow-free conditions by the end of January and a net reduction in ice thickness over four consecutive days of rain. On February 4th, however, up to 2 cm of snow still existed on the lake. The predicted reduction in ice thickness due to rain is due to melting both at the surface and at the ice-water interface. The latter melting is probably well predicted since its only dependence on the surface balance is through the value of T_o, which, for melting conditions, must be 0°C. The amount of surface melt, however, depends directly on H, of which Q_r is an important part. As described in Chapter 4, the latent heat was included in the surface balance because both sensible and condensation heat is under-predicted due to the use of average daily meteorological data.

The trend in ice thickness between the 18th of January and the 4th of February does not seem to be consistent with the observations. Ice growth appears to be under-estimated between these dates. There are two likely explanations for this. First, the snow conductivity may be under-estimated using Equation 2.15. Secondly, there is considerable rainfall and snow-ice production over the interval. The incorrect prediction of complete snowmelt, and a further melting of ice from the top has been discussed, but it is also possible that ice melt from the bottom due to snow-ice production has been over-estimated. This would have occurred if the prediction of heat generated by the snow-ice is excessive. Such a problem, however, would be offset by an over-estimation of snow-ice production. Finally, with the accumulation of a significant amount of snow-ice in the latter part of January, the snow-ice conductivity increases in importance (although it was assumed that the initial ice cover was 50% snow-ice). If snow-ice conductivity is more accurately represented by the higher value of pure ice, then greater ice thicknesses would be expected during subsequent cold weather.

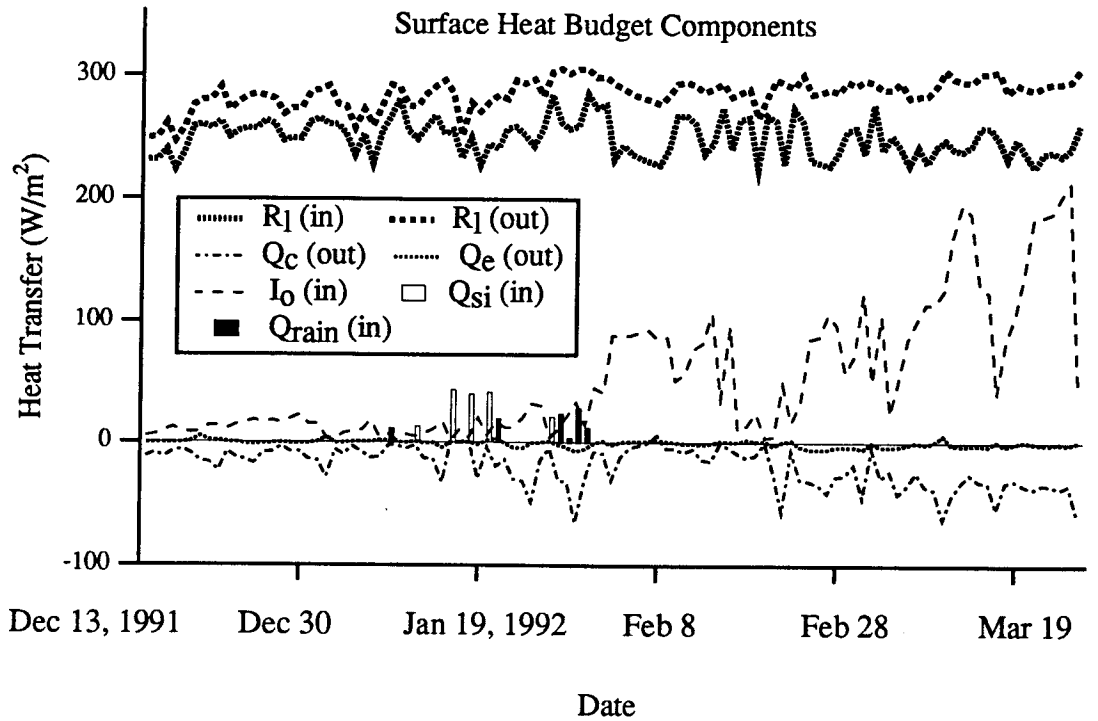

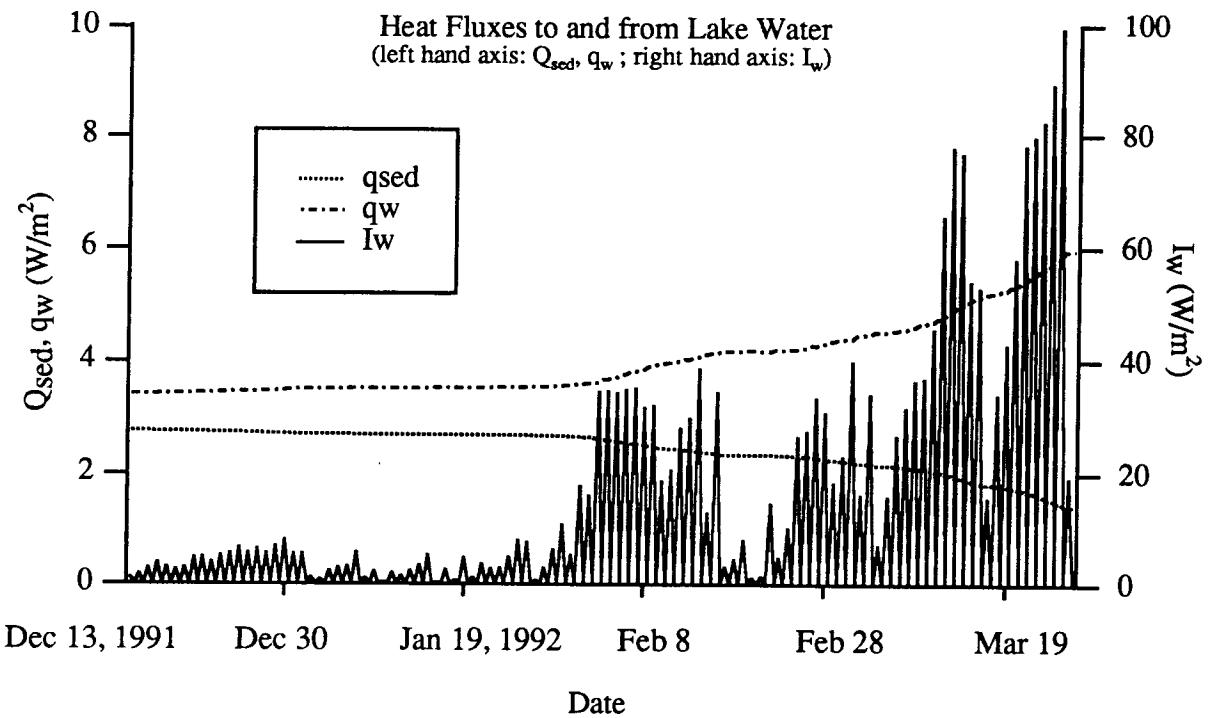

Figure 5.2 MLI: Surface Heat Budget Components and Heat Fluxes to and from Lake Water

The rate of ice melt in March is also under-predicted. Several explanations are available. The difficulty of accurately predicting the presence (or absence) of very thin layers of snow, which may have a huge effect on the albedo, is recognized. The weather station tilt likely resulted in some error in the radiation data. The open ice area around the perimeter of the lake which developed in March probably served to encourage convective circulation in the lake, resulting in an increased transfer of heat from the water to the ice. Convective circulation is discussed further in Chapter 3. It is probable that this last mechanism was most important in increasing ice melt since it does not necessarily involve an increase in lake temperature, the trend of which is quite well predicted over the last month of the simulation.

The lake temperature is actually very well predicted on the whole, aside from the improbable surge in mid-February. The Menzies Lake weather station data (see §5.2) indicate that a minor surge in temperature was likely but, with the incorrect prediction of complete snowmelt, solar penetration would have been over-estimated, thereby causing too large an increase in the rate of lake warming.

The effect of varying the most influential and least well established parameters on snow, ice and temperature will be studied in §5.1.4. In the section which follows, the results will be interpreted in terms of the individual heat flux terms, and the surface heat budget.

5.1.3 Components of the Heat Budget

The Surface Heat Balance

The components of the surface heat budget and the direct heat fluxes to and from the lake water are shown in Figure 5.2. The meteorological balance results in a net loss of heat from the lake surface over the first half of the simulation, facilitating a period of sustained ice growth. Most important in the early winter balance is a net emittance of

long-wave radiation. The evaporative flux is generally negligible over the entire modeling period. The sensible heat transfer almost always constitutes a source of heat to the lake surface, not a sink. This latter result is due to the fact that the solution to the conduction equation yields surface temperatures, T_o, which are consistently below air temperatures, T_{air} (more on this later). Both Ashton (1986) and the U.S. Army Corps of Engineers (1956) provide thermal profile measurements across the air-snow interface which are consistent with these results. No examples were found in the literature where $T_o > T_{air}$ for a snow covered surface.

Although there is, on average, an increase in the net emittance of long-wave radiation towards the end of the simulation period, both solar radiation and sensible heat transfer increase substantially. This results in a reverse in the flux imbalance at the ice-water interface thereby causing the ice to melt.

Although most of the transmitted solar radiation is absorbed in the cover (about 90% in December, decreasing to about 75% in March), the heat is distributed throughout the cover, albeit not uniformly, thereby diminishing the tendency to counter the heat flux out of the lake. Therefore, when solar radiation appears to tip the balance in favour of a net gain of heat in early February, there is actually a continued period of heat loss and ice formation until well into the latter half of the month.

It can be seen from Figure 5.2 that the heat due to rainfall is in most instances, sufficient when combined with high rates of sensible heat transfer into the lake to reverse the direction of the surface heat flux, and cause surface melting. The rainfall of January 9th, was described as freezing rain by the Menzies Lake resident, which explains the relatively low sensible heat transfer on this date compared with the other rainy days. (Although the latent portion of the heat produced by the rain was not removed on this date, the total rainfall was light, and surface melt was not predicted. The reduction in

snow thickness on this date is due to the assumed increase in maximum snow density which occurs when rain falls).

Since almost all of the heat generated by the rainfall is assumed to be latent heat, there would not be sufficient melt predicted if this heat were not included in the surface meteorological balance. According to Harr (1981), there should have been significant amounts of heat derived from condensation (as quantified by Q_e) to produce surface melt. The warm temperatures and high humidity which likely persisted over the rainfall periods are not reflected in the daily averages. Although daily average meteorological data are useful for computing daily average heat fluxes which are active over the entire day, they are clearly not appropriate for determining heat transfer due to precipitation which is usually only active over much shorter periods, when the meteorological variables are at extreme values. It is therefore concluded that a purely theoretical representation of snowmelt due to rain will not produce accurate results unless sub-daily averages of meteorological data are used.

The heat produced by ice cover flooding is substantial (again, the bulk of the heat is latent). The impact of this term on the heat budget is considered in §5.1.4.

The heat fluxes to and from the unfrozen lake are also shown in Figure 5.2. Although solar radiation is responsible for almost all of the heat absorbed by the lake water over the modeling period, there are a few significant periods over which sediment heat transfer rates exceeded the rate of solar heating. In fact, from December 13th until the end of January, the average rate of solar heating was less than the average 2.8 W/m^2 delivered from the sediments to lake water. As described in §5.1.4, however, the model results agree more with the field observations if the sediment heat conductivity is reduced by 50%. In that case, the solar heating over this period would be slightly greater than

sediment heating. By February, however, solar heating dominates strongly as the sediment heat transfer begins to fall in response to a reduced thermal gradient.

Over most of the period, sediment heating is only slightly more than offset by heat conduction through the ice. The gap widens, however, starting in February, as the lake begins to heat up more rapidly. By the end of the simulation period, conduction through the ice cover is more than four times the diminishing sediment heat transfer rate. At this time, however, conduction of heat to the ice is only 5 to 10% of the daytime averages of solar heating.

Comparisons with DYRESMI

With a few notable exceptions, there is little difference between the DYRESMI and MLI surface heat balance. Of course, Q_r and Q_{si} do not appear in the DYRESMI heat balance, but the R_{li} term is identical, and there is no significant difference in Q_e which is again negligible. The remaining terms for both models are shown in Figure 5.3. The different albedo representations account for the mismatch in I_o. The difference is most significant in mid-February, and during some periods in March, when MLI predicts snow-free conditions, allowing a great increase in the quantity of solar heat penetration into the lake. This comparison emphasizes the importance of a good albedo estimate in late winter when solar radiation dominates the heat budget.

Both R_{io} and Q_c correspond much more closely. The most significant deviations occur at the start of the simulation, when immediate snow-ice formation is predicted using DYRESMI, and in early February when MLI predicts complete snowmelt. The differences in these two terms are due to T_o. At the start of the simulation, the immediate snow thickness discrepancy, coupled with the relatively high conductivity of DYRESMI snow produces a greater conduction of heat to the surface, thereby increasing T_o. The prediction of a snow layer in mid-February, according to DYRESMI, means that there is

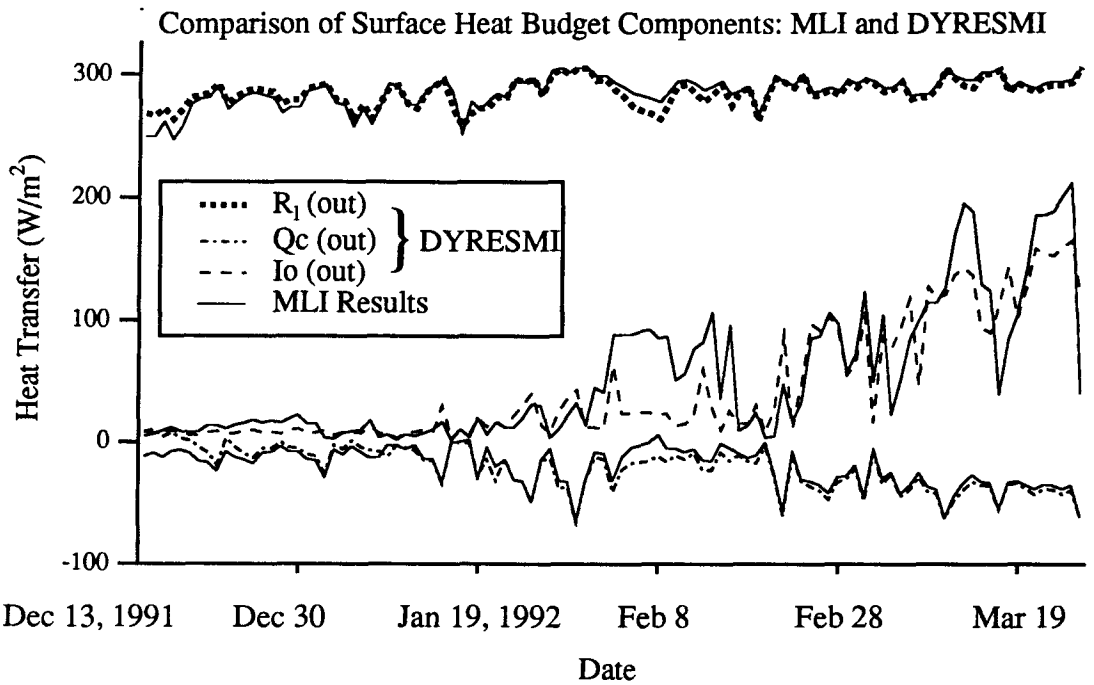

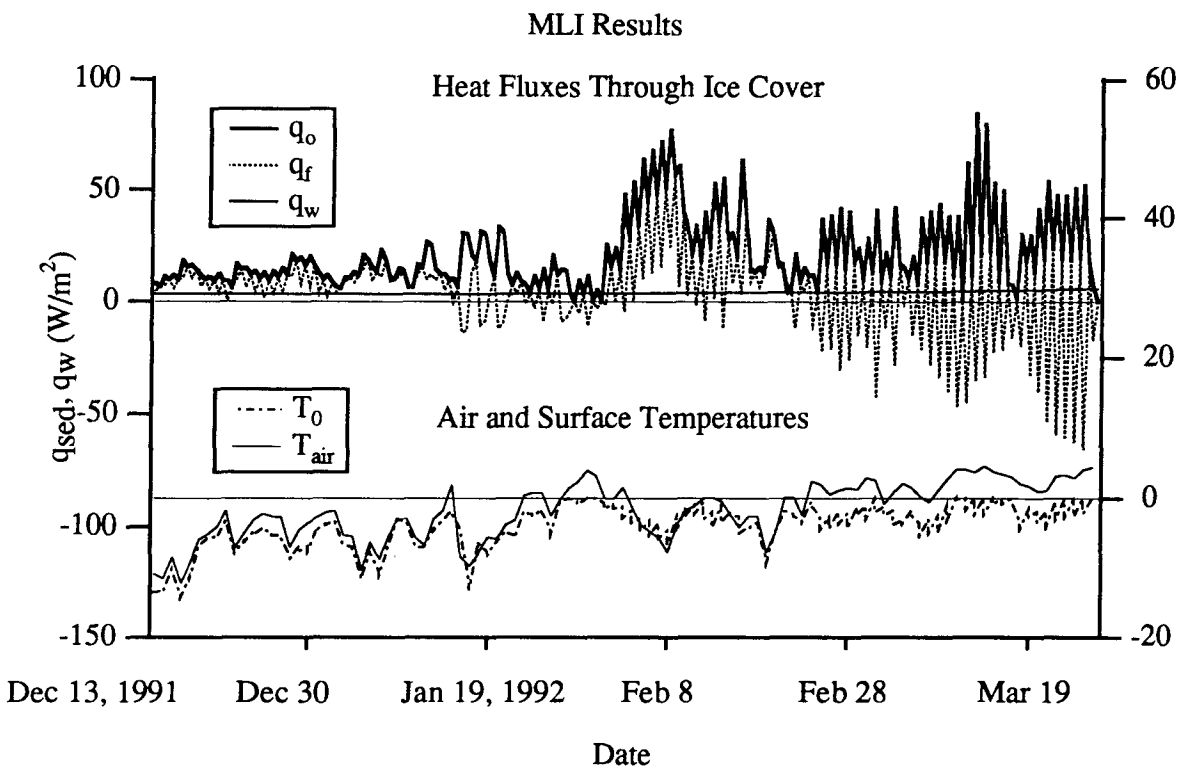

Figure 5.3 a) MLI & DRESMI: Comparison of Surface Heat Budget Components
b) MLI: Heat Fluxes Through the Cover; Air and Surface Temperatures

reduced heat conduction to the surface, resulting in an under-estimation of T_o. The lack of solar heat in the surface layer due to the high snow albedo also contributes to this latter result. Hence the sensible heat transfer into the lake is over-estimated and the long-wave emission is under-estimated in this case, while the reverse is true at the start of the simulation.

As described earlier in explaining the rate of ice melt predicted by DYRESMI, relatively high conductivity leads to slightly more sensible heat transfer into the lake and somewhat less outgoing long-wave radiation during the melting phase to offset the relatively low predictions of solar heating.

Heat Flux Through the Cover

The heat fluxes q_o and q_f are shown in Figure 5.3. These two terms are equal over the night time step, when there is no solar heat distribution in the cover. The extreme daytime deviation from this equilibrium illustrates the importance of solar radiation in causing melt at the ice-water interface. The exception to this rule occurs during snow-ice production in January, since the associated heat is distributed over both daily time steps.

A consistent net upward flux of heat through the ice, which nearly always exceeds the rate of heat conduction to the ice, results in the almost steady gain in ice thickness up until mid-February. The model predicts that this flux is reversed for a significant part of the latter half of January, resulting in a small net loss of about 1 cm of ice. This is due to ice cover flooding, rainfall, and warm air temperatures. The actual ice melt predicted at the ice-water interface is much higher, since there are significant accumulations of snow-ice during this period. Evidence from the field observations, however, suggest that there was little ice melt to offset the snow-ice growth. Further work is required to better quantify both Q_r and Q_{si}. In the latter half of the simulation, daytime solar heating results in significant melting at the ice-water interface. Even in late March, however,

there is some ice growth at night, although it is much less significant than the daytime melt.

Both T_{air} and T_o are plotted for the simulation period in Figure 5.3. As described earlier, it is predicted that T_o is almost always less than T_{air}, which explains the sensible heat transfer into the lake. The temperature data indicate a sustained surface melt over several days in late January. This was made possible by including Q_{rl} in the surface heat budget. During this brief period, surface melt is predicted for both time steps. In contrast, surface melt only occurs in the first time step in late March due to high levels of solar heat in the cover.

5.1.4 Impact of MLI Parameters on Predictions

The impact of change to some of the default parameters and functions are examined here. The most likely combination of changes is considered in Chapter 6.

Effect of Ice Cover Flooding

The impact of flooding on the Harmon Lake heat budget is illustrated in Figure 5.4. Here, results are given based on the expected snow-ice formation, but with no associated heat addition to the snow (Q_{si} = 0). Several snowfalls occur in mid-January which exceed the bearing capacity of the ice cover. Figure 5.3 indicates that the flooding causes a significant reversal in the balance between q_f and q_w, which translates into substantial melting at the ice-water interface. The primary source of this heat, however, is the latent heat of fusion resulting from the formation of snow-ice. The net effect of this process is an increase in the total ice thickness. In fact, the net rate of growth is substantially higher over the period of these snowfalls than over the preceding month.

If the formation of snow-ice produced no heat at all, the total ice thickness would have been expected to be about 2 cm greater over most of the remainder of the modeling

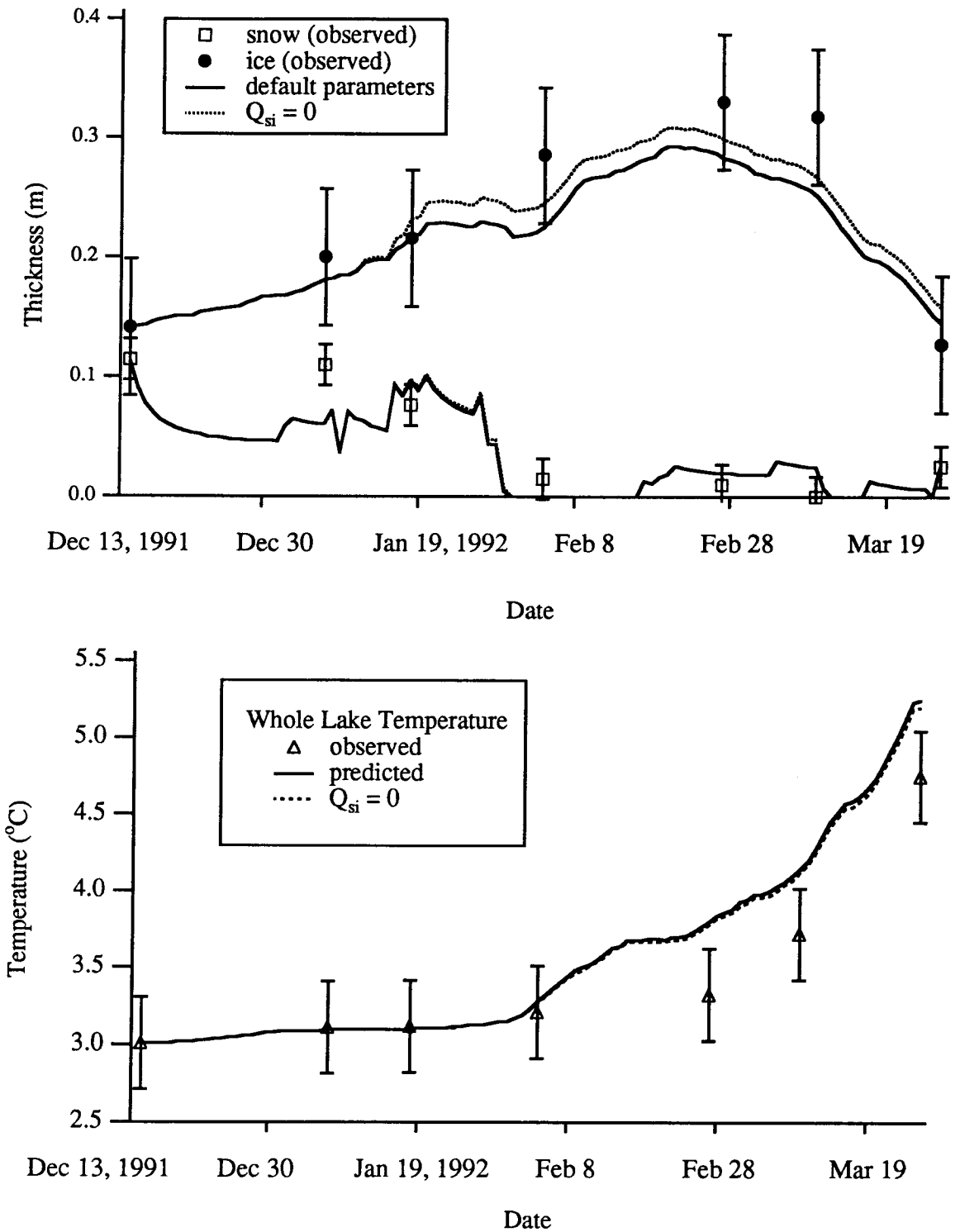

Figure 5.4 Effect of Heat Associated with the Formation of Snow-ice on Ice and Snow Thickness and Whole Lake Temperature

period. This heat, however, appears to have virtually no impact on either the expected snow thickness, or the whole lake temperature.

More work is needed to quantify both the snow-ice thickness and the associated heat. One likely possibility is that high densification of the flooded snow occurs before it actually freezes. This would mean both less snow-ice and heat production. The expected reduction in flooding depth may be offset by capillary rise of flood water in the snow.

Effect of Snow-Ice Solar Attenuation Coefficient

The impact of doubling the attenuation coefficient associated with the visible band of solar radiation for snow-ice is shown in Figure 5.5. With regard to ice cover, there is little dependency on these coefficients in the first two months of the simulation when the non-reflected solar energy is well below daily averages of 100 W/m^2. Despite these low levels of radiation, the impact on the lake temperature is more notable because radiation is absorbed twice as quickly through the snow-ice (which is assumed to constitute 50% of the ice cover at the start of the simulation) before reaching the water. There is a significant reduction in lake warming due to the higher attenuation coefficient by early February. By the end of March, however, there is effectively no difference in the rate of warming because the higher attenuation results in a greater rate of melting, and therefore less material through which absorption may take place.

Regarding ice cover, the maximum impact over the entire modeling period is only less than half the expected error in the measurements. By the end of the simulation period, The lake temperature is less than the prediction based on the default coefficient by more than the expected error.

It seems reasonable to assume that solar attenuation may increase with snow density. In the early winter, when the average density is low, there would presumably be less

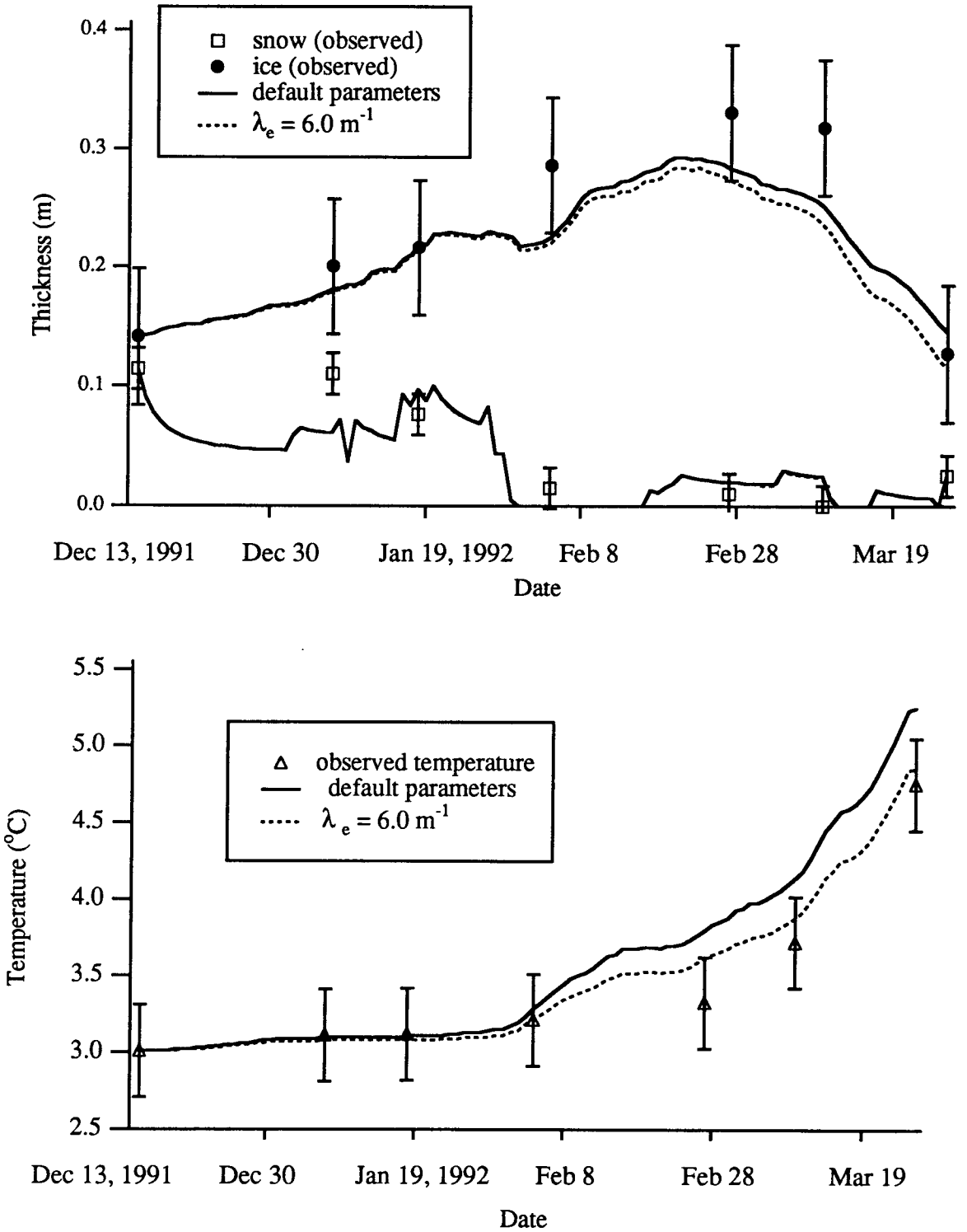

Figure 5.5 Effect of Increased Solar Attenuation Through Snow-ice on Ice and Snow Thickness and Whole Lake Temperature

attenuation than in late winter when the average density can be up to four times higher. This possibility is beyond the scope of this project but should be considered in future improvements to MLI.

Effect of Snow Density and Conductivity

The important effect of snow density on the lake condition is shown in Figure 5.6. The maximum snow density in Equation 4.15 was increased to 300 kg/m^3 for $T_o < 0$ °C, and 400 kg/m^3 for $T_o > 0$ °C. This results in a substantial increase in predicted ice thickness over almost all of the simulation period. The increased density translates into a greater heat flux out of the cover because of the corresponding increase in snow conductivity as quantified by Equation 2.15, and a reduction in snow thickness. This increases the imbalance between q_f and q_w, thereby creating more ice. Almost all of the increase over the default condition occurs in the first 3 weeks of the simulation. The ice thickness thereafter changes at essentially the same rate as the default case for the following reasons:

a) When rain falls, the maximum density is assumed in both cases to rise to 400 kg/m^3. Therefore, following the first rainfall in early January, there is much less disagreement in the average snow density.
b) The increase in q_f due to the higher snow conductivity is reduced due to the increased insulation of the additional ice previously produced.
c) The extra ice provides greater snow bearing capacity, thereby increasing the mass of snow which could be supported. In spite of the higher rate of snow densification, the net effect is slightly increased snow thicknesses over the default case in the latter part of January. The extra snow provides a little more insulation to further temper q_f. (The greater snow thickness in late January can also be attributed to a reduced rate of surface snowmelt because this rate is inversely proportional the density.)

In summary, the increased snow density facilitates a substantial increase in ice thickness, but has little impact on the whole lake temperature. A slight decrease in the latter

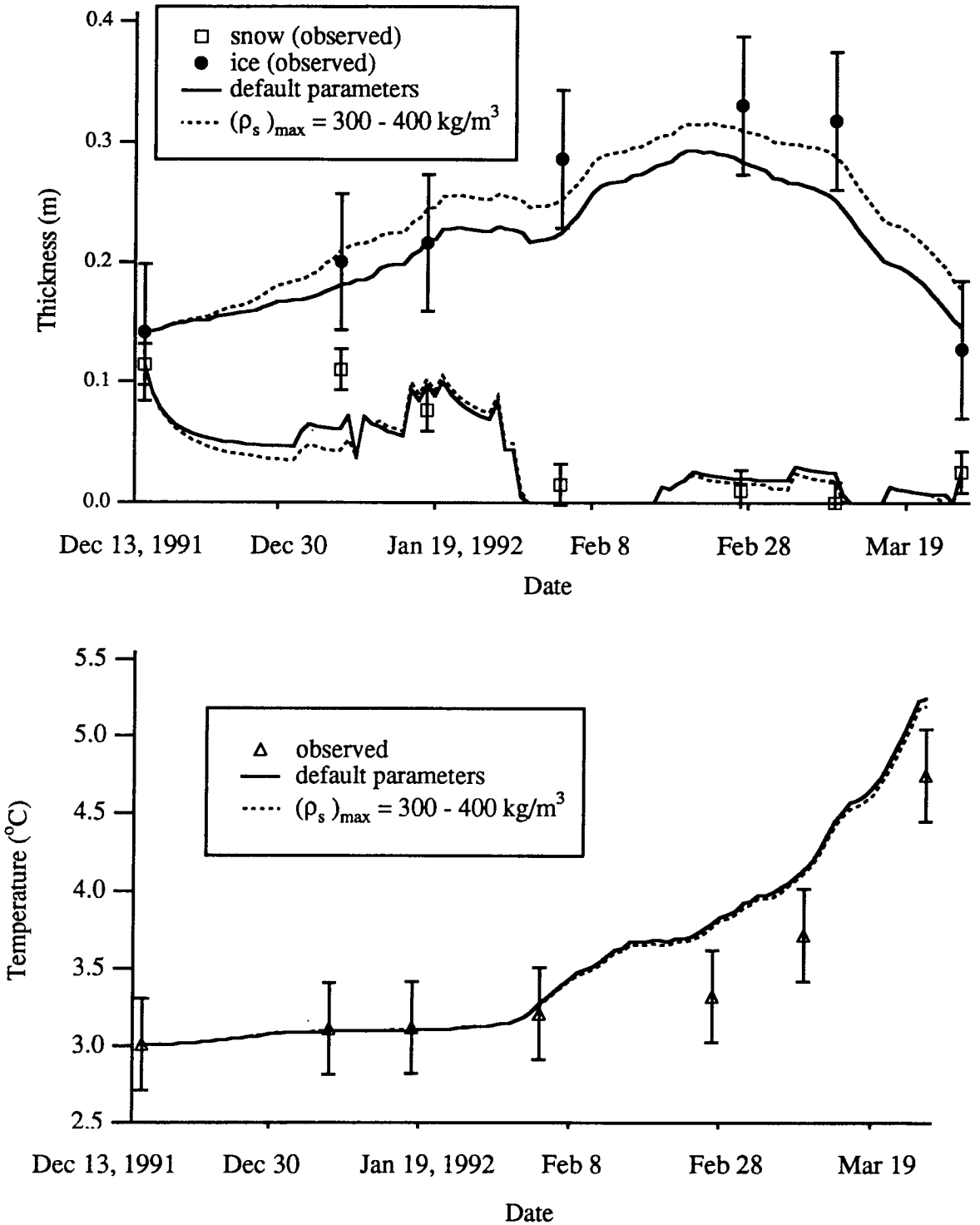

Figure 5.6 Effect of Increased Maximum Snow Density on Ice and Snow Thickness and Whole Lake Temperature

variable occurs due to the increased solar attenuation caused by the extra ice in the latter part of winter.

The impact of increased maximum snow density on snow thickness is most substantial when there is a completely fresh, low density cover and a subsequent period free of snowfall and surface melting.

Patterson & Hamblin (1988) assume a constant snow density of 330 kg/m^3, and a constant snow conductivity of 0.31 W/m^{o}C. If this density is substituted in Equation 2.15, the result is a conductivity of only 0.24 W/m^{o}C. To examine the effect of snow conductivity while maintaining the original density function, Equation 2.15 was multiplied by the ratio of these two conductivities, 0.31/0.24. The result is given in Figure 5.7. The result is almost identical to the density adjustment described above. The increase in ice thickness is slightly less, but the predicted lake temperature is almost identical to the previous case. The only substantial difference is the lack of a reduced snow thickness (as caused by increased densification) in the early stages of the simulation.

Effect of Sediment Conductivity

In the majority of the investigations regarding sediment heat transfer which were reviewed for this project, the sediment conductivity, K_{sed}, was found to equal that of water (about 0.6 W/m^{o}C). A substantially higher conductivity was assumed for the default case because values of up to 3.5 times that of water have been reported in the literature (see Chapter 2). If K_{sed} were reduced from the assumed value of 1.2 W/m^{o}C back down to 0.6 W/m^{o}C, the predicted agrees with the observed lake temperature to within the expected observation error on all dates as shown in Figure 5.8. The cumulative deviation from the default case, however, is only about 0.2 ^{o}C, which is also within the expected error.

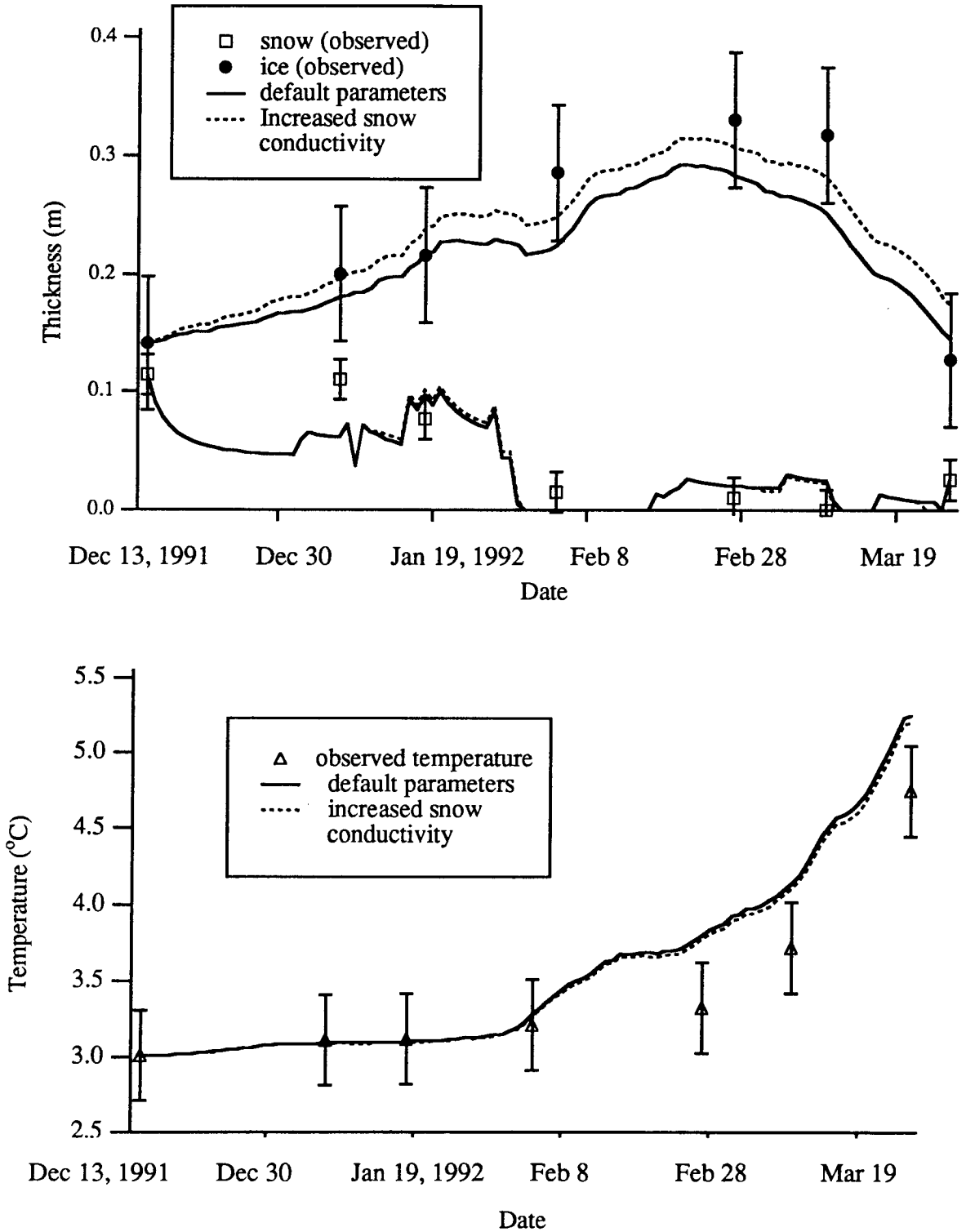

Figure 5.7 Effect of Increased Snow Conductivity on Ice and Snow Thickness and Whole Lake Temperature

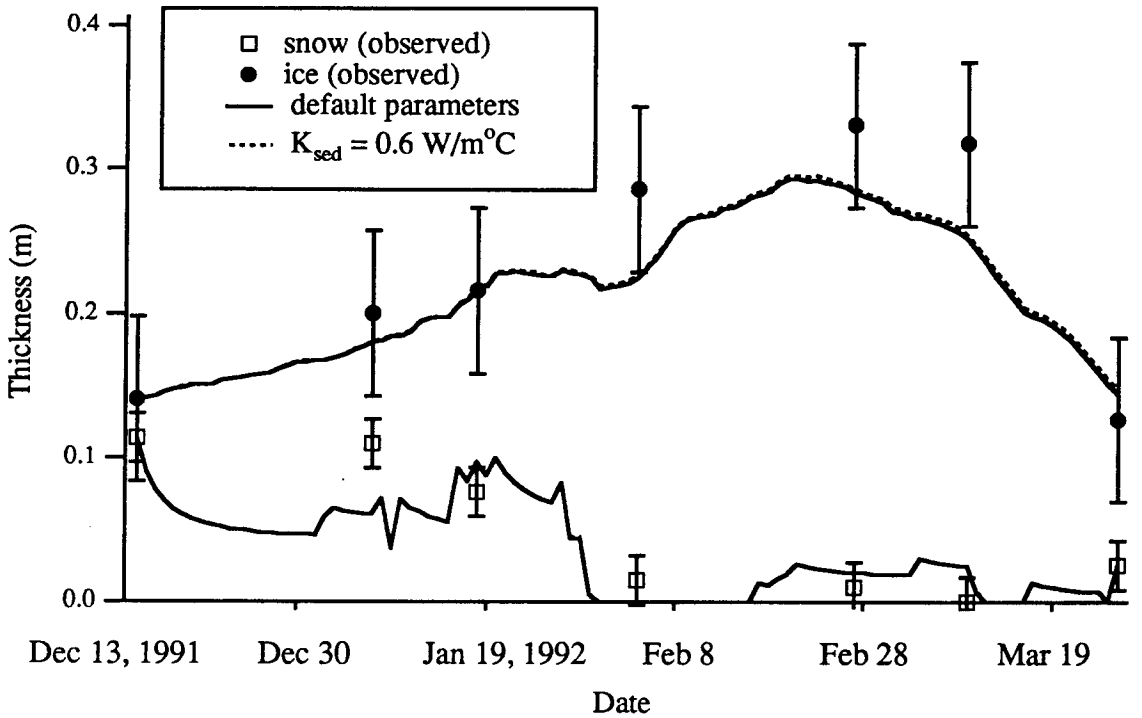

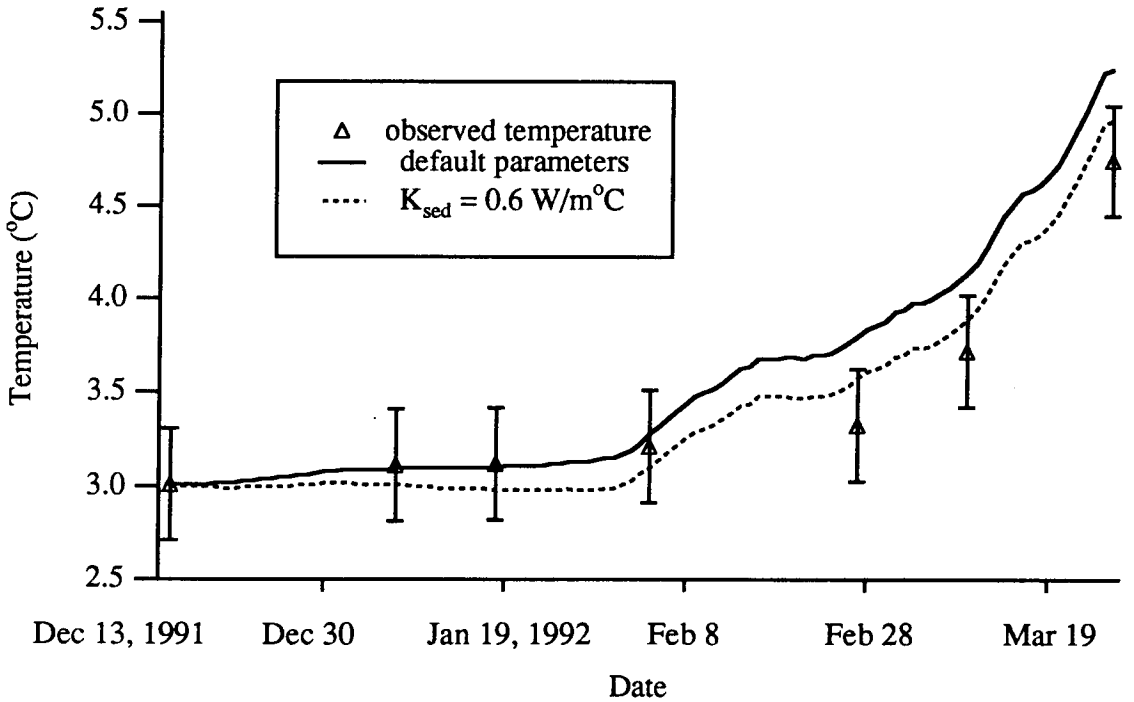

Figure 5.8 Effect of Decreased Sediment Conductivity on Ice and Snow Thickness and Whole Lake Temperature

There is effectively no impact on the ice and snow cover aside from a negligible increase in ice thickness late in the period owing to the reduction in heat conducted from the water to the ice.

Effect of Albedo Decay Rate

The result of multiplying the USACE decay functions (Equations 2.16) by a factor of 0.5 is presented in Figure 5.9. The higher albedos which are produced result in a substantial increase in ice thickness over the default case during the period spanning from late February to early March. At that time, there is a light snow cover and solar radiation is more than an order of magnitude more intense than over the first month of the simulation. Although solar heating is as important in early February, there is no snow cover during that period and therefore no change in the results. The only change in the predicted snow cover occurs in mid-March. The reduced absorption of solar energy at that time causes a delay in the complete loss of snow due to melting. Clearly, the albedo is of extreme importance to the whole lake temperature in late winter, especially if the meteorological conditions produce a situation where an extended snow-free period may or may not occur, depending on how much solar heat is reflected at the surface. Although this is not a significant factor for the two albedo functions compared here, careful examination of Figure 5.9 reveals that the impact on lake temperature is still quite substantial over the few days in March when this condition occurs using the two decay rates. The average rate of change in whole lake temperature over the last month is only about 70% of the default case, producing results which are more consistent with observations. As suggested below, however, it is more likely that the deviations from the observed are more likely due to other parameters.

These results suggest that the predicted albedo should have been lower over most of March in order to match the rapid ice melt. Complete snow melt actually occurred earlier

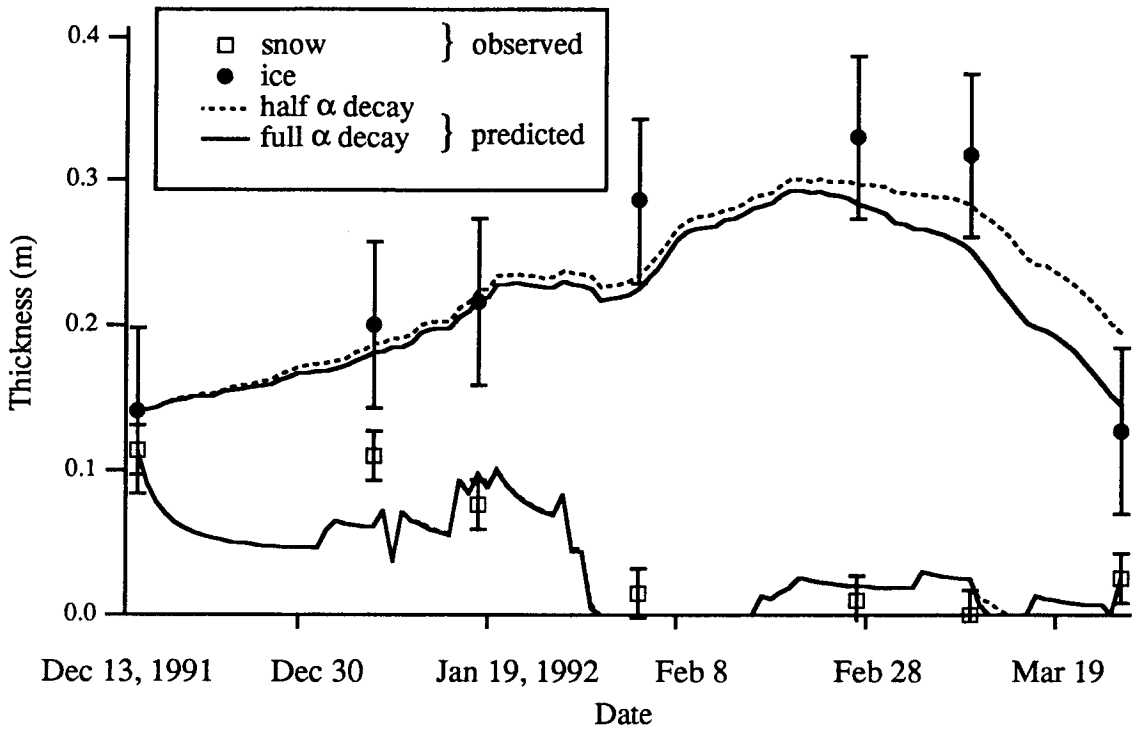

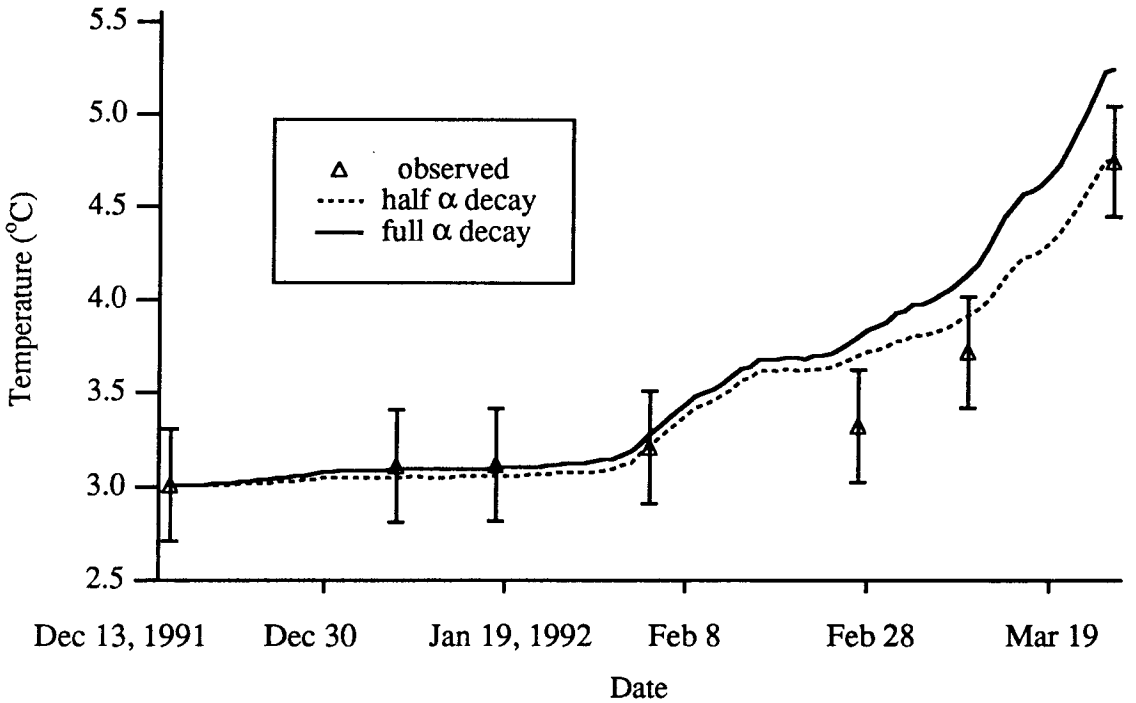

Figure 5.9 Effect of Reduced Albedo Decay Rate on Ice and Snow Thickness and Whole Lake Temperature

than either decay rate predicted in the first half of the month. This may be partly due to the heavy snowmobile traffic on the lake at this time. Whatever the cause, there would have resulted a much reduced albedo over several days due to snow-ice exposure.

More research is required in order to establish a more reliable relationship between albedo and meteorological conditions. A more likely solution which would produce more accurate results is direct albedo measurement.

Effect of the Thermal Gradient at the Ice-Water Interface

The effect of reducing the thermal gradient at the ice-water interface by 62.5% is illustrated in Figure 5.10. (The assumed distance, dz, over which the lake temperature linearly decreases to 0 ^{o}C at the interface is increased from 0.5 to 0.8 m.) As far as ice and snow thicknesses are concerned, the reduced conduction from the lake water produces results which are similar to those obtained from increasing the snow conductivity (Figure 5.7). This is due to the fact that the reduction in q_w in the first case is of similar magnitude to the increase in q_f in the latter case. The result is similar flux imbalances which leads to similar rates of ice growth.

While the lake temperature effectively does not change with increased snow conductivity, it undergoes a substantial increase as a result of the reduced thermal gradient. By the end of the simulation period, the lake temperature is more than twice the expected error greater than the observed value. Although this result suggests that the lower gradient is unlikely, the probability of decreased lake temperature predictions due to reasonable variations in sediment conductivity, solar attenuation and albedo must be assessed. Furthermore, it is also quite possible that the gradient is significantly variable over the course of the winter. Convective mixing, as described in Chapter 3, may have resulted in turbulent heat transfer to the ice in late winter, thereby greatly reducing the rate of increase in lake temperature caused by solar heating.

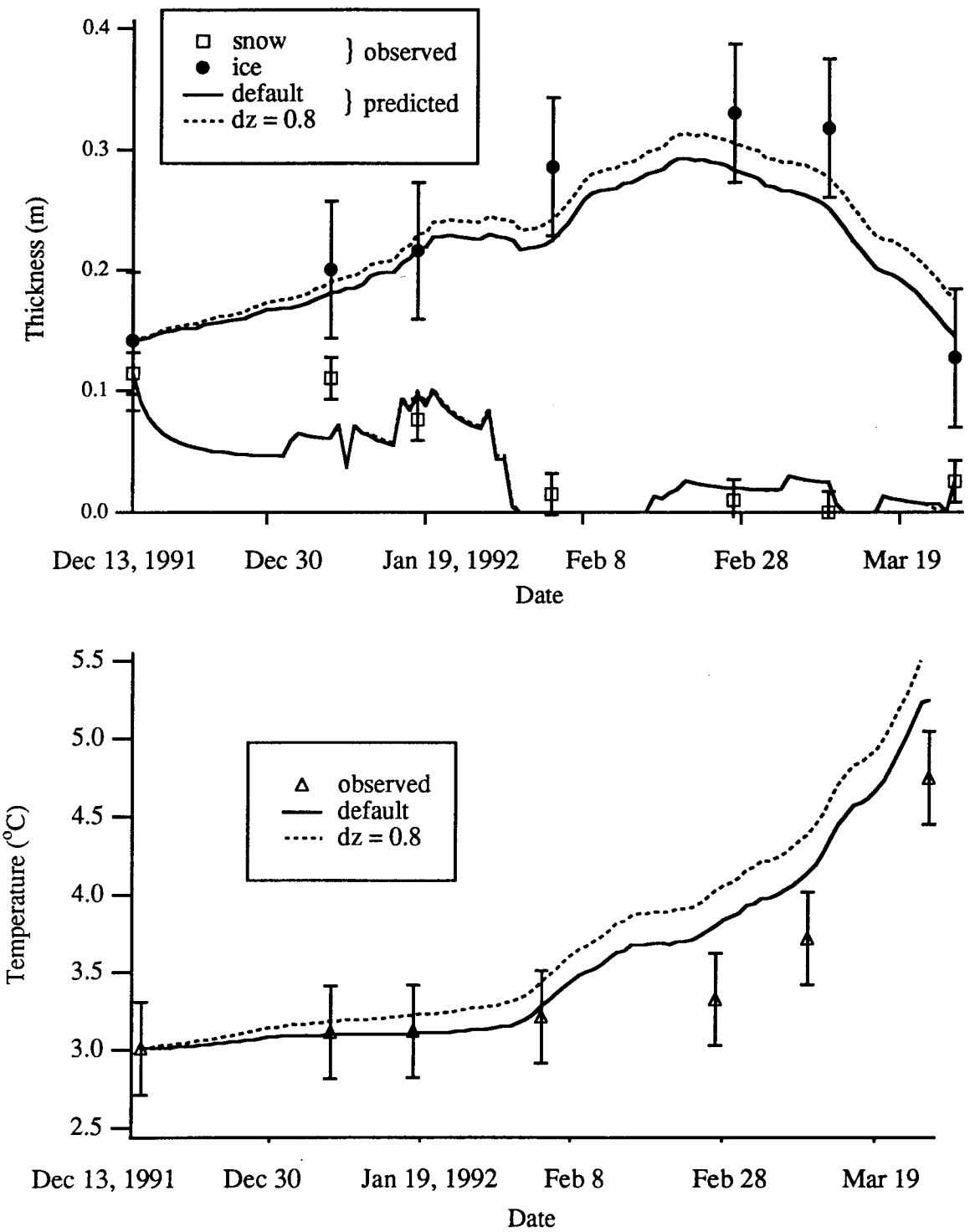

Figure 5.10 Effect of Reduced Thermal Gradient at Ice-Water Interface on Ice and Snow Thickness and Whole Lake Temperature

5.2 ARTIFICIALLY CIRCULATED LAKE

5.2.1 Analysis of MLI-C Predictions

Results from MLI-C using the Menzies Lake data set are given in Figure 5.11. All parameters used in MLI were set to their default values. Although reasonable variations in some of these parameters have shown to produce better predictions, the correct combination of variations remains unknown. The most likely changes to these parameters are considered in Chapter 6. One of the key recommendations which stems from this work is that more effort be made to narrow the range of possible parameter values for a given location and set of (easily measurable) conditions.

Model Adjustments

Some modifications to the subroutines which are specific to MLI-C were required in order to avoid unlikely polynya radius predictions. It was found that the incorporation of surface melt into the polynya edge heat balance produced improbable radii on those days when surface melt was predicted. This is attributed to the small value assigned to h_{min} (the value is discussed later in this section). Significant surface melt results in a proportionally large reduction in this parameter. This significantly increased the sensitivity of the polynya radius to the warm weather conditions associated with surface melt, resulting in very large radius predictions. The predictions were much improved when the MELTPE subroutine was removed. This is justified by the fact that the snow-free zone around the polynya is limited in extent (see Chapter 4). Therefore, if there were to be a large increase in polynya radius, then some snow melt must occur. Since this snow is assumed not to exist, the incorporation of surface melt results in under-estimation of the thermal energy required to expand the polynya.

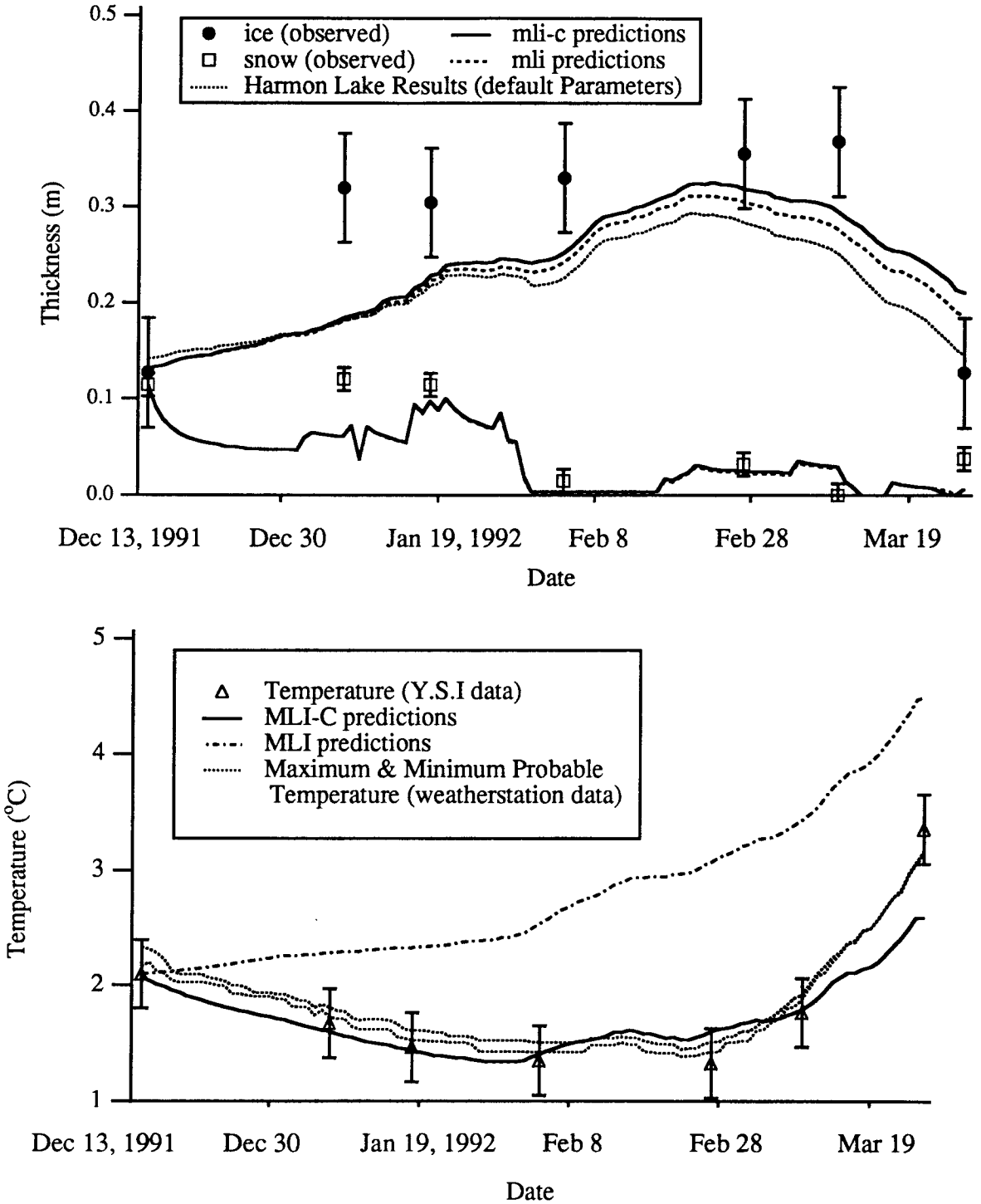

Figure 5.11 Snow and Ice Thickness and Whole Lake Temperature Predctions: A Comparison of MLI and MLI-C Ouput for Menzies Lake

Testing MLI-C at extreme values of Δr resulted in water temperatures which dipped below 1°C (see §5.2.3). Even on warm days with $H_p > 0$, (and therefore a small value of $(q_f)_{pe}$), Equation 2.25 did not yield a melting rate which would satisfy the polynya expansion criterion. This is due to the low value of q_t associated with the very cold lake temperature. Hence Equations 4.26, 4.23 and 2.30 would be solved to calculate a new, presumably contracted, radius. With $H_p > 0$ however, the solution gives an extremely large polynya radius. In response to this result, the model was changed so that when H_p is greater than zero, expansion is assumed and Equations 4.25 (which is based on $(q_f)_{pe}$, not H_p), 4.23 and 2.30 are solved for the new radius.

Ice and Snow Predictions

Figure 5.11 includes ice and snow predictions for Harmon Lake, as well as results for Menzies Lake in the case of no artificial circulation. All three results are nearly identical for snow cover, and only minor differences in ice thickness are predicted over the latter two-thirds of the simulation. All differences are accounted for by q_w which is lower for a lower T_w. The artificially circulated lake, being the coolest, therefore results in the greatest ice thicknesses.

Since both the snow cover results and observations are almost identical to those at Harmon Lake, it is unlikely that artificial circulation has any direct impact on the snow cover. There are sound explanations, however, for the small differences observed. The observed ice thickness was significantly greater at Menzies than at Harmon Lake between late December and mid-January. This translates into a higher snow bearing capacity at Menzies Lake which explains the greater snow thickness observed at the lake on January 19th. Following the late January rain the snow thicknesses are similar because the snow bearing capacity at both lakes greatly exceed snow loading. The small observed differences may be, to a lesser degree, also due to dissimilar sheltering

characteristics and slight variances in the rates of surface melt due to the indirect influence of heat conduction through the ice.

Unfortunately, the MLI-C does not predict the Menzies Lake ice cover satisfactorily. It seems unlikely that errors were made in the observations given the simplicity of the measurement, as well as the fact that significant differences from the Harmon Lake observations were noted on almost half of the field trip dates. As described in §5.2.4, however, improper sampling may have led to poor estimates of average lake ice thickness. The greatest discrepancies between the predicted and observed ice thicknesses occur in the first month of the simulation when the lake water is experiencing its highest rate of cooling. If the observations are reliable, MLI-C must significantly under-predict the conduction of heat through the ice and snow cover. There are two possible explanations for this. First, the conductivity of ice and snow at Menzies Lake may be much greater than what is assumed. Second, the meteorological balance is improperly represented. These possibilities are considered in §5.2.4. It should be noted that, as explained in §5.2.3, although the calibration parameters C_t, h_{min}, and Δr have a significant impact on lake temperature and polynya radius, they have virtually no effect on the ice cover.

With regard to the latter half of the winter, the explanations for any differences in observed ice and snow thickness at Harmon Lake using MLI apply equally well here.

Water Temperature Predictions

The predicted water temperature at Menzies Lake is also given in Figure 5.11. The best results were achieved for the following calibration parameter values:

C_t	1.1×10^{-3}
h_{min}	0.02 m
Δr	13 m

These values produced reasonable estimates of whole lake temperature, although the rate of warming in March is under-estimated. As described in §5.1, this may be due to low radiation measurements resulting from weather station tilt or poor albedo representation. Furthermore, factors which are particular to Menzies Lake include under-estimation of the polynya radius and boundary effects . This latter factor may be of great importance given that the polynya edge was only two to three metres from the North shore of the lake, in very shallow water.

The above value of C_t is slightly above the range given by Hamblin & Carmack (1990). In their study, C_t is based on velocities measured 1 m below the ice-water interface. In this study, a relatively high value of C_t is expected since the velocity distribution used is assumed to describe the water motion immediately below the interface. For a more accurate model, C_t should be determined for the Air-o-lator® in a manner like that which is described by these authors.

Initially r_∞ was set to the average lake radius, but this produced much too high a rate of lake water cooling. The average lake radius would be expected to be an appropriate choice provided that:

a) Equation 4.23 is based on the true velocity field below the ice cover. It is likely that the ice roughness accelerates the velocity decay, thereby reducing the turbulent heat transfer to below the rates predicted using extrapolated polynya surface measurements.
b) The polynya is located closer to the centre of the lake, well away from shore.

Minimum ice thicknesses of approximately the same magnitude as the selected h_{min} have been observed at both Harmon and Menzies Lakes. The value of h_{min} should drop with reduced fetch length because the maximum wind speed and wave height development is limited, resulting in less turbulent energy available to melt ice. Although the circulator creates turbulence it is quickly dissipated as the radial jet spreads, and the wave

amplitudes produced are small. Therefore a relatively thin ice sheet is able to persist around the polynya edge. Although no direct measurements were made, ice thicknesses of order 0.02 m were observed around the perimeter of the polynya. Direct measurements made when both Menzies and Harmon Lakes were beginning to freeze also indicated that this minimum ice thickness is appropriate.

Further fine-tuning of both h_{min} and Δr are unlikely to produce more reliable results without making the model more sophisticated, or by providing better velocity field data. In order to improve the model, much attention must be given to the shape and characteristics of the ice edge at the polynya boundary and to the hydrodynamic and thermal boundary layers.

If the reason for the under-prediction of ice thickness is adequately addressed, it is nonetheless possible that the parameter values given may produce reasonable results for other artificially circulated lakes (any changes to the MLI parameters examined in §5.1.4 may result in minor alterations to the MLI-C calibration parameters). Indeed the fact that the weather station thermistor data (Figure 5.11) confirms that all of the trends in temperature are predicted by MLI-C (including the slight rise and subsequent fall in mid-February) is encouraging. It should be pointed out, however, that the value of Δr used here may be dependent on the lake morphometry given the proximity of the polynya to the lake edge.

The effect of varying the three calibration parameters is described in §5.2.3.

Polynya Radius

As suggested in Chapter 3, the errors involved in estimating the average polynya radius generally exceed its variability over the observation period. The most detailed observations were made on March 10th, 1992 when ten measurements of polynya radius

were made each with an estimated accuracy of ±0.3 m. Given the great local variability however, the average radius is considered only to be accurate to ±2 m. Nine measurements were made on February 27th, and only 2 on all the remaining field trip dates. The errors in all cases were estimated by scaling the estimated error of March 10th in the manner described in §5.1.2. An error of ±10 m is assigned to the final observation, on March 28th since no actual measurements were made and the polynya was very large and irregular in shape. The location of the polynya edge relative to distinct features were merely noted in this case for an off-site size estimate (the edge had almost reached the north shore of the lake by this time).

MLI-C correctly predicts a narrow range in the polynya size as shown in Figure 5.12. There is a sharp diurnal trend due to the effect of solar heating in the first time step. The trend cannot be confirmed given the available data since all observations were made near mid-day. Aside from this diurnal variation, there are, at times, some significant day to day changes notable, especially during the January rainy period and near the end of the simulation. The sampling was insufficiently frequent to confirm any rapid day to day changes.

MLI-C produces results which agree quite well with the observations but the lack of long term variations which exceed the expected error does not provide an adequate test of the model. Given the asymmetries in the jet and the potential impact of the lake boundaries on the hydrodynamics and the heat transfer processes, better results are not likely without increasing both the sophistication of the model and the input data requirements.

5.2.2 Components of the Heat Budget

The surface heat budget components for the ice-covered portion of Menzies Lake is given in Figure 5.13. The indirect effect of much cooler lake temperatures has virtually no effect on any of the components in relation to the Harmon Lake simulation. If the ice

thickness were more accurately predicted, some minor differences may appear, the most important of which may be a reduction in Q_{si} due to the greater snow bearing capacity.

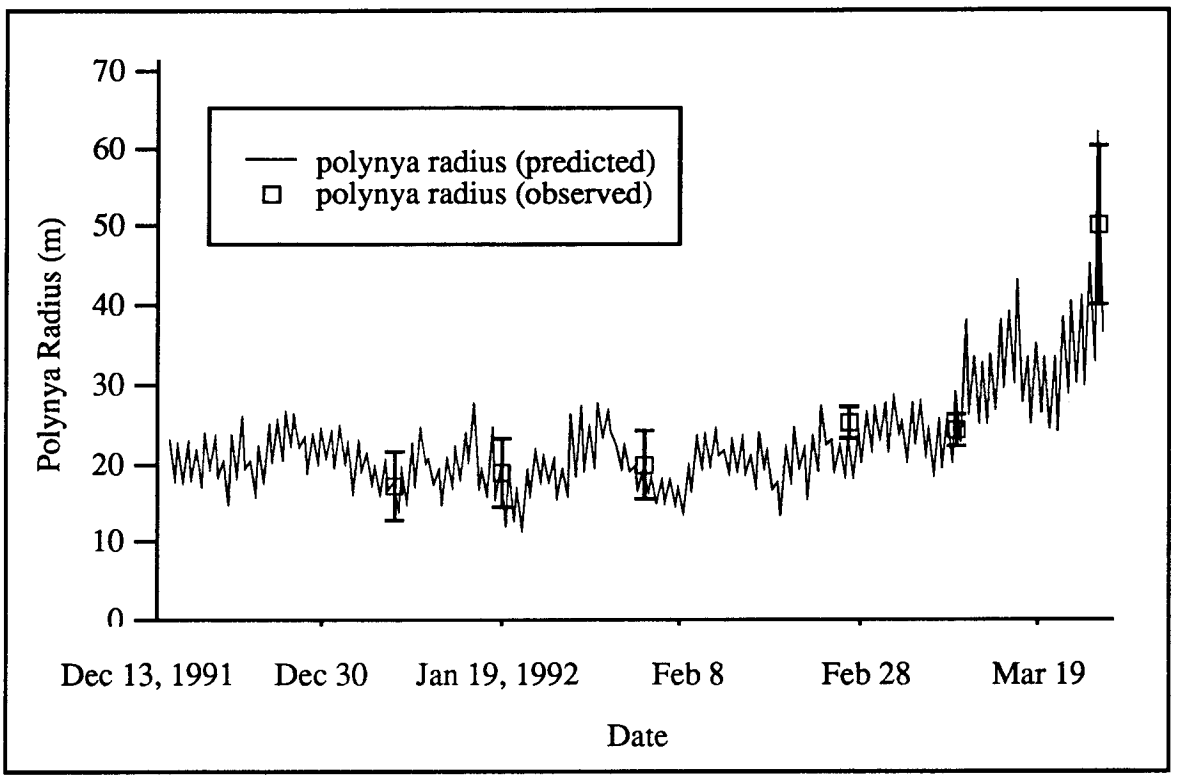

Figure 5.12 Predicted and Observed Polynya Radius

The heat fluxes to and from the lake water are also given in Figure 5.13. All of the fluxes shown have been adjusted to apply over the entire lake surface to facilitate direct comparisons. The only flux which is virtually identical to the Harmon Lake simulation is the solar radiation which penetrates the ice cover, I_w. This is explained by the similarity of the snow and ice predictions. Initially the sediment heat transfer rate is almost the same because the reduced thermal reserve in the sediments at Menzies Lake is offset by a lower lake temperature. The sediment heat transfer rate, q_{sed}, continues to increase, however, as the lake cools before a gradual reduction which begins in earnest at the end of February. The opposite trend is observed in q_w. As the lake cools, there is a reduced thermal gradient between the lake water and the ice. As a result, the heat transfer rate

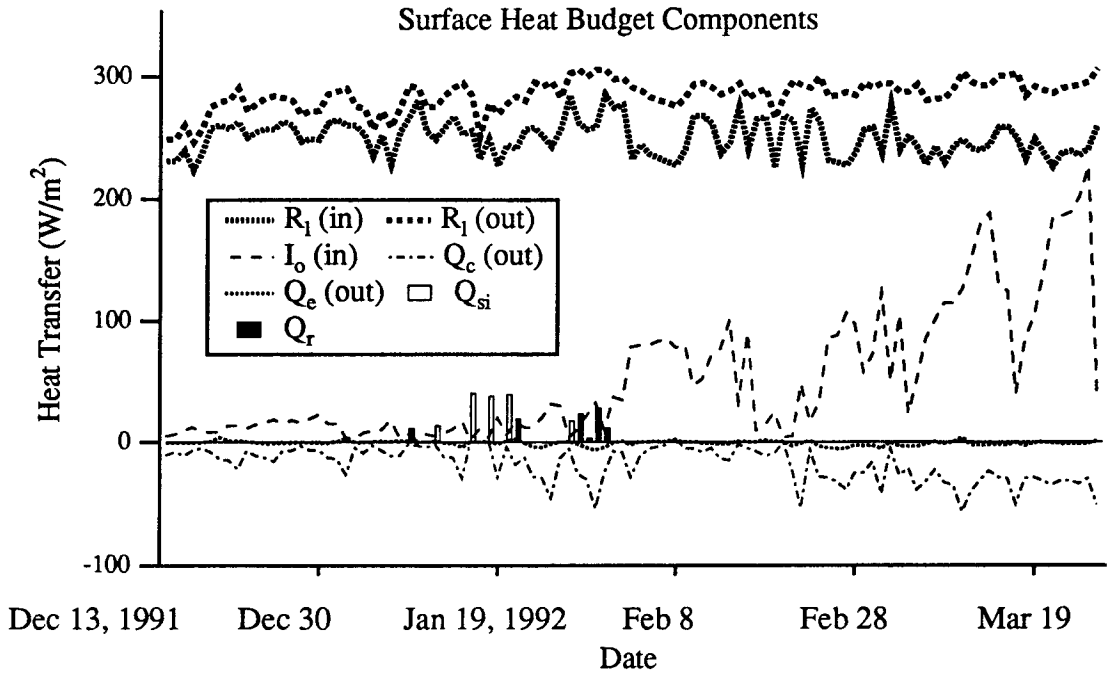

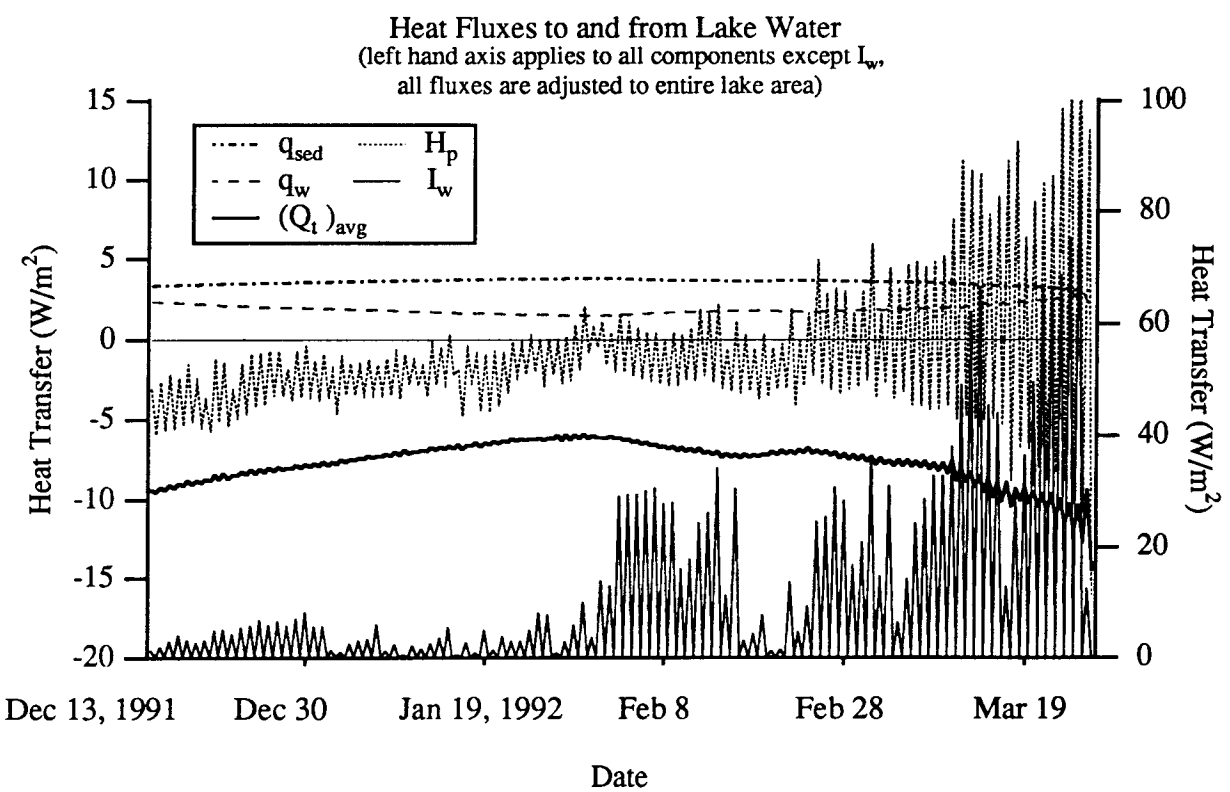

Figure 5.13 MLI-C: Surface Heat Budget Components and Heat Fluxes to and from Lake Water at Menzies Lake

goes down until a steady recovery begins as the lake warms up at the end of February. In general both q_{sed} and q_w vary little compared with the remaining sources and sinks of heat.

Menzies Lake cooled steadily down to a minimum temperature of less than 1.4°C. From the start of the simulation until the end of January, when this minimum was reached, $\bar{Q}_t$ averaged about 7.6 W/m^2 over the entire lake area. This rate was over three times the rate of cooling across the polynya (averaged over the lake area) over the same period. From the start of February until the end of March, there was, on average, a slight net transfer of heat into the lake across the polynya, while $\bar{Q}_t$ increased to an average rate of 8.6 W/m^2 due to elevated water temperature. It is noteworthy that there is only about a 4 W/m^2 range in $\bar{Q}_t$ over most of the simulation, mainly due to gradual changes in lake temperature. This is explained by the opposing effects of lake temperature and polynya radius. Over the course of the winter no dramatic variations are seen in these key variables. A sharp diurnal trend in polynya size is predicted due to the lack of solar heating in the second time step (see §5.2.1). This trend is only mildly reflected in $\bar{Q}_t$ because $\bar{Q}_t$ is more dependent on Δr (which is assumed constant) than the actual polynya area (see Equation 4.24). There is no diurnal trend in T_w, so as r is reduced in the second time step, there is only a small corresponding increase in $\bar{Q}_t$. By mid-March, the polynya begins its rapid expansion and there is an equally rapid increase in temperature. $\bar{Q}_t$ is shown to steadily increase on average over this time. The area over which $\bar{Q}_t$ is assumed active must increase for the given Δr when the polynya area increases. This factor is offset, however, by the inverse relationship between q_t and r (Equation 2.30). So as r_p increases, the effective area of $\bar{Q}_t$ also increases but q_t decreases, resulting in little change in $\bar{Q}_t$. Since $\bar{Q}_t$, however, is proportional to T_w, it must follow the same trend as the lake temperature. It is likely that there is a dependency of Δr on r_p. That is, the distance over which the energy associated with the jet is dissipated decreases as the polynya radius

increases. If this is so, then MLI-C would tend to over-predict the heat loss due to $\bar{Q}_t$ near the end of the simulation when the polynya is large. This provides another possible explanation for the under-prediction in the rate of temperature increase in March (see Figure 5.11). In addition it provides further impetus for future study of the hydrodynamics at the polynya edge.

H_p varies strongly due to diurnal changes in the meteorological balance, but average heat loss over the first two months is only in the order of about 3 W/m2. In terms of heat loss from the entire lake, this means that H_p is only slightly more important than simple conduction of heat from quiescent water to ice. Furthermore, when warmer conditions prevail, as early as the late January rainy period, the average daily heat exchange across the polynya is close to zero. Following a brief cooling period in mid-February, when average daily heat losses were only about 1 W/m^2, the direction of net heat transfer is reversed. Greatly increased solar energy penetrating through the ice-covered area more than offsets the consistent turbulent heat transfer, $\bar{Q}_t$, to produce warming of the lake water. The range in H_p is shown to increase dramatically at the end of March because both solar heating and polynya area also increase in the same manner. Hence for each time step, the importance of H_p increases greatly with respect to the other sources and sinks of heat in the lake. In terms of average daily heat exchange, however, H_p remains a modest term compared with both I_w and $\bar{Q}_t$.

The components of the polynya heat budget are plotted in Figure 5.14. (They have <u>not</u> been adjusted to apply over the entire lake area.) As the lake surface is relatively warm compared with the snow surface, net emission of long-wave radiation is much greater from the polynya than the rest of the lake. Net long-wave heat loss ranges from about 25 to 100 W/m^2 over the entire period. The greater temperature difference between the water and the atmosphere also translates into greater evaporative and sensible heat transfers. In this case, however, the sensible component removes heat from the polynya

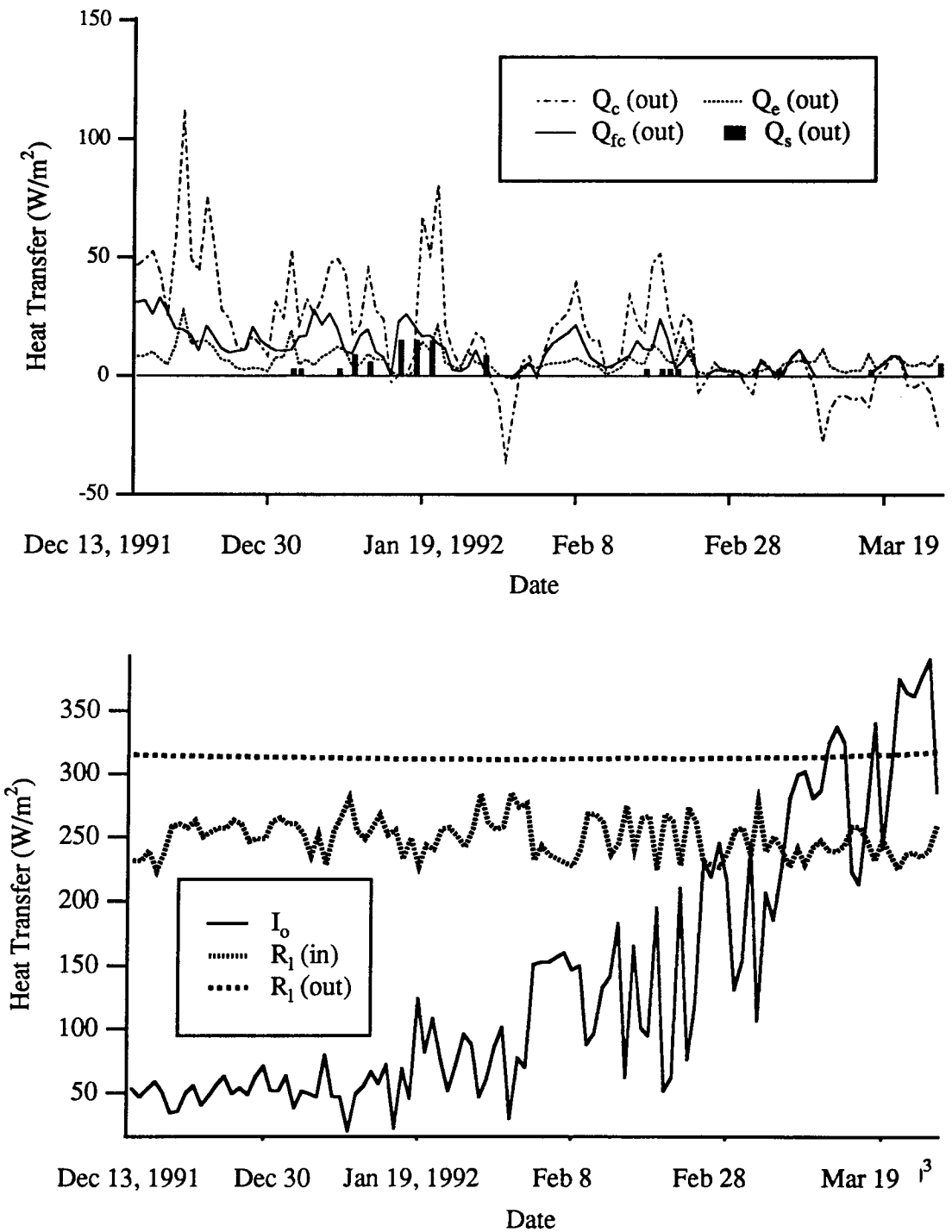

Figure 5.14 MLI-C: Surface Heat Budget Components Across Polynya at Menzies Lake

surface over most of the simulation (up to an occasional maximum of over 100 W/m^2). This is in spite of wind speeds which rarely exceed about a daily average of about 3 m/s, but are more commonly in the range of 1 to 2 m/s. Although the lake cools more in response to turbulent heat transfer to the ice cover, increased exposure to high winds during cold periods may lead to more significant heat loss across the polynya surface. From Figure 5.14, it is also clear that heat loss due to free convection, Q_{fc}, is much more important than the evaporative loss as quantified by the standard aerodynamic formula. Maximum heat transfer rates due to this mechanism are in the range of 25 to 35 W/m^2. Heat loss due to the cooling and melting of snow, Q_{sp}, falling into the polynya is also important when the total daily accumulation is greater than about 5 cm. For this amount of precipitation, about 10 W/m^2 of heat is lost.

By early February, solar heating begins to overcome all of the heat sinks described above. Following another brief cooling period later that month, only the long-wave heat loss term is significant, but is no match for the solar heating which ranges from about 100 W/m^2 at the beginning of March to over 400 W/m^2 at the end of the simulation.

5.2.3 Impact of Varying MLI-C Calibration Parameters

Any reasonable change in the calibration parameters has virtually no impact on the lake ice and snow cover. The impact of each on lake temperature and polynya radius, however, is substantial. The effect of changing the parameters on these two key variables are studied in this section.

Radial Extent of Turbulent Heat Transfer

The impact of increasing Δr from 13 to 26 m is shown in Figure 5.15. The temperature predictions must first be examined in order to explain the effect on the polynya radius. By doubling Δr, the area over which turbulent heat transfer more than doubles.

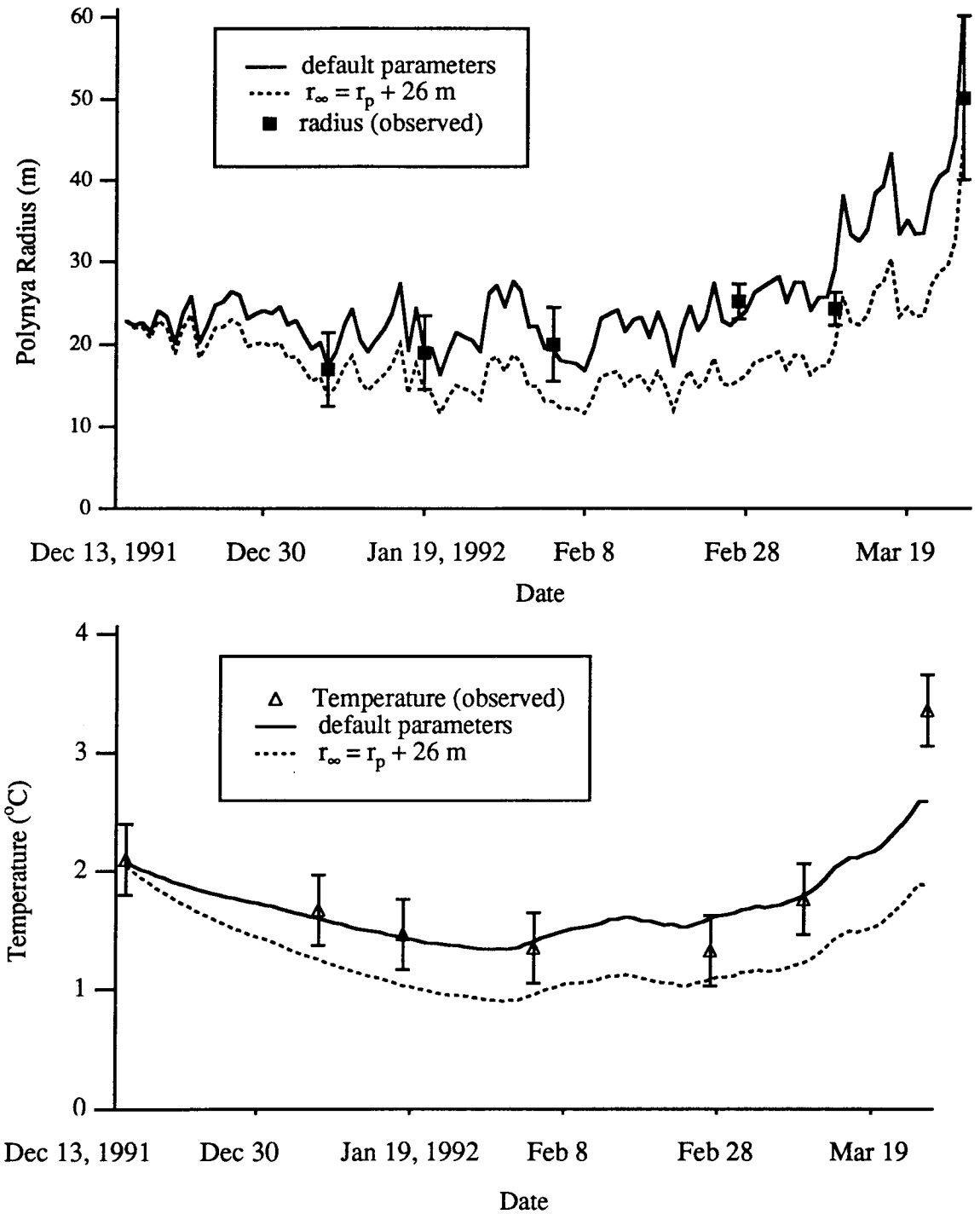

Figure 5.15 Effect of Increased Radius of Turbulent Heat Transfer on Polynya Radius and Whole Lake Temperature

Therefore, there is greater heat loss from the lake on each and every day of the simulation by virtue of increased $\bar{Q}_t$. The divergence in the temperature predictions is gradual because there is limited day to day variation in $\bar{Q}_t$ for a given Δr. The divergence proceeds at a somewhat higher rate in December because of the relatively high thermal reserve from which heat can be drawn. This rate of divergence is not regained when the lake heats up again because $\bar{Q}_t$ by then is relatively unimportant term compared with solar heating. H_p is relatively unimportant throughout much of the simulation. Therefore the slight reduction in polynya size (see below) results in less heat loss across the polynya but this is insignificant compared with the increased $\bar{Q}_t$.

In order to produce a clear picture of the effect on the polynya radius, only the first time step predictions of this variable are shown (this gives an improved look at how well the model agrees with observations since all of the observations were made during daylight hours). About a 15 m difference from the default case gradually builds up over the simulation period. This is due primarily to the difference in lake temperature. For cooler water, there is less heat available to keep the ice edge from encroaching on the polynya area. It is not $\bar{Q}_t$ that is important to the polynya radius, but the value of q_t right at the ice edge. As q_t is proportional to T_w, the decrease in temperature results in a shrinking polynya.

Minimum Ice Thickness

The effect of increasing the minimum possible ice thickness from 2 to the 10 cm used in DYRESMI for much larger lakes is shown in Figure 5.16. Since this entire thickness must be melted in order for the polynya to increase, then q_t must be larger for a larger h_{min} in order for expansion to occur. Since q_t is proportional to r^{-1}, but not dependent on h_{min}, a balance will only be struck at a much smaller r_p for the larger h_{min}. Hence the predicted radii are less than half those for the default case. In addition, since a great deal

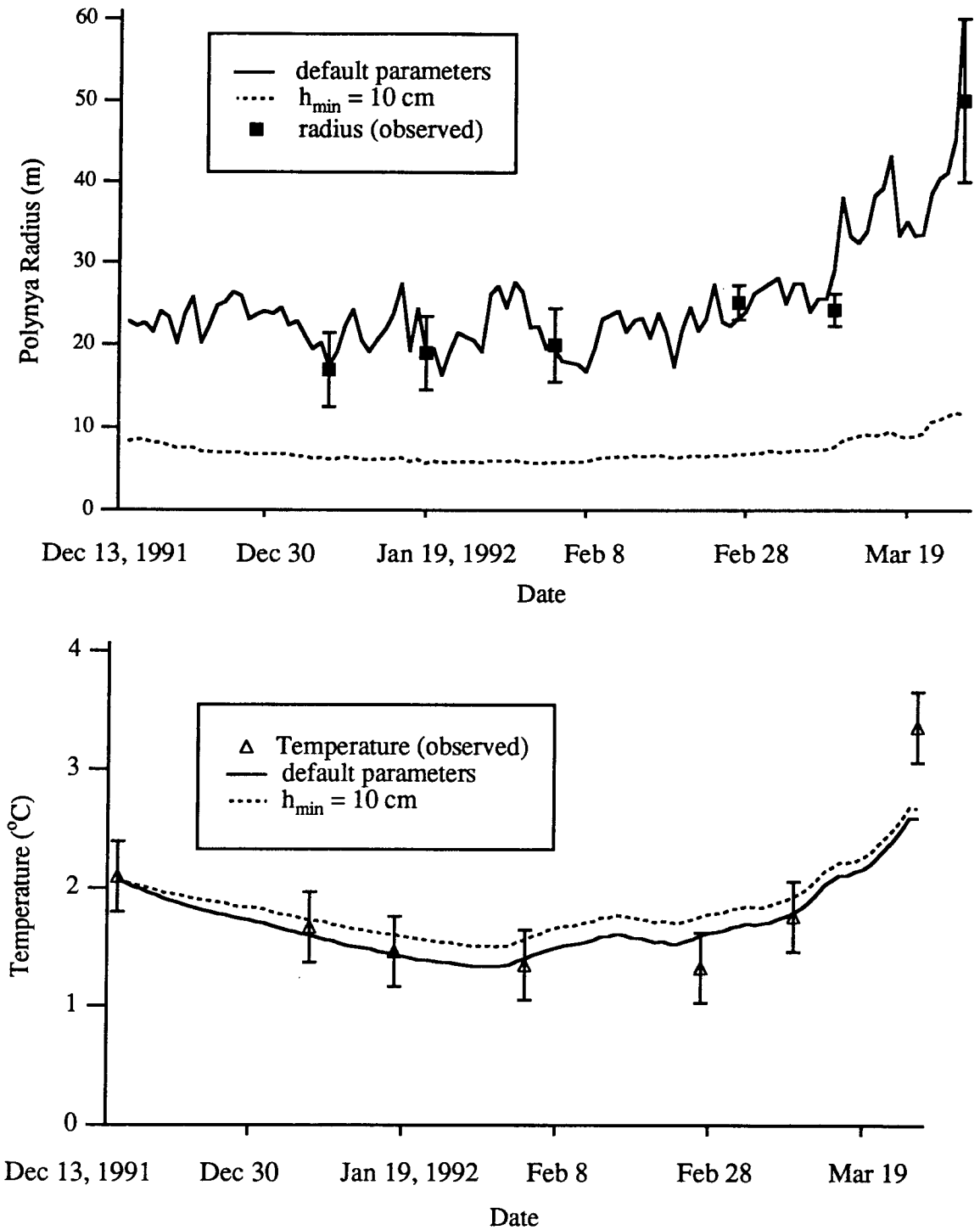

Figure 5.16 Effect of Increased Minimum Possible Ice Thickness on Polynya Radius and Whole Lake Temperature

more heat is required to melt 10 cm of ice than 2 cm, there is almost no day to day variation in the predicted radii. Over the long term, there is a very slight trend which follows that of the lake temperature. Since the thermal reserve is important in determining the heat balance at the polynya edge, the size of the polynya decreases as the lake temperature goes down, and increases as it goes up.

It is only with this strong variation in h_{min} that a significant change in water temperature due to the change in H_p occurs. With less than half the radius, the area over which H_p is active is less than one quarter of the default area. Hence there is a significant reduction in the heat loss from the lake. Essentially none of this change can be attributed to $\bar{Q}_t$ because it is only very weakly dependent on r_p. The temperature curves stop diverging in late January when the daily average flux approaches zero. With further cooling in February, there is little further widening in the temperature gap because H_p is unimportant relative to both $\bar{Q}_t$ and I_w. The gap closes almost completely as the end of the simulation is approached, because the smaller polynya now restricts the heat transfer back into the lake.

Turbulent Heat Transfer Coefficient

The effect of reducing the turbulent heat transfer coefficient from 1.1×10^{-3} to 0.8×10^{-3}, the average value found by Hamblin & Carmack (1990), is shown in Figure 5.17. The impact on the polynya radius is immediate since, from the start, there is only about 70% of the turbulent heat transfer to the ice edge. This contraction of about 7 m reduces H_p due to the smaller area across which the heat transfer can take place. The relatively warmer temperatures, however, are mainly due to the 70% reduction in $\bar{Q}_t$ which has been shown to be more important to the lake temperature than H_p. As warmer temperatures are produced, however, there is more heat available to melt the ice at the polynya edge, and the gap between the polynya radius for $C_t = 1.1 \times 10^{-3}$ and $C_t = 0.8 \times$

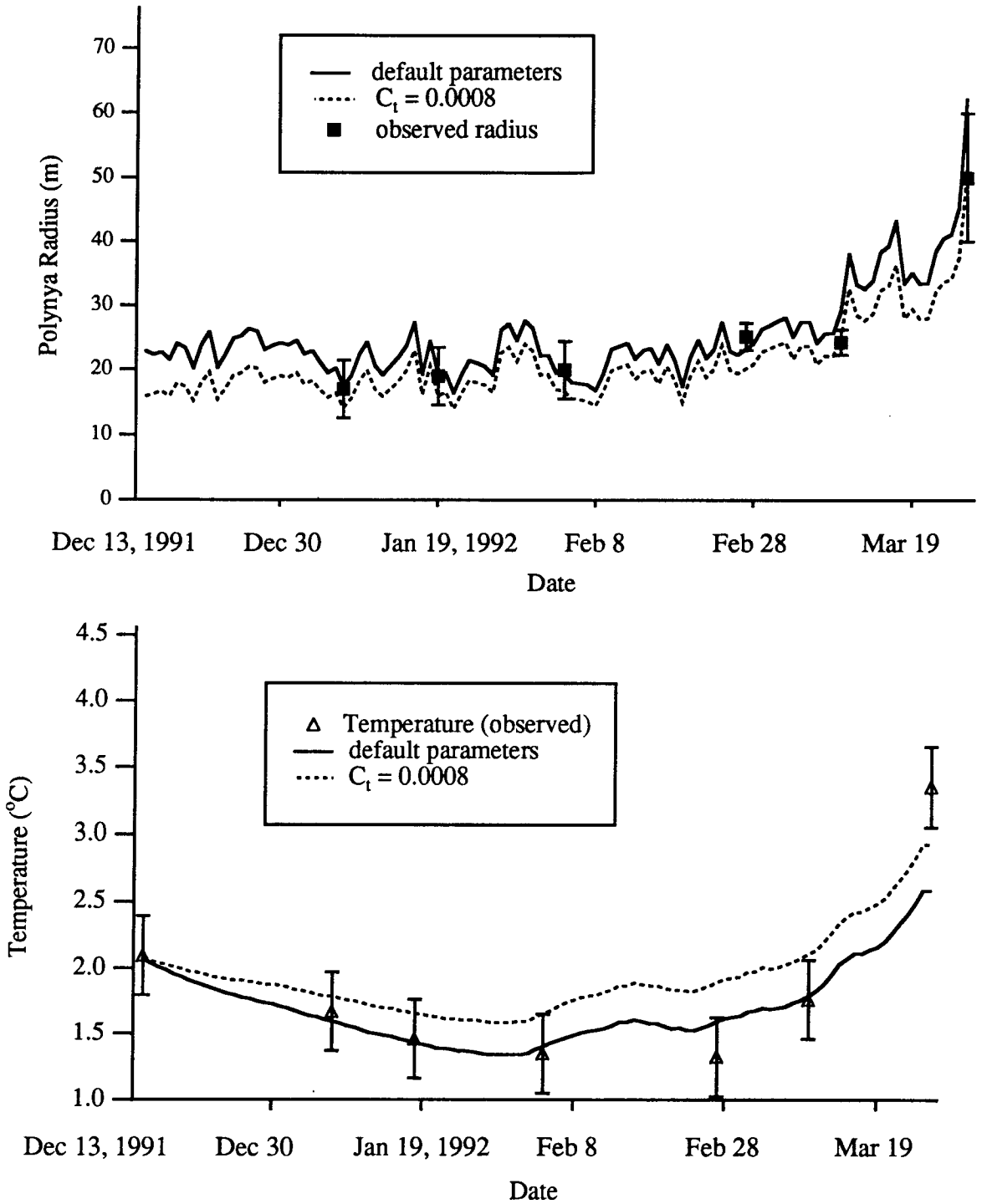

Figure 5.17 Effect of Decreased Turbulent Heat Transfer Coefficient on Polynya Radius and Whole Lake Temperature

10^{-3} is reduced. As $\bar{Q}_t$ reduces in relative importance with increased solar heating, the temperature no longer increases over the default case. With the temperatures rising together, the difference in C_t values increases in importance again with regards to the heat balance at the polynya edge, and the radius must therefore decrease relative to the default case.

5.2.4 Improving Ice Thickness Predictions

In §5.2.1, it was shown that the MLI-C ice thickness predictions are somewhat less than satisfactory due to the under-prediction of heat conduction through the cover during the cooling period of the simulation. Three possible explanations have been identified:

a) under-estimation of ice and snow conductivity
c) improper selection of ice thickness measurement location
b) improper representation of the meteorological balance

Given the good results for the Harmon Lake simulation using the same snow and ice properties, the first explanation is unlikely. One possibility, however, is the tendency to form white instead of black ice at Menzies lake due to the turbulence induced by the circulator. Although, given the lower density of white ice, it is more likely that this would tend to decrease conduction, not increase it. The second explanation deserves more consideration. In retrospect, ice measurements were often made too close to the weather station, which probably served as a heat sink. An increased flux of heat from the water up through the weather station would have resulted in greater local ice thicknesses. This possibility, which brings the ice cover data into question, emphasizes the need for a more thorough sampling procedure, so that statistically reliable estimates can be calculated for each observation date.

The third explanation deserves detailed examination, as it provides a starting point for further research. To illustrate the potential impact of the polynya on the conduction of heat through the ice cover in the rest of the lake, the analogy of parallel electrical resistors may be considered. Typically, the heat flux through a material which is characterized by variable conductivity over its surface is calculated using this concept. In this manner, reasonable results may be obtained for many heat transfer problems without resorting to a two-dimensional model. The best results are obtained if the variability is well distributed over the surface of the material, such as in the case of equally spaced steel bolts passing through an insulated wall. Although this is clearly not the case at Menzies Lake, the resistance concept could nonetheless be applied in future work to see if the results improve. It is likely that increased melt from the underside of the ice due to turbulent heat transfer in the vicinity of the polynya would be offset by the tendency of the heat flux through the ice cover to increase in this region due to the effect of the low relatively thermal resistance associated with the polynya. Again this suggests the need for more thorough ice thickness sampling in the future.

The thermal resistance approach provides explanations which are specific to the poor representation of the rate of ice growth in early winter, and the rate of melt late in the season. Both of these rates are under-estimated using MLI-C, especially the former. Referring back to Figure 5.13, it can be seen that the importance of heat transfer across the polynya, H_p is most significant during these two periods. Hence the impact of the polynya on the ice thickness would be most important at these times. Although the range in H_p is greatest in late winter, the average daily value per unit area of the polynya is much less significant. (Recall that the polynya at this time is large, and so H_p, per unit area of the entire lake surface, as given in Figure 5.13, would also tend to increase in importance.) It follows that, as the results indicate, the impact of the thermal resistance of the polynya on ice growth should be most significant in early winter.

Chapter 6
CONCLUSIONS AND RECOMMENDATIONS

6.1 GENERAL REMARKS

The field observations at Menzies and Harmon Lakes coupled with the modeling results provide conclusive evidence of the severe impact that artificial circulation has on the temperature of a small mid-latitude lake. It has been confirmed that a gradual increase in temperature would likely take place at Menzies Lake if it were left in a natural state. Instead, significant cooling takes place, bringing the lake dangerously close to a temperature which is intolerable to the aquatic life. (As described in Chapter 1, deleterious effects on aquatic life may occur below about 1°C). Over the uncharacteristically warm winter of 1991-92, the average temperature in Menzies Lake dipped to 1.4°C. This fact alone suggests that the peril of harming the biota of lakes subjected to artificial circulation should not be under-estimated.

MLI constitutes a first attempt to fine-tune an ice and snow cover model for small mid-latitude lakes left in a natural state. It has been shown in Chapter 5 that the extensions to DYRESMI provide significant improvements to ice, snow and temperature predictions. Although highly simplified, MLI-C also provides good predictions of water temperature. Given the questions which are arisen regarding the quality of the ice cover observations, it is possible that the model may also provide better ice cover predictions than the observation suggests. Certainly it would appear that the trend in ice thickness is well predicted once the ice thickness approaches its maximum. Furthermore it should be emphasized that the ultimate goal of this project was to determine if there would be a

deleterious effect on the aquatic life in an artificially circulate lake due to excessively low lake temperatures. To this end, the project has been successful. As described later in this chapter, however, more work is required before reliable predictions can be made based on a hypothetical meteorological data set.

An important feature of MLI and MLI-C is the reduced computing power requirement compared with DYRESMI. It has been shown that good results are achieved for small lakes even when the internal hydrodynamics are ignored. Hence the short time steps employed by DYRESMI can be avoided, resulting in significant savings in computing time. For this project MLI was run on a 80386 (25 MHz) PC. Less than 10 seconds were required for both MLI and MLI-C to produce results for the 105 days of simulation.

In this chapter, the results of both the Menzies and Harmon Lakes simulations will be summarized and conclusions drawn regarding the DYRESMI extensions, the actual heat transfer processes, and the parameter values.

6.2 MLI

6.2.1 Summary of Results

MLI provides good predictions of ice thickness and water temperature, and reasonable predictions of snow thickness. It has been found that solar heating is the main cause of lake warming over the ice-covered period but that sediment heat transfer may at least counter conductive heat loss to the ice cover to prevent a reduction in temperature in early winter. In addition, rain events may lead to a significant increase in lake warming due to reduced albedo. Ice thicknesses may be reduced as a result of the heat associated with rain, but it may eventually cause an increase in ice thickness if the insulation provided by the snow cover is lost and cold conditions follow. The impact of snow-ice

formation is similar in that mass is added to the total ice thickness, but the associated latent heat may result in melting at the ice-water interface.

The following extensions to DYRESMI are most important in achieving the results as described in Chapter 5:

a) rain melt
b) solar attenuation through snow-ice
c) a snow density function appropriate for mid-latitudes
d) sediment heat transfer
e) variable albedo

It is clear that the water which floods the snowpack when the bearing capacity of ice is exceeded constitutes a source of heat within the cover. As described in §5.1.4, this heat, as represented by Q_{si}, may be over-estimated since further snow densification likely occurs prior to the snow-ice formation. In addition, capillary rise may contribute to the snow-ice thickness.

The latent heat associated with rainfall was needed to produce the order of observed surface melting. Although the results are reasonable, the mechanism is unlikely. As described in Chapter 2, condensation melt should be the main driving force behind snowmelt for the given amounts of precipitation. It is suspected that the use of daily average meteorological data leads to an under-representation of condensation melt. Results indicate that the surface melt due to rainfall is over-estimated. Accurate predictions of snowmelt is essential, especially when the snow cover is thin. Even slight inaccuracies may lead to much more significant inaccuracies in ice and temperature predictions because of the significant drop in albedo (and to a lesser extent, the increase in conduction) associated with ice exposure when the snow is completely melted. This explains why the unlikely surge in lake temperature due to solar heating following the incorrect prediction of complete snowmelt in mid-February.

The correct combination of parameter values which would provide more accurate predictions is not completely evident from this study. Much work is required to quantify narrow ranges of possible values for mid-latitude locations. The relationships between snow density, conductivity, solar attenuation and albedo are of the greatest importance. A physically based model of snow densification is also needed.

From §5.1.4 however, it is hypothesized that the following combination of parameter changes are most likely to produce a more accurate representation of the heat budget:

a) Increased K_s: Figure 5.7 illustrates the significant impact of snow conductivity on ice thickness. A similar impact was only achieved by increasing maximum snow densities, but this leads to less likely snow cover predictions. The initial density cannot be increased by much to improve this latter result because of the restricted load bearing capacity of ice.

b) Increased λ_e: Figure 5.5 shows the impact of increasing the visible radiation attenuation coefficient of snow-ice from 3.75 m^{-1} to 6.0 m^{-1}. The result is a more likely rate of ice melt in March due to the absorption of more heat. This extra heat does not penetrate to the water, thereby producing improved temperature predictions.

c) Reduced α in March: The impact of reduced albedo in March is suggested by Figure 5.9. More than a simple parameter change is required here, since the results are very much dependent on whether or not a thin snow layer is predicted. From the few observations, made, it would appear that snow free conditions persist for a longer period of time than what is suggest by the predictions. The effect of heavy snowmobile traffic is suspected a being important in reducing the albedo to below those values predicted by MLI. The result would be a faster rate of ice melt and temperature increase.

d) reduced K_{sed}: It is suspected that the conductivity of the sediments is close to that of water as suggested by most of the studies available in the literature. Included in this majority is a study of gelatinous, organic sediments which are qualitatively similar to the sediments of Menzies and Harmon Lakes (see Chapter 2). It is expected that this change, in combination with the increase in λ_e would

appropriately offset the lake temperature increase due to a reduced albedo in March.

6.2.2 Recommendations for Future Research

Further research should concentrate on confirming that the parameter changes described in §6.2.1 are appropriate. This would involve including direct measurements of snow density, conductivity, solar attenuation, albedo, and sediment conductivity, in addition to repeating the data collection and modeling process over a full winter at Harmon Lake. In order to show that there are no other parameters of importance to the results, additional steps will be required to prove the accuracy of the model. These include a better understanding of Q_r, Q_{si}, q_w and q_{sed} as described below. Furthermore, the observation errors must be reduced. For the ice and snow cover, many more observations should be made over the entire lake area. With regard to lake temperature, more measurements over the thermal boundary layer at the ice-water interface may improve estimates (this would also help to better quantify q_w). In addition, instrumentation error may be reduced slightly by measuring the lake temperature over several profiles. If field measurements are restricted by time, however, the emphasis should be on making several ice and snow measurements. Temperature estimates would be improved to a greater extent by a highly accurate bathymetric survey and by better quantifying boundary effects.

More research is required to assess the importance of convective stirring near the temperature of maximum density. This condition probably occurred in March to result in increased rates of ice melt due to turbulent (convective) heat transfer from the water to the ice. It is possible that this mechanism may entirely explain the difference between the observed and predicted rates of ice melt. If this were the case, then the changes to λ_e and α described in §6.2.1 would be less likely.

Of great importance is the need to develop a more accurate rain melt model without resorting to sub-daily meteorological data. The apparent importance of condensation melt, which is not reflected in the MLI model, is iterated in Chapters 2, 4 and 5. Related issues include the impact on both the snow albedo and density. Furthermore, the role of latent heat due to the freezing of rain water as it approached the ice layer should be better understood.

The nature of the thermal boundary layers both at the ice-water interface and the lake bottom should be explored further. Of particular importance are the thermal gradients at both interfaces. In a global sense, the heat flux from the water to the ice is treated independently of the heat flux through the ice and snow cover in the MLI formulation. If this is so, further research may produce a model which predicts the thermal gradient based on the water temperature outside the boundary layer alone if the water is still. Any turbulent motion in the water below the ice, such as that created by convective mixing should also be considered. With regard to sediment heat transfer, a relationship that the thermal gradient may have with the annual average lake temperature and time since turnover would be useful for modeling purposes.

Q_{si} should be better quantified. This could be accomplished by making several field measurements of snow density, flooding depth, and snow, ice, and snow-ice thicknesses over the period in which snow falls, flooding occurs and snow-ice formation takes place. The spatial variation of these quantities should also be assessed by sampling over the entire lake area. It is likely that bending of the ice cover under the weight of snow results in significantly more flooding and snow-ice production near the centre of the lake, as observations have indicated. Establishing the importance of capillary rise of water through snow would also be useful.

Finally, the cloud cover estimate algorithm should be tested thoroughly by comparing actual long-wave radiation measurements to model predictions. Given the importance of cloud cover to both the long-wave radiation balance and albedo predictions, the need to better quantify this variable is substantial.

6.3 MLI-C

6.3.1 Summary of MLI-C Results

The MLI-C model provides good predictions of temperature at Menzies Lake throughout the entire simulation period. The deviations from the observations can be attributed to inappropriate choices of parameters which are independent of the artificial circulation process. This issue is dealt with in §6.2. However, the reliability of the results are brought into question by the apparently poor ice predictions in early winter. Throughout most of the period, the predicted trend in ice thickness is good, and the deviations may simply be explained in terms of the MLI parameters. Further field work is required in order to determine if the lack of agreement in early winter was due to an improper sampling procedure as described in §5.2.4.

The following values for the calibration parameters have been found to give the best predictions:

h_{min}	0.02 m
Δr	13 m
C_t	1.1×10^{-3}

Although determined through calibration, the values of h_{min} and C_t make good physical sense as described in §5.2.1. Only Δr has no physical meaning except that it is the radial distance over which the turbulent heat transfer for frictionless flow is equal to that

produced by a velocity field which is dissipated by friction at the ice-water interface over the entire ice-covered area. According to visual observations through ice holes, the velocities became negligible below the ice at much less than the average lake radius away from the polynya edge.

In spite of an apparently low value of Δr, the turbulent heat transfer from the water to the ice, $\bar{Q}_t$, at an average of about 7.6 W/m^2, is over three times as important as the heat transfer across the polynya, H_p, over the lake cooling period. After the lake had reached its minimum temperature, there is, on average, a slight net transfer of heat across the polynya until the end of the simulation. Meanwhile, $\bar{Q}_t$ increased in importance in the latter half of the simulation, with a lake average heat transfer rate of about 8.6 W/m^2. Furthermore, in spite of such a small value of h_{min}, there is little day to day variation in r_p until late March when ice-free conditions are rapidly produced. In this regard, the model simulates field conditions well.

The results described in Chapter 5 indicate that there is a delicate heat flux balance which results in lake temperatures which are just adequate in supporting aquatic life. For example, the heat which is provided to the lake by the sediments could, over cold winters, often constitute the difference between fish survival and fish mortality. Similarly, if overcast skies prevailed, the lake may be deprived of the solar energy it needs (fortunately, extremely cold weather is often associated with clear skies). Extremely windy conditions could also increase the importance of H_p through substantial gains in sensible heat loss. Furthermore, although snow cover does insulate the lake, its main impacts are to reduce the growth in ice thickness and to prevent solar radiation from penetrating into the water. Hence a winter characterized by consistently thick snow cover may deprive an artificially circulated lake of the solar heat it needs over the winter.

Finally, if a large lake, characterized by a larger value of h_{min}, were equipped with a proportionately large circulation system, a proportionately large polynya would not be expected. Similarly, a polynya which is larger than expected may develop at a very small and highly sheltered lake.

6.3.2 Recommendations for Artificial Circulator Design

From the results of this study, it is not the polynya size which must be controlled to avoid over-cooling a lake, but the turbulence beneath the ice. If aeration is improved merely by increasing the polynya size (without increasing the pumping rate) then a lake which persistently experiences winterkill due to inadequate aeration could be rehabilitated without increasing $\bar{Q}_t$. Unfortunately, for the given system, a larger polynya could only be created by increasing the radial jet velocity. As both q_t and $\bar{Q}_t$ are proportional to this velocity, then the polynya cannot be increased in size without increasing $\bar{Q}_t$.

The cost associated with the option of virtually eliminating $\bar{Q}_t$ by installing large baffles in a suitable geometry at some distance away from the circulator would, in possibly all cases, be prohibitive. A more viable option may involve the installation of two or more smaller units in such a way that an adequate polynya surface area (and adequate total pumping rate if required) is maintained. In this manner, $\bar{Q}_t$ is reduced since, although the same surface velocities must exist along the perimeter of the polynya for a given polynya radius and any system configuration, the use of several units should mean that the rate at which this velocity decreases beyond the polynya edge should be higher. This is explained by the inverse relationship between velocity and the radial distance from each individual circulator. The net effect is a reduction in Δr. Figure 5.15 suggests that both the average lake temperature and the average polynya radius would increase. Such a strategy may therefore actually improve re-aeration over the use of one large unit, while diminishing the impact on lake temperature.

A third option involves the use of a distributed air bubble diffuser system. In most systems described in the literature (see, for example, Ashton, 1979), a point source bubble diffuser creates a rising plume which entrains water, strikes the water surface where it is redirected in the form of a radial jet. Such systems would create a similar velocity decay function as the Air-o-lator®. An alternative would be to install a distributed source diffuser which would create a grid of smaller plumes impinging at the surface. The principal regarding reduced $\bar{Q}_t$ is the same as that described above. This alternative may be less costly, since only one air compressor would be required.

A final suggestion involves the use of a pump which could produce a relatively fine spray of water. In this case the jet would be projected high into the air, such that trajectory of the falling drops of water are nearly vertical. The larger the required polynya, the greater the maximum height of the fountain would have to be. This system would almost completely avoid any significant turbulent heat transfer to the ice. The design would involve calculation of the minimum rate of constant rainfall required to maintain ice-free conditions, and the amount of cooling that the drops of water would experience. If the drops were to cool substantially, or even freeze, the result could be very high rates of lake cooling.

6.3.3 Recommendations for Future Research

The first step in improving MLI-C must be to re-evaluate the MLI parameters as described in §6.2.2. Once MLI is fine-tuned, attention should be focused on the characteristics of the polynya edge and the hydrodynamic boundary layer which becomes established at the ice-water interface. Once the hydro/thermodynamics are better understood, it may be possible to abandon the h_{min} approach in favour of a more theoretical boundary layer heat transfer model in which the growth of ice from the polynya edge out the full ice thickness is also predicted. If this could be done, then there

would also be no further need for the Δr calibration constant. The remaining parameter, C_t, would best be assessed in the field specifically for the Air-o-lator®. Alternatively, C_t could be determined with better confidence by means of calibration once the hydrodynamic model is established.

The model described above would ideally be verified in the field. The use of under-ice drogues such as those described by Hamblin (1990) would allow for measurement of the velocity field below the ice. In addition, large sections of the ice could be cut away for a direct measurement of the ice profile in the vicinity of the polynya. Furthermore, detailed measurements of the thermal boundary would provide critical information on the turbulent heat transfer rates.

More thorough ice thickness observations is also recommended for any future studies involving artificially circulated lakes. Several measurements would be useful both for meaningful values of average thickness, and for providing more insight on spatial variations which may be dependent on the circulator. This may allow for an indirect evaluation of the velocity decay below the ice, and $\bar{Q}_t$.

Finally the impact the polynya has on the heat flux through the ice covering the remainder of the lake should be well established and quantified. A first attempt at solving this problem could involve the thermal resistance approach described in Chapter 5.

REFERENCES

Ashley, K.I., 1987, Artificial Circulation in B.C., Review and Evaluation, Province of British Columbia, Ministry of the Environment and Parks, Fisheries Technical Circular no. 78, 34 pp.

Ashley, K.I., 1991, personal communication, Fish and Wildlife Branch, B.C. Ministry of the Environment, Vancouver, B.C.

Ashton, G.D., 1974, Air Bubbler Systems to Suppress Ice, Cold Regions Research Engineering Laboratory, Special Report 210, AD-A008867.

Ashton, G.D., 1979, Point Source Bubbler Systems to Suppress Ice, Cold Regions Science and Technology, no. 1, pp. 93-100.

Ashton, G.D., 1986, ed., River and Lake Ice Engineering, Water Resources Publications, Colorado.

Bandow, F., 1986, Evaluation of Winter Lake Aeration Techniques in Minnesota, Pub. No. 386, Minnesota Dept. of Natural Resources, Division of Fish and Wildlife, St. Paul, Minnesota.

Bauer J., Martin, S., 1983, A Model of Grease Ice Growth in Small Leads, J. Geophys. Res., 88(C5), pp. 2917-2925.

Bergen, J.D., Hutchinson, B.A., McMillan, R.T., Ozment, A.D., Gottfried, G.J., 1983, Short-wave Reflectivity of Recent Snow, Journal of Applied Meteorology, 22(2), pp.193-200.

Birge, E.A., Juday, C., March, H.W., 1927, The Temperature of the Bottom Deposits of Lake Mendota; a Chapter in the Heat Exchanges of the Lake, Trans. Wisc. Acad. Sci. Arts Lett. 23, pp. 187-231.

Böer, K.W., 1980, The Terrestrial Solar Spectrum, Solar Energy Technology Handbook, Part A (W.C. Dickenson & P.N. Cheremisinoff [eds.]), Dekker, pp. 65-87.

Bohren, C.F., and Beschta, 1979, Snowpack Albedo and Snow Density, Cold Regions Science and Technology, 1(1), pp.47-50.

Chen, C.W., Orlob, G.T., 1975, Ecological Simulation for Aquatic Environments, System Analysis and Simulations in Ecology, B. Patton, ed., Vol. 3, Academic Press, New York.

Choudhury, B.J., 1982, Spectral Albedos of Mid-latitude Snowpacks, Cold Regions Science and Technology, 6(2), pp.123-139.

Den Hartog, G., Smith, S.D., Anderson, R.J., Topham, D.R., Perkin, R.G., 1983, An Investigation of a Polynya in the Canadian Archepelago, 3. Surface Heat Flux, Journal of Geophysical Research, 88(C5), pp. 2911-2916.

Eranti, E., Leppänen, E., Penttinen, M., 1983, Ice Control in Finnish Harbours, Proceedings, 7th International Conference on Port and Ocean Engineering Under Arctic Conditions, Vol. 1, Espoo, Finland, pp. 370-380.

Gardon, R., Akrifirat, J.C., 1966, Heat Transfer Characteristics of Two-Dimensional Air Jets, Trans. Am. Soc. Mech. Eng., series C, J. Heat Transfer, 88, pp. 101-108.

Geiger, R., 1965, The Climate Near the Ground, Cambridge, Harvard, University Press, 611 pp.

Gilpin, R.R., Hirata, T., Cheng, K.C., 1980, Wave Formation and Heat Transfer at an Ice-Water Interface in the Presence of a Turbulent Flow, Journal of Fluid Mechanics, pp. 619-640.

Gosink, J.P., 1987, Northern Lake and Reservoir Modeling, Cold Regions Science and Technology, no. 13, pp. 281-300.

Grant, L.O., Rhea, J.O., 1973, Elevation and Meteorological Controls on the Density of New Snow, Advanced Concepts and Techniques in the Study of Snow & Ice Resources, U.S. Committee of the International Hydrological Decade, pp. 169-181.

Gray, D.M., 1970, Handbook on the Principles of Hydrology, Canadian National Committee for Hydrological Decade, Ottawa.

Gray, D.M., and Male, D.H., 1981, Handbook of Snow: Principles, Processes, Management and Use, Pergamon Press.

Grenfell, T.C., Maykut G.A., 1977, Optical Properties of Ice and Snow in the Arctic Basin, Journal of Glaciology, 18, pp. 445-463.

Grenfell, T.C., Perovich, D.K., Ogren, J.A., 1981, Spectral Albedos of an Alpine Snowpack, Cold Regions Science and Technology 4(2), pp. 121-127.

Hamblin, P.F., 1990, Yukon River Headwater Lakes Study, 1983 and 1985: Observations and Analysis, Environment Canada, Scientific Series No. 175, Lakes Research Branch, Canadian Centre for Inland Waters.

Hamblin, P.F., 1992, personal communication, Lakes Research Branch, Canadian Centre for Inland Waters (National Water Research Institute), Burlington, Ont.

Hamblin, P.F., Carmack, E.C., 1990, On the Rate of Heat Transfer Between a Lake and an Ice Sheet, Cold Regions Science and Technology, 18, pp. 173-182.

Harr, R.D., 1981, Some Characteristics and Consequences of Snowmelt During Rainfall in Western Oregon, Journal of Hydrology (53), pp. 277-304.

Henderson-Sellers, B., 1984, Engineering Limnology, Pitman Publishing Ltd., 356 pp.

Hill, J.M., Kucera, A., 1983, Freezing a Saturated Liquid Inside a Sphere, Int. J. Heat Mass Transfer, 26, pp. 1631-1638.

Hiratia, T., Gilpin, R.R., Cheng, K.C., 1979, The Steady State Ice Layer Profile on a Constant Temperature Plate in a Forced Convection Flow, II. Turbulent Regime, International Journal of Heat and Mass Transfer, 22, pp. 1435-1443.

Holman, J.P., ed., 1990, Heat Transfer, 7th ed., McGraw-Hill Publishing.

Hutchinson, G.E., 1957, A Treatise on Limnology, Vol. 1: Geography, Physics and Chemistry, Wiley, New York.

Imberger, J., & Patterson, J.C., 1981, A Dynamic Reservoir Simulation Model -DYRESM:5, in Transport Models for Inland & Coastal Waters: Proceedings of a symposium on Predictive Ability (H.B. Fischer, ed.), Academic Press, New York.

Jirka, G.H., Katavola, D.S., 1980, Supercritical Withdrawal from Two-Layered Fluid Systems, Part 2: Three-Dimensional Flow into Round Intake, Journal of Hydraulic Research 17, No.1, pp. 53-62.

Kirk, J.T.O., 1983, Light and Photosynthesis in Aquatic Ecosystems, Cambridge.

Kraus, E.B., 1972, Atmosphere-Ocean Interaction, Clarendon Press, Oxford, 275 pp.

Lackey, R.T., Holmes, D.W., 1972, Evaluation of Two Methods of Aeration to Prevent Winterkill, Prog. Fish Cult., 34(3), pp. 175-178.

Likens, G.E., Johnson, N.M., 1969, Measurement and Analysis of the Annual Heat Budget for the Sediments in Two Wisconsin Lakes, Limnology & Oceanography, 114(1), pp. 115-135.

Maykut, G.N., Untersteiner, N., 1971, Some Results from a Time Dependent, Thermodynamic Model of Sea Ice, J. Geophys. Res. (83), pp. 1550-1575.

McKay, G.A., 1968, Problems of Measuring and Evaluating Snowcover, Snow Hydrology: Proceedings of the Canadian National Committee of the International Hydrological Decade

Mortimer, C.H., 1941-42, The Exchange of Dissolved Substances Between Mud and Water in Lakes, Journal of Ecology, 29, pp. 280-329; 30, pp. 147-201.

Mortimer, C.H., 1971, Chemical Exchanges in the Great Lakes - Speculations on Probable Regulatory Mechanisms, Limnology & Oceanography, 16(2), pp. 387-404.

Mortimer, C.H., and Mackareth, 1958, Convection and its Consequences in Ice-covered Lakes, Verh. internat. Ver. Limnol., pp. 923-932.

National Research Council of Canada, 1985, National Building Code of Canada, 1985, Supplement, Report No. 23178.

Neumann, J., 1953, Energy Balance and Evaporation from Sweet-Water Lakes of the Jordan Rift, Bull. Res. Coun. Israel, 2, pp. 337-357.

O'Neill, K., Ashton, G.D., 1981, Bottom Heat Transfer to Water Bodies in Winter, U.S. Army Corps of Engineers, Special Report 81-18.

Patterson J.C., & Hamblin, P.F., 1988, Thermal Simulation of Lakes with Winter Ice Cover, Limnol. Oceanogr. 33(3): 328-338.

Petzold, D.E., 1977. An Estimation Technique for Snow Surface Albedo, Climatological Bulletin, McGill University, Dept. of Geography, 21, pp.1-11.

Rajaratnam, N., 1976, Developments in Water Science: Turbulent Jets, Elsevier Scientific Publishing Co., Amsterdam, 304 pp.

Raphael, J.M., 1962, Predictions of Temperature in Rivers and Reservoirs, Journal of the Power Division, A.S.C.E., 88(PO2), Proc. paper 3200, pp. 157-182.

Robinson, D.A., and Kukla, G., 1984, Albedo of a Dissipating Snow Cover, Journal of Climate and Applied Meteorology, 23(12), pp.1626-1634.

Ryan, P.J., Harleman, D.R.F., Stolzenbach, K.D., 1974, Surface Heat Loss from Cooling Ponds, Water Resources Research, 10(5), pp. 930-938.

Semter, A.J., 1976, A model for the Thermodynamic Growth of Sea Ice in Numerical Investigations of Climate, J. Phys. Oceanogr., 6, pp. 379-389.

Stauffer, R.E., 1987, A Comparative Analysis of Iron, Manganese, Silica, Phosphorus and Sulpher in the Hypolimnia of Calcareous Lakes. Water Research 9(21), pp. 1009-1022.

Stigebrandt, A., 1978, Dynamics of an Ice-Covered Lake with Through Flow, Nordic Hydrology, 9, pp. 219-244.

Strickland, N., 1982, Factors Affecting Temporal Variations in the Albedo of Snow Cover, Western Snow Conference, Proceedings, pp. 186-187.

Tennessee Valley Authority (TVA), 1972, Heat and Mass Transfer Between a Water Surface and the Atmosphere, Division of Water Control Planning, Report No. 0-6803, Water Resources Research Laboratory Report No. 14, Norris, Tennessee.

United States Army Corps of Engineers (U.S.A.C.E.), 1956 , Snow Hydrology, Summary Report of the Snow Investigations, North Pacific Division, Portland, Oregon, 437 pp.

United States Army Corps of Engineers (U.S.A.C.E.), 1986, CE-QUAL-R1: A Numerical One-Dimensional Model of Reservoir Water Quality (User's Manual), Instructional Report E-82-1, Environmental Laboratory, Vicsburg, Mississippi.

Urban, T.C., Diment, W.H., 1988, Thermal Regime of the Shallow Sediments of Clear Lake, California, Late Quaternary Climate, Tectonism, Sedimentation in Clear Lake, Northern California Coasts, Geol. Soc. of America, Boulder, CO., pp. 207-221.

Welch, H. E., and Bergmann, M.., 1985, Water Circulation in Small Arctic Lakes in Winter, Can. J. Fish. Aquat. Sci. 42, pp. 506-520.

Wetzel, R.G., 1983, Limnology, 2nd Edition, Sanders College Publishing.

Wiscomb, W.J., and Warren, S.G., 1980, Model for the Spectral Albedo of Snow, Journal of the Atmospheric Sciences, 37(12), pp. 2712-2733.

Witze, P.O., Dwyer, H.A., 1976, The Turbulent Radial Jet, J. Fluid Mech., 75(3), pp. 401-417.

Wood, I.R., 1978, Selective Withdrawal from Two-Layered Fluid, Journal of the Hydraulics Division, ASCE, pp. 1647-1659.

APPENDIX A

Theoretical Solar Radiation Under Clear Skies

The Tennessee Valley Authority (1972) has published a comprehensive report covering empirical formulae which permit calculations of heat and mass transfer between at water surface and the atmosphere. Included in the report are the formulae required to calculate the total amount of solar radiation, SWCS, which could reach the earth's surface under clear skies at a given location and at any time of the year. SWCS requires estimates of atmospheric attenuation which is controlled by the optical air mass, precipitable water content and atmospheric dust. In addition, since the total daily radiation includes both direct and indirect energy, an estimate of the local albedo is also required. First, however, the solar radiation at the top of the atmosphere must be calculated as follows:

$$Qs = \frac{24 \cdot I_c}{\pi r_d^2} [\ hss \sin(\theta) \sin(\delta) + \cos(\theta) \cos(\delta) \sin(hss)\ ]$$

where, I_c = solar constant

= 4871 kJ / m^2 / hr

r_d = ratio of actual to mean distance of the earth from the sun

$= 1 + 0.017 \cos(\frac{2\pi}{365} (186\text{-}jd))$

jd = Julian day

θ = latitude of geographical location

δ = solar declination

h_{ss} = hour angle at sunset

The hour angle at sunset, h_{ss}, is given by:

$$\cos(h_{ss}') = \frac{\sin(\psi_{ss}) - \sin(\theta) \sin(\delta)}{\cos(\theta) \cos(\delta)}$$

where, ψ_{ss} = solar altitude at sunset ($\approx 15^o$ at Menzies and Harmon Lakes due to topographic obstructions; assumed to be equal to the solar altitude at sunrise)

If $\cos(h_{ss}') = 0$, then $h_{ss} = \pi/2$

If $\cos(h_{ss}') < 0$, then $h_{ss} = \pi - \cos^{-1}|\cos(h_{ss}')|$

If $\cos(h_{ss}') < 0$, then $h_{ss} = \cos^{-1}|\cos(h_{ss}')|$

An accurate formulation for the sun's declination, δ, is given as:

$$\sin(\delta) = \sin(\delta_{max}) \sin(\sigma)$$

where, $\sigma = \frac{2\pi}{360}[279.9348 + \frac{360}{2\pi} d + 1.914827 \sin(d) - 0.079525 \cos(d) + 0.019938 \sin(d) - 0.001620 \cos(2d)]$

d = angular fraction of a year

$= \frac{2\pi}{365.242}(jd - 1)$

$\delta_{max} = 23.445 \frac{\pi}{180}$

Two transmission coefficients are required for the calculation of SWCS:

$$a' = \exp[-(0.465 + 0.134\, w)\,(0.129 + 0.171 \exp(-0.88\, m_p))\, m_p], \text{ and}$$

$$a'' = \exp[-(0.465 + 0.134\, w)\,(0.179 + 0.421 \exp(-0.721\, m_p))\, m_p]$$

where, a' = mean atmospheric transmission coefficient after scattering

a'' = mean atmospheric transmission coefficient after scattering and absorption

w = precipitable water content in the atmosphere

$= 0.85 \exp(0.110 + 0.0614\, T_d)$

T_d = mean dew point temperature (^oC)

$= \frac{265.5\,(\log(svpd) - 0.7858)}{9.5 + 0.7858 - \log(svpd)}$

m_p = optical air mass

$= \frac{[(288 - 0.0065\, z)/288]^{5.256}}{\sin(\psi) + 0.15(\psi\, 180/\pi + 3.885)^{-1.253}}$

z = local elevation

ψ = solar altitude (the altitude at solar noon is used in MLI)
= $\sin(\theta)\sin(\delta) + \cos(\theta)\cos(\delta)$

Although the equation for the precipitable water content, w, has been calibrated for a monthly average T_d (TVA, 1972), daily averages are used here since they are available.

SWCS may be computed as:

$$SWCS = Q_s \frac{a'' + 0.5(1 - a' - dust)}{1 - 0.5\, R_g\, (1 - a' + dust)}$$

Where, dust = depletion coefficient of the direct solar beam by dust scattering
R_g = local reflectivity of the ground in the vicinity of the site

A value of 0.13 for dust was selected. Few data are available but the range given in TVA (1972) for the winter season is 0.06 to 0.13, depending on the air mass, m_p. It was found that a value chosen from the high end of the range produced the most reasonable cloud cover predictions. The local reflectivity is dependent on the surrounding forest, the small area of snow-covered fields adjacent to the lake, and the lake surface itself. The lake surface must only have an indirect effect on the reflected solar radiation measured at the pyranometer since it is entirely below the elevation of the instrument. The tall trees surrounding the lake, however, have a more direct impact. R_g was estimated by adding 70% of the forest reflectivity to 30% of the lake surface albedo. An average value of 0.07 for forest cover was selected with reference to TVA (1972). This is much less than the lake surface albedo with either snow or snow-ice cover. Since the lake surface albedo may vary substantially from day to day, then SWCS will not necessarily be expected to steadily increase each day as time progresses beyond the winter solstice.